Unraveling phenological and stomatal responses to extreme flash drought and implications for water and carbon budgets

Nicholas K. Corak[1,2], Jason A. Otkin[3], Trent W. Ford[4], and Lauren E. Lowman[1,2]

[1]Department of Physics, Wake Forest University, Winston-Salem, NC, USA
[2]Department of Engineering, Wake Forest University, Winston-Salem, NC, USA
[3]Cooperative Institute for Meteorological Satellite Studies, Space Science and Engineering Center, University of Wisconsin-Madison, Madison, WI, USA
[4]Illinois State Water Survey, Prairie Research Institute, University of Illinois at Urbana-Champaign, Urbana-Champaign, IL, USA

Correspondence: Lauren E. L. Lowman (lowmanle@wfu.edu)

Abstract. In recent years, extreme drought events in the United States have seen increases increased in frequency and severity underlining a need to improve our understanding of vegetation resilience and adaptation. Flash droughts are extreme events marked by rapid dry down of soils due to lack of precipitation, high temperatures, and dry air. These events are also associated with reduced preparation, response, and management time windows before and during drought which exacerbate their detrimental impacts on people and food systems. Improvements in actionable information for flash drought management are informed by atmospheric and land surface processes, including responses and feedbacks from vegetation. Phenologic state, or growth stage, is an important metric for modeling how vegetation interacts with the atmosphere. modulates land-atmosphere interactions. Reduced stomatal conductance during drought leads to cascading effects on carbon and water fluxes. We investigate how uncertainty in vegetation phenology and stomatal regulation propagates through vegetation responses during drought and non-drought periods by coupling a land-surface hydrology model to a predictive phenology model. We identify plant processes that influence vegetation responses to drought and also assess the role of vegetation in the partitioning of carbon, water, and energy fluxes during flash drought and compare against drought and non-drought periods. We selected study sites in Kansas, USA where extreme drought events have been observed, in particular that were impacted by the flash drought of 2012, and where AmeriFlux eddy covariance towers provide data which can be used to evaluate water movement between the land (surface and subsurface) and the atmosphere. We evaluate the evolution of plant phenology, water use, and productivity using different water stress events. Results show that phenological ground observations to validate and compare against model estimates. Results show the compounding effects of reduced precipitation and high vapor pressure deficit (VPD) on vegetation distinguish flash drought from other drought and non-drought periods. High VPD during flash drought shuts down stomatal conductance resulting in rates of evapotranspiration (ET), gross primary productivity (GPP), and water use efficiency (WUE) falling below average drought conditions. Phenological responses using model parameters generated from periods of average precipitation show slower responses to drought as compared to parameters generated to reflect isohydric or anisohydric tendencies. Evapotranspiration (ET) and gross primary productivity (GPP) show similarly timed responses to water stress. We find plants alter water use strategies under extreme drought, with plants nearly halting atmospheric water and carbon exchanges

when under stress. Decreases in uncertainty from ensemble estimates of GPP and ET during the flash drought period reduce to winter levels implying variability in plant life stage and functionality during drought periods are similar to those of dormant months. These results have implications for improving predictions of drought impacts on vegetation.

1 Introduction

Frequency and severity of extreme droughts are predicted to increase within the next century (Dai, 2013). Flash droughts are a particular type of extreme drought characterized by their rapid intensification (Svoboda et al., 2002; Ford and Labosier, 2017; Otkin et al., 2018, 2022). The flash drought of 2012 that impacted the Central United States amplified the need to understand and predict flash droughts because of its estimated $30 billion of impacts to agriculture (Otkin et al., 2018). Work over the last decade has improved methods for identifying flash droughts based on development time and concurrent meteorological conditions (see Lisonbee et al., 2021, for a summary of flash drought definitions and indicators). Many studies have examined the drivers (e.g., lack of precipitation, greater atmospheric demand for water, above average temperatures) and impacts (e.g., soil moisture deficits and damages to agriculture) of flash drought (e.g., ?Christian et al., 2023, 2022; Jin et al., 2019; Otkin et al., 2018) (e.g., Lowman et al., 2023; Christian et al., 2023, 2022; Jin et al., 2019; Otkin et al., 2018) while others have examined vegetation-atmosphere interactions (Chen et al., 2021; Zhang and Yuan, 2020; Gerken et al., 2018; Otkin et al., 2016; Novick et al., 2016) (Hosseini et al., 2022; Chen et al., 2021; Zhang and Yuan, 2020; Gerken et al., 2018; Otkin et al., 2016) and stomatal functioning (Novick et al., 2016; Roman et al., 2015).

Further assessment of vegetation-atmosphere feedback mechanisms may help improve identification of flash drought onset (Qing et al., 2022). Gross primary productivity (GPP), or carbon assimilation by plants during photosynthesis, is one such vegetation-atmospheric interaction impacted by drought (Zeng et al., 2023). Large reductions in GPP due to soil moisture and temperature anomalies can be used to mark the beginning and duration of flash drought events (Zhang and Yuan, 2020; Poonia et al., 2022) (Poonia et al., 2022; Zhang and Yuan, 2020), as seen in the 2012 flash drought (Jin et al., 2019). Flash droughts can intensify through land-atmosphere feedbacks (Basara et al., 2019); for example, vegetation expediting water stress by pulling water from deeper soil layers and further drying soils (Qing et al., 2022). Otkin et al. (2016) studied the evolution of soil moisture and vegetation conditions during the 2012 event, finding that changes in soil moisture and evaporative stress indicators preceded rapid drought intensification in the US Drought Monitor (USDM, Svoboda et al. (2002)). Chen et al. (2019) found declines in evapotranspiration (ET), another interaction between the vegetation and the atmosphere, to be a major sign of flash drought intensification.

Interactions between vegetation and the atmosphere are altered during flash drought events, thus it is necessary to consider vegetation state when studying the effects of flash drought (Chen et al., 2021). Additionally, capturing differences across plant types is essential for modeling vegetation response to drought. Failure to account for differential responses across plant function functional types (PFTs) could result in underestimating the plant's ability to maintain its function under water stress (Zhou et al., 2013). Roman et al. (2015) showed that tree species in a forested region behaved differently during drought, with some species exhibiting isohydric tendencies, whereas others were more anisohydric. Isohydric plants

are more conservative with their water use strategies when under stress and tend to regulate their stomatal conductance making them less susceptible to hydraulic failure (Konings and Gentine, 2017). These tendencies dictate how much photosynthesis occurs and thus how much carbon is exchanged (Roman et al., 2015). However, Garcia-Forner et al. (2017) cautions against making links between carbon assimilation and water potential regulation by showing similar rates of carbon assimilation under controlled drought simulations between two species of Mediterranean trees with opposing drought responses (one isohydric and one anisohydric). For some species, ~~hydraulic~~ stomatal regulation exists on a spectrum and can shift between isohydric and anisohydric in response to atmospheric and water conditions ~~(Guo et al., 2020; Wu et al., 2021)~~ (Wu et al., 2021; Guo et al., 2020) leading to variation and uncertainties in water use strategies (Kannenberg et al., 2022). Ecosystem scale modeling may be able to incorporate the plant level spatial and temporal variability in water use strategies ~~(Kannenberg et al., 2022)~~ (Giardina et al., 2023; Konings and Gentine, 2017) by taking into account concurrent meteorological and environmental conditions that influence plant water use tendencies beyond the ~~species~~ specie's physiological characteristics (Hochberg et al., 2018).

Vegetation state parameterization in ecohydrological models could also dictate whether an area experiences carbon uptake changes during a flash drought due to the linkage between ET and GPP that couples the carbon and water cycles (Hosseini et al., 2022). There is evidence connecting vegetation changes in response to flash drought to lower plant production (Zhang et al., 2020; Jin et al., 2019; He et al., 2018; Otkin et al., 2016; Hunt et al., 2014). Jin et al. (2019) and He et al. (2018) found that croplands, grasslands, and shrublands experienced the majority of loss to carbon uptake rates during the droughts of 2011 and 2012 across the central US and similar rates of ET were found in croplands in the US northern plain flash drought of 2017 (He et al., 2019; Kimball et al., 2019). Chen et al. (2021) showed increases in LAI led to increased ET and that in a low moisture regime the amount of latent heat released due to ET was sensitive to changes in LAI. Hunt et al. (2014) showed that maize experienced decreases in stomatal conductance, which led to declines in GPP and ET, during a flash drought. ~~Multiple studies showed crop yield losses following flash drought (e.g., Otkin et al., 2016; Hunt et al., 2014)~~Roman et al. (2015) show that species specific stomatal control can lead to different drought responses implying that some plants that exhibit more drought tolerant behavior might be accessing deeper stores of water (Giardina et al., 2023).

Previous studies have used remotely sensed or ground measurements and indicators to study vegetation responses to flash drought ~~(e.g., Christian et al., 2022; Zhang et al., 2020; Basara et al., 2019)~~(e.g., Christian et al., 2022; Zhang et al., 2020; Basara et al., 20
. In contrast, Chen et al. (2021) used an earth system model to gauge plant behavior during flash drought while Hosseini et al. (2022) used models with different phenological forcing to investigate impacts on the water and carbon cycles during drought. Remotely sensed and eddy covariance data provide snapshots of the state of the system at point or preset spatial resolutions, and fixed temporal resolutions, while models can scale in space and time. Inherently simplified due to the complexity of systems, numerical models incorporate physical and biological processes and statistical techniques to make predictions based on current states and their uncertainties (Dietze, 2017). Data assimilation procedures and Bayesian inference allow modelers to incorporate observations while also identifying sources of uncertainty in both processes and scale ~~(Dietze et al., 2013; Dietze, 2017)~~ (Dietze, 2017; Dietze et al., 2013).

Capturing phenology has implications for photosynthetic activity ~~(Lowman and Barros, 2018; Stöckli et al., 2008; Jolly et al., 2005)~~ (Lowman and Barros, 2018, 2016; Stöckli et al., 2008; Jolly et al., 2005) which will influence the water, carbon, and energy fluxes coupled between the land and atmosphere. We use two versions of the Duke Coupled Land-Surface Hydrology Model (DCHM) that incorporate physically parameterized routines for photosynthesis (Garcia-Quijano and Barros, 2005; Gebremichael and Barros, 2006) and predictive phenology, or plant life stage ~~(Lowman and Barros, 2016, 2018)~~ (Lowman and Barros, 2018, 2016) to more closely investigate if and how vegetation water use strategies accelerate or decelerate dry down before and during flash drought. Data assimilation techniques allow us to capture model uncertainty around processes controlling vegetation activity, and in particular, assimilating vegetation phenology can improve the detection of drought (Mocko et al., 2021). We investigate whether plants exhibit anisohydric tendencies thereby exacerbating the dry down, or whether they regulate their water intake to preserve soil moisture to mitigate the effects of flash drought. In turn, we also investigate if plant behavior can be altered during periods of water stress by predicting phenology model parameters from hydrologic model outputs in dry and wet periods. We hypothesize that simulated transpiration and carbon uptake rates will taper during flash drought due to limited soil water availability and increased atmospheric demand and that the phenological changes are directly related to changes in transpiration rates and GPP (Figure ~~1~~1). Our specific hypotheses are:

H1 ~~Evaporation initially increases before completely shutting down due to lack of precipitation and increased atmospheric demand for water. Water will also evaporate shortly after precipitation events leaving little to no chance of infiltration~~ During flash drought, there is an increase in days between precipitation events leading to larger reductions in total precipitation and infiltration as compared to non-flash drought events.

H2 ~~Infiltration and root-uptake slow~~ Lower total infiltration and higher atmospheric demand for water observed during flash drought ~~causing declines in~~ reduces soil water available for root water uptake. This decreases stomatal conductance, subsequently leading to reduced rates of transpiration~~and carbon uptake~~, carbon uptake, and water use efficiency as compared to non-flash drought within a subseasonal time frame.

H3 In response to ~~decreases in water availability~~ decreased water availability during flash drought, vegetation phenological states will ~~diminish~~ be diminished as compared to non-flash drought years exacerbating the reduction ~~in plant-atmosphere interactions~~of transpiration and carbon uptake.

Here we use phenological responses ~~, (i.e., FPAR,~~ of fraction of photosynthetically active radiation (FPAR) and leaf area index (LAI) to examine how flash droughts affect vegetation state and ultimately impact the surface fluxes governing the movement of water and carbon between the land and atmosphere. We use the well-studied flash drought of 2012 to compare vegetation growth state and water use strategies during flash drought and non-drought periods to better understand how plants modulate water and interact with the atmosphere when under stress. We compare our model results with eddy covariance and remotely sensed values of vegetation state and atmospheric interactions. Discrepancies between observations and models with predictive versus forced phenology illuminate physical processes dictating plant water use strategies ~~, for example,~~ (e.g., suppressing transpiration by closing stomata and limiting carbon intake). This study extends previous research on the water

and carbon movement between plants and the atmosphere during flash drought by simulating the propagation of uncertainty after implementing a predictive phenology routine to understand how variability in the representation of vegetation state within a modeling framework impacts land-atmosphere exchanges during extreme drought events.

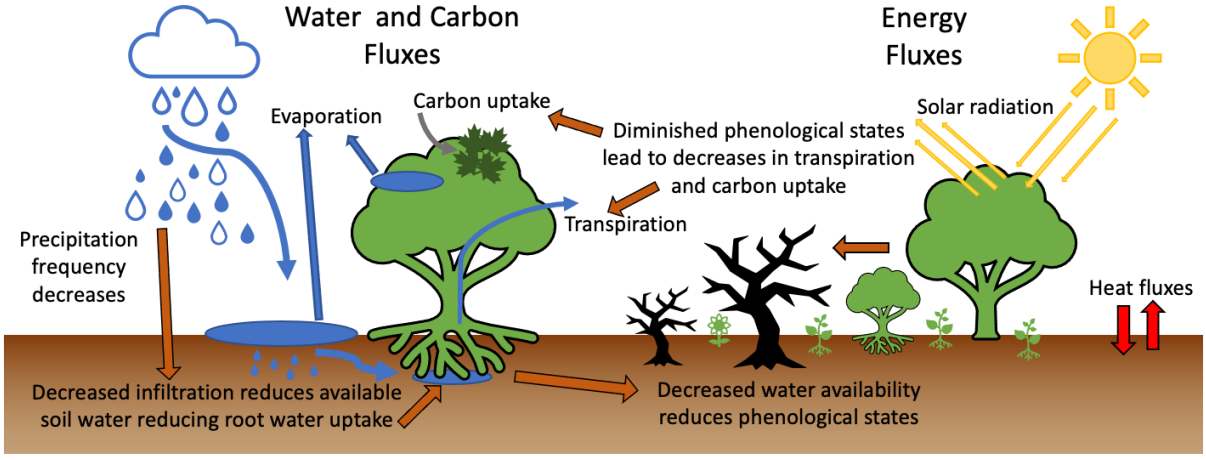

Figure 1. Schematic of water, carbon, and energy fluxes with hypotheses about ecological ~~responses~~ response to flash drought indicated with orange arrows. ~~Evaporation initially increases before completely shutting down due to lack~~ Decreased frequency of precipitation ~~and increased atmospheric demand for water. Water will also evaporate shortly after precipitation~~ events ~~leaving little~~ leads to ~~no chance of~~ decreased infiltration ~~. Infiltration~~ and ~~root-uptake slow~~ less water available for plant use during flash drought ~~causing declines in rates of transpiration and carbon uptake. In response~~ as compared to ~~decreases in~~ non-flash drought periods. During flash drought, the cascading effects of decreased water availability, ~~vegetation~~ exacerbated by the reduced phenological states ~~will diminish exacerbating the reduction~~ and stomatal conductance, include rapid reductions in ~~plant-atmosphere interactions~~transpiration and atmospheric carbon uptake to levels below other drought periods.

2 Methods and Data

2.1 Overview of Modeling Approach

Remotely sensed or ground observations of land and atmospheric responses to flash drought are useful in identifying changes in plant phenology, soil moisture, and evaporation rates, ~~etc.~~among others, but observations alone are unable to fully explain the mechanisms driving ~~the~~ ecological responses and water use ~~strategy adaptations~~strategies. Physically-based models can help fill the gaps in understanding what drives these changes by identifying key processes in the land-atmosphere interactions. For example, decreases in ground-based or satellite-derived GPP do not illuminate what processes caused the change, whereas a process based model might be able to signal that changes in root water uptake lead to decreased transpiration rates, which ultimately lead to decreased photosynthesis and carbon assimilation.

Within physical models, changes in ~~state~~ land-surface variables (e.g., soil moisture, root uptake, evaporation rates, etc.) are dependent upon ~~forced meteorological conditions~~meteorological conditions, either forced or dynamic (Sellers et al., 1997). Water use strategies are dictated by vegetation phenological states (Hu et al., 2008) and stomatal regulation (Novick et al., 2016) and strongly influence GPP and ET (Beer et al., 2009). Therefore, physical, process-based models are able to adapt to changing meteorological conditions and capture mechanistic changes in vegetation-atmosphere interactions. Our goal is to identify vegetation responses that occur as a result of flash drought and associate those changes with the physical ~~parameterizations used~~ processes represented in a land-surface hydrology model.

~~In order to~~ To identify physical mechanisms driving plant responses to flash drought intensification, we use two configurations of the physically based Duke Coupled surface-subsurface Hydrology Model ~~with dynamic vegetation~~ (DCHM) with dynamic Vegetation (DCHM-V) ~~. We provide the~~ and Predictive Vegetation (DCHM-PV). The DCHM-V ~~with plant life stage updates from Moderate Resolution Imaging Spectroradiometer (MODIS)fraction photosynthetically active radiation (FPAR) and LAI products in order to establish baseline outputs of~~ provides baseline estimates soil moisture (SM), root uptake (RU), ET, and GPP ~~from the DCHM-V. We then implement an ensemble Kalman filter (EnKF) data assimilation procedure following Lowman and Barros (2018) to establish ensembles of parameters to use in a dynamic canopy biophysical properties (DCBP) model within the DCHM-V yielding the DCHM with prognostic vegetation (~~using forced phenology from the from Moderate Resolution Imaging Spectroradiometer (MODIS) fraction photosynthetically active radiation (FPAR) and LAI products. Instead of using forced phenology, the DCHM-PV ~~). The~~ uses a prognostic vegetation (i.e. phenological) model ~~uses seasonal parameters~~ to predict the vegetation states of FPAR and LAI using parameters that correspond to seasonality (e.g., temperature and photoperiod)~~as well as meteorological parameters~~ , water availability (e.g., soil and ~~atmospheric water availability)to predict vegetation state and functionality (e.g., Lowman and Barros, 2018; Kim et al., 2015; Caldararu et al., 2014; Stöckli et al., 2008; Moradkha . In addition to recomputing the same outputs of interest from the DCHM-V, we run~~ vapor pressure deficit), and local vegetation characteristics (Lowman and Barros, 2018; Kim et al., 2015; Caldararu et al., 2014; Stöckli et al., 2008; Moradkhani et al., 2005) . An ensemble Kalman filter (EnKF) data assimilation procedure following Lowman and Barros (2018) is used to estimate ensembles of parameters for use in the predictive phenology model. Monte Carlo simulations of the DCHM-PV with the ~~ensemble~~ ensembles of predictive phenology parameters from the ~~EnKF in order to predict FPAR and LAI from the DCBP rather than forcing phenology with MODIS~~data assimilation step are used to explore the propagation of error and uncertainty. We validate model simulations against ground observations, remotely sensing data, ~~remotely sensed,~~ and other modeled ~~observations. The data sets~~ products. A summary of the data sets used to force or validate ~~all versions~~ both configurations of the DCHM ~~are summarized~~ is provided in Table 1~~and described in the following subsections~~.

2.2 Forcing Data Sets for DCHM

2.2.1 Meteorological

The 1-D ~~DCHM (-V~~ DCHM-V and -PV ~~)~~ spatial and temporal resolution is set to the ~~scale of the available~~ same scale as the highest quality precipitation forcing data available. For this study, ~~we use the~~ the model uses the native resolution of

Table 1. Summary of data products and uses

Dataset	Variable(s)	Spatial Resolution	Temporal Resolution	Use	Reference
~~StageIV~~ Stage-IV	Precipitation	4 km	hourly	Forcing	Baldwin and Mitchell (1998) Du (2011)
NLDAS-2 Forcing File A	Atmospheric	0.125°	hourly	Forcing/Data Assimilation	Mitchell et al. (2004)
NLDAS-2 Mosaic	Vegetation Fraction/ Albedo	0.125°	hourly	Forcing/Data Assimilation	Xia et al. (2012)
MODIS MOD15A2H	LAI/FPAR	500 m	8 day	Forcing/Data Assimilation	Myneni et al. (2015)
MODIS MOD12Q1	Land Cover	500 m	yearly	Forcing	Friedl and Sulla-Menashe (2015)
STATSGO	Soil Texture and Porosity	30 arcsec	fixed	forcing	Miller and White (1998)
AmeriFlux	GPP, latent heat, SM	point	30 min.	Validation	Baldocchi et al. (2001)
MODIS MOD17A2H	GPP	500 m	8 day	Validation	Running et al. (2015)
~~Noah-LSM~~ NLDAS-2	SM	0.125°	hourly	Validation	Xia et al. (2012)
SMERGE	SM	0.125°	hourly	Validation	Tobin et al. (2019)

the Stage-IV precipitation forcing from the National Oceanic and Atmospheric Administration (NOAA) National Centers for Environmental Prediction (NCEP) (Baldwin and Mitchell, 1998; Du, 2011). The Stage-IV dataset has 4 km spatial resolution and 1 h temporal resolution and ~~is available beginning from~~ with a record beginning in 2002. All forcing data sets were interpolated to the Stage-IV resolution for the entire continental US (CONUS) before study site specific data were extracted. Atmospheric forcing data (downward short and long wave radiation, air temperature, specific humidity, surface pressure, wind velocity) used in the DCHM are from the North America Land Data Assimilation System Phase 2 (NLDAS-2) Forcing File A. NLDAS-2 is a combination of observational and reanalysis data sets (Mitchell et al., 2004) intended for use in land surface models like the DCHM. The data are available at 0.125 degree spatial resolution and 1 h temporal resolution. They are spatially interpolated to the 4 km Stage-IV grid. No temporal interpolation was necessary.

2.2.2 Land Cover

The land surface albedo and fraction of vegetation cover ~~come from~~ used in the DCHM-V and -PV come from the NLDAS-2 Mosaic Land Surface Model L4 dataset at 0.125 degree spatial resolution and 1 h temporal resolution (Xia et al., 2012; Mitchell et al., 2004). NASA's ~~Moderate Resolution Imaging Spectroradiometer (MODIS)~~ MODIS Land Cover (MCD12Q1) remotely sensed satellite ~~data~~ land cover classification product is used to ~~inform the model of land cover classification~~determine land cover type within the DCHM. In particular, we use the University of Maryland classification scheme (Sulla-Menashe and Friedl, 2018). Within the model, ~~the classification~~ land cover type is updated yearly. The native spatial resolution of this data set is 500 m and ~~we~~ it is interpolated to the 4 km ~~size for model implementation using a most frequent~~ resolution using a nearest neighbor approach.

2.2.3 Soil Texture and Porosity

Soil texture and porosity data was acquired from Soil Information for Environmental Modeling and Ecosystem Management CONUS-Soil (Miller and White, 1998). The CONUS-Soil spatial resolution is 1 km with 11 layers. We upscaled the raw soil texture and porosity data to the 4-km Stage-IV grid ~~. For each pixel, we~~ using two different methods. By averaging over the top 100 cm, we avoid averaging layers interpolated as bedrock, and thus near zero porosity. We approximate soil porosity by averaging the top eight layers (100 cm) and we represent texture using the ~~most frequent texture . By averaging over the top 100 cm, we avoid averaging layers interpolated as bedrock, and thus near zero porosity~~texture mode across each grid cell and layer.

2.2.4 Vegetation

MODIS LAI and FPAR data were ~~downloaded~~ obtained for all of CONUS at the native 500-m spatial and ~~8 day~~ 8-day temporal resolution. Before ~~scaling to the DCHM grid and time scale~~linearly interpolating the data to the Stage-IV grid and timestep, the data for each pixel were smoothed using a Savitsky-Golay filter (Savitzky and Golay, 1964) algorithm following Chen et al. (2004) in order to preserve seasonality and reduce noise ~~associated with cloud cover~~ in the data from cloud

contamination and other atmospheric ~~effects~~ disturbances that may alter surface reflectance observations (Cihlar et al., 1997; Tanré et al., 1997). We use ~~the~~ m=6 scaling window and d=4 degree ~~of~~ for the interpolating polynomial as ~~in Chen et al. (2004) and Lowman and Barros (2016). After the smoothing filter is applied, the data is up-scaled from 500 m to 4 km resolution and linearly interpolated to a 1 h temporal resolution.~~ (Chen et al., 2004; Lowman and Barros, 2016).

2.3 ~~Validation~~ Data Sets Used for Model Comparison

We ~~use the~~ assess vegetation responses to the Kansas flash drought of 2012 ~~to compare model results~~ by comparing model results of land surface, sub-surface and atmospheric carbon and water fluxes (e.g., SM, GPP, ET) to multiple ground and remotely sensed observations. Modeled ~~soil moisture (SM) fluxes~~ SM fluxes from the DCHM-V and -PV are compared to SoilMERGE (SMERGE), NLDAS-2 NOAH model output, and AmeriFlux eddy covariance. SMERGE is a 0.125 degree root-zone (0-40 cm) SM product obtained from 'merging' NLDAS-2 outputs with European Space Agency Climate Change Initiative surface satellite data ~~which~~ that can predict vegetation health anomalies (Tobin et al., 2019). Because SMERGE only provides root-zone SM, we only compare it to the DCHM middle layer SM output. We also validate SM estimates against ~~simulated SM from~~ NLDAS-2 estimates Noah land-surface model (LSM) for all three ~~root zones~~ soil layers used in DCHM ~~. Noah-LSM is a physically based model forced with NLDAS-2 Forcing File A~~ (Xia et al., 2012)). When AmeriFlux SM data is available, we compare with modeled soil moisture from the top layer since most AmeriFlux SM sensors are in the top few centimeters of soil. ~~Computed outputs~~ DCHM-V and -PV estimates of GPP are compared to MODIS (MOD17A2H) GPP product and AmeriFlux eddy covariance outputs of GPP. We ~~computed ET from~~ also compare DCHM estimates of ET to AmeriFlux eddy covariance flux tower ~~values by dividing~~ estimates by dividing observed latent heat flux by the latent heat of vaporization of water ~~and use the results to validate model outputs of ET~~($\lambda_w = 2.5$ MJ kg^{-1}, Dingman, 2015)).

2.4 ~~Model Site Locations~~Description of Study Sites

This study ~~employs eddy covariance data from~~ focuses on three AmeriFlux sites in Kansas (US-KFS, US-KLS, US-Kon, Figure 2 and Table 2)~~. Each site was~~ , chosen because of the availability of GPP and latent heat (converted to ET) data during the flash drought year of 2012 and at least one wet year after 2012. When available, we used gap-filled FLUXNET FULLSET data for US-KFS and US-Kon (Pastorello et al., 2020). All three sites are classified as grasslands according to the International Geosphere-Biosphere Programme (IGBP) land cover and all three sites have Cfa (humid, subtropical) Köppen Climate Classifications (Brunsell, 2020a, 2021, 2020b). US-KFS is located within a grassland-deciduous forest boundary area and receives 1014 mm of precipitation annually (Brunsell, 2020a). US-KLS is a perennial agricultural study sties receiving 812 mm of rainfall each year (Brunsell, 2021). US-Kon is part of the Konza Prairie Long-term Ecological Research (LTER), recieves 867 mm of precipitation, and is burned annually. Static characteristics of PFT, soil texture and porosity, and geographic information for the study sites are shown in Table 2. According to the MODIS land cover classification product (MCD12Q1), each site had a unique vegetation cover type (savanna, grassland, cropland, Table 2). The PFT is a result of interpolating MODIS MCD12Q1 Land Cover Type 2 to the 4-km grid and does not necessarily align with the land cover from AmeriFlux. The soil texture and porosity are interpolated CONUS-Soil (Miller and White, 1998) values.

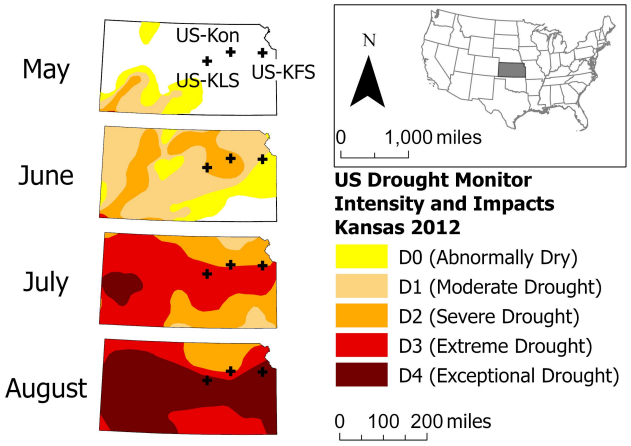

Figure 2. ~~Maps~~ Evolution of the ~~U.S.~~ 2012 flash drought from May - Aug in the US Drought Monitor with the three AmeriFlux tower study sites (US-KFS, US-KLS, and US-Kon)~~showing the evolution of the U.S. flash drought of 2012.~~

Table 2. AmeriFlux study sites contained within ~~StageIV~~ Stage-IV pixels.

Site	Latitude	Longitude	PFT	Soil Texture	Soil Porosity	~~Reference~~ Mean Precipitation [mm yr^{-1}]	~~AmeriFlux mean StageIV 2012 StageIV 2019~~Reference
US-KFS	39.0561	-95.1907	SAV	silty clay loam	0.4225	~~Brunsell (2020a)~~ 1012	~~597 1373~~ Brunsell (2020a)
US-KLS	38.7754	-97.5684	CRO	silt loam	0.4812	~~Brunsell (2021)~~ 812	~~558 1425~~Brunsell (2021)
US-Kon	39.0824	-96.5603	GRA	silty clay loam	0.4588	~~Brunsell (2020b)~~ 867	~~490 1346~~Brunsell (2020b)

Plant functional type (PFT), soil texture, and soil porosity determined after interpolation to the Stage-IV grid. Abbreviations: SAV = Savanna, CRO = Cropland, GRA = grassland. Precipitation totals listed as AmeriFlux annual mean.

2.5 ~~Model~~ Description of Modeling Work

2.5.1 Land-Surface Hydrology Model

We employ two 1-D versions of the DCHM coupled land-surface hydrology model that accounts for ~~mass (water) and energy transfers~~ water and energy exchanges between three soil layers, the surface, and the atmosphere ~~(Devonec and Barros, 2002)) applied on a~~ (Lowman and Barros, 2018, 2016; Tao and Barros, 2014, 2013; Yildiz et al., 2009; Yildiz and Barros, 2007, 2005; Gebremich . A 4-km ~~grid. The 4-km~~ grid ~~was chosen since it is the~~ resolution and 1-hr timestep were chosen to run the model to match the native spatial resolution of the Stage-IV precipitation data, as precipitation is the main source of uncertainty when modeling drought (Trenberth et al., 2014). ~~The soil depths we use best match the USDA Kansas soil profile (Soil Survey Staff). We maintain 8 cm~~ We use 80 mm for the top ~~soil layer for~~ layer soil depth to ensure model stability, but ~~use 35 in. (approx 89 cm) for root zone depth and 72 in (89-183 cm) for the impermeable layer. This yields the~~ middle and deep layers were selected to best match the USDA Kansas soil profile (Soil Survey Staff). The this yields three soil layers: top (~~0-8 cm~~0-80 mm), middle (~~8-89 cm) ,~~ 80-890 mm) and bottom (~~89-183 cm). Each PFT has its own root distribution function dictating root water uptake through the three layers (Lowman and Barros, 2016; Zeng, 2001; Lai and Katul, 2000; Clausnitzer and Hopmans, 1994).~~ 890-1830 mm). Rooting depth and density, which are used to determine the total root water uptake in the DCHM, are calculated using empirical exponential root distribution functions that vary by PFT. (Lowman and Barros, 2016; Zeng, 2001; Lai and Katul, 2000; Jackson et al., 1996 . Soil layer and rooting depths align with the different combinations of soil textures and PFTs found in Thornthwaite and Mather (1957) .

The DCHM water balance includes subroutines for evaporation from the different ~~land surfaces (~~components of the land surface (i.e., bare soil, and vegetation), ponding and groundwater runoff, snow ~~hydrology~~accumulation and melt, and root water uptake while energy balance routines solve for net ~~radiative fluxes, sensible and latent heat transfers~~radiation, and sensible, latent heat, and ground heat fluxes (Lowman and Barros, 2018, 2016; Tao and Barros, 2014, 2013; Yildiz and Barros, 2007, 2005; Garcia-Quijano and Barros, 2005; Devonec and Barros, 2002; Barros, 1995). The water and energy balances ~~are linked through parameterized routines for photosynthesisfollowing~~ both influence photosynthesis, which is simulated using the Farquhar model (Lowman and Barros, 2016; Garcia-Quijano and Barros, 2005; Farquhar and Caemmerer, 1982; Farquhar et al., 1980).

~~The main~~

2.5.2 Predictive Phenology

The key difference between the ~~DCHM-V and DCHM-PV is that~~ two versions of the DCHM used for this study is that within the DCHM-V ~~has vegetative phenology forced with updates from~~ vegetative phenology is forced using the MODIS MOD15A2H FPAR and LAI products~~and~~ , while the DCHM-PV ~~implements a subroutine for predicting phenology (DCBP). The DCHM-PV is run using an ensemble of parameters (Table 4) generated using an EnKF from outputs from the DCHM-V following Lowman and Barros (2018) with a separate simulation for each ensemble member.~~

predicts phenology for the next day based on the current day conditions. Establishing differences in the outputs from DCHM-V and -PV ~~illuminate~~ illuminates changes in plant ~~behavior~~growth strategies. MODIS is a passive sensor and ~~observes~~ uses only the red (648 nm) and near-infrared (NIR, 858 nm) spectral bands to estimate values of LAI (Myneni et al., 2015). ~~The DCBP~~Within the DCHM-PV, the dynamic canopy biophysical properties (DCBP) model predicts plant life stage based on climatological properties of water availability, air temperature, and evaporative demand (Lowman and Barros, 2018). ~~We updated~~ FPAR and LAI ~~instead of forcing them with~~ are dynamically estimated instead of forced using MODIS observations to evaluate impacts on estimates of ET and GPP (Lowman and Barros, 2018; Kim et al., 2015; Caldararu et al., 2014). ~~Predicting phenological state variables also provides updates on daily time scales rather than through interpolation from the 8 day measurements of MODIS. We compare model outputs for a wet year and a dry year to illuminate the vegetation responses to flash drought.~~

~~The data assimilation procedure within the~~

The DCBP is the predictive phenology model that determines future plant growth based on differences between current and potential phenological states. The growing season index (GSI) determines potential phenological state based on current climate conditions (Jolly et al., 2005; Stöckli et al., 2008). Specifically it is a function of temperature, photoperiod, soil water potential, and VPD (Lowman et al., 2023; Lowman and Barros, 2018). Lowman and Barros (2018) adapted the framework to incorporate soil water parameters that affect predictions of plant growth stage. The DCBP is implemented within the DCHM-PV to estimate phenologic state with the the land-surface hydrology model. However, in order to implement the predictive phenology model ~~jointly estimates the current phenological state (FPAR, LAI) along with eleven parameters (Table 4) required to calculate the next phenological state (Lowman and Barros, 2018)~~within the DCHM-PV, we first must estimate parameters that determine plant growth rates and sensitivity to meteorological and soil conditions.

A Bayesian hierarchical approach is used to estimate the parameters for the DCBP. Specifically, a dual state-parameter ensemble Kalman filter (EnKF) is used to jointly estimate the phenologic states of FPAR and LAI and the eleven other parameters within the DCBP (Table 4 Lowman et al., 2023; Lowman and Barros, 2018). This method was ~~first introduced~~ described by Moradkhani et al. (2005) as a way of simultaneously predicting states and parameters in ~~hydrology~~ hydrologic models, and ~~it was~~ later implemented by Stöckli et al. (2008) ~~specifically for assimilating remotely sensed data in phenological models. Lowman and Barros (2018)) added additional soil water parameters to the data assimilation system to improve phenological state predictions. Using outputs from the DCHM-V and updating phenological states from MODIS FPAR and LAI in the DCBP, we generate ensembles of phenology parameters representing different precipitation regimes (above average, below average, and mixed conditions). We run Monte-Carlo simulations of the DCHM-PV with~~ to assimilate remotely sensed observations of LAI and FPAR into a predictive phenology model.

The parameter estimation procedure first consists of creating a prior distribution by sampling each state and parameter from a Gaussian distribution. This generates N=2000 ~~ensembles of the DCBP model parameters. Ensembles were generated using the final mean and standard deviations of the parameters from each inference period~~ensemble members. Phenological states and input parameters are updated at every timestep for the duration of the data assimilation period using the EnKF. We assimilate

MODIS LAI and FPAR every 8 days (the native MODIS temporal resolution) to reduce error and ensure that phenological state predictions do not stray too far from observations (Lowman et al., 2023; Lowman and Barros, 2018).

2.6 Model Simulations

We ~~begin by running~~ run both the DCHM-V and -PV from 2002-2019 ~~(~~at a 1 h timestep and 4 km spatial resolution, spinning-up 2002 three times to allow for model stabilization ~~, Lowman and Barros (2016, 2018)) for all three sites. Using the~~ (Lowman and Barros, 2016, 2018). The DCHM-V ~~outputs from 2003-2005 along with the DCBP, we generate ensembles (N=2000) of~~ simulations provide a baseline for changes in water, energy, and carbon exchange using forced phenology from MODIS while the DCHM-PV simulations implements a predictive phenology scheme that allows us to investigate how dynamic changes in plant growth strategy impact the aforementioned fluxes.

In order to run the DCHM-PV, we first generate phenology model parameters for ~~three meteorological scenarios for each site (Table 3)yielding a total of twelve simulations (one DCHM-V and three~~ the predictive phenology routine. Specifically, we use 2003 (DRY), 2005 (WET), and 2003-2005 (3YR), as the data assimilation periods in the DCBP to generate parameters that correspond to wet, dry, or average precipitation regimes (Table 3). We use three different assimilation periods in order to capture the sensitivity of phenology model parameters to the meteorological conditions. It has been shown under varied climatological conditions plants can be highly adaptable, transitioning from isohydric to anisohydric in a single season (Guo et al., 2020) . Lowman and Barros (2018) showed that assimilation period can determine the water stress adaptations for the modeled vegetation state. Broadly speaking vegetation model parameters predicted using data from years with minimal rainfall represent plants that are accustomed to drier conditions and therefore exhibit more regulation in their water use tendencies (Lowman and Barros, 2018 .

To incorporate uncertainty from the phenology parameter estimation step into the DCHM-PV ~~for each of the three sites). Each of the nine phenology ensembles consist of~~ simulation, we run the model as Monte Carlo simulations with N=2000 ~~sets of parameters so each of the nine DCHM-PV simulations consist of 2000 Monte Carlo experiments. We chose the~~ members. Each ensemble member is sampled from a Gaussian distribution using the final mean and standard deviation of the parameter estimates from each of the assimilations period. In our results, we focus on analyzing model output from 2006-2019 to omit from our analysis the 2003-2005 ~~period because it allows us to establish ensembles of phenology parameters associated with dry, wet, and mixed condition periods. The parameters used in~~ period used in the ~~DCHM-PV simulations are from the one-year periods of 2003 (DRY) and 2005 (WET), and from the three-year period2003-2005 (3YR). The chosen assimilation period is prior to the case studies described in Section 2.7, thereby preventing the use of over fit model parameters when investigating the behavior of the DCHM-PV results.~~ data assimilation step.

~~The three sets of phenology parameters for each site allows us to investigate vegetation-atmosphere feedbacks through different causal lenses by generating phenology model parameters in several climate scenarios. Furthermore, this type of simulation permits us to investigate if meteorological conditions alter plant behavior (become more isohydric or anisohydric), rather than investigating if vegetation behavior affects the development of flash drought . Broadly speaking, vegetation model parameters trained on dry conditions will represent isohydric vegetation and vice versa for vegetation trained on wet conditions~~

Table 3. Summary of precipitation conditions during assimilation periods.

Year(s)	~~Abbreviations~~ Assimilation Period*	Stage-IV Annual Precipitation Accumulation [mm]		
		US-KFS	US-KLS	US-Kon
2003-2005	3YR	1066	770	847
2003	DRY	804	756	670
2005	WET	1242	806	956

*The data assimilation periods: 3YR represents a period with average annual precipitation, WET and DRY are periods with above and below average annual precipitation, respectively.

~~because vegetation adapted to minimal rainfall is more conservative in its water use (Lowman and Barros, 2018; Sade et al., 2012) . By using the three different data assimilation periods, we are able to capture the sensitivity of phenology model parameters to the meteorological conditions.~~

2.7 ~~Study Period and Outputs~~

~~We run the DCHM-V and DCHM-PV for 2002-2019. We are able to generate phenology parameters using a subset of this time frame (2003-2005), allowing us to investigate land-atmosphere interactions outside of the parameter inference period. We highlight~~

2.7 Analysis of Model Outputs

In this manuscript, we are interested in exploring whether land-surface, subsurface, and atmospheric interactions are distinct in flash drought compared to drought and non-drought periods. We focus on results from the three AmeriFlux sites for 2012 (flash drought), 2018 (drought), and 2019 (~~above average precipitation~~non-drought) to draw conclusions about plant ~~responses~~ response during flash drought ~~. We are also able to compute yearly totals of GPP and ET~~ and how they differ from drought and non-drought years. We also evaluate model outputs from 2006-2019 to assess ~~interannual variability of outputs from~~ the differences between the DCHM-V and DCHM-PV ~~.~~ model configurations during drought and non-drought years compared to a flash drought year. During this time period, we identified drought years as 2006, 2011, 2013, 2014, 2018 and non-drought years as 2007-2010, 2015-2017, 2019 using the USDM for the Central and East Central Kansas climate regions (Svoboda et al., 2002) . Drought years were determined by whether parts of the region reached the D2 "Severe Drought" classification or higher. When computing drought and non-drought averages, we use the years listed here. In many time series results, we display the water year (April-October) rather than the entire year because plants are largely dormant outside of the water year in a temperate region (Dai et al., 2016; Wang et al., 2003; Towne and Owensby, 1984). Transpiration is calculated from total root water uptake through the three soil layers and total evaporation is computed from summing evaporation from ground and

canopy surfaces allowing us to partition ET into evaporation and transpiration (Lowman and Barros, 2018; Lai and Katul, 2000). Water use efficiency is represented as the ratio of GPP and ET (WUE = GPP/ET, Beer et al. (2009)). We highlight differences between the DCHM-V and DCHM-PV model simulations and compare outputs to remotely sensed and in situ observations where available.

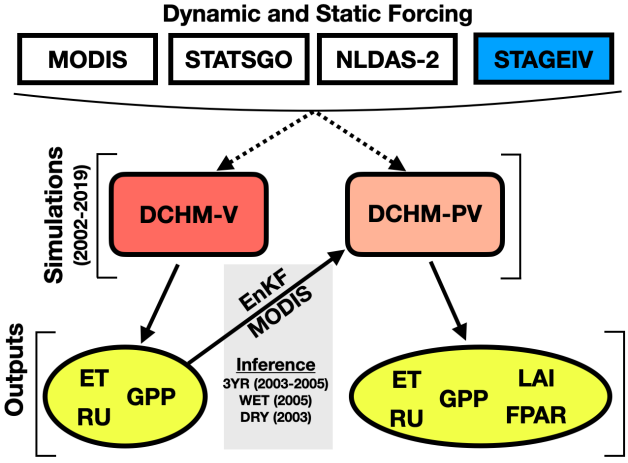

Figure 3. Schematic of modeling workflow. Spatial and temporal resolutions of all forcing data are interpolated to match the resolution of the Stage IV precipitation (4 km and 1 h) ~~and dictate~~ which is the resolution used for the DCHM ~~scales~~in this study. Land cover, soil properties, and atmospheric forcing inputs come from MODIS, STATSGO, and NLDAS-2, respectively. Simulations are run from 2002-2019. Three ensembles of parameters for the predictive phenology routine in the DCHM-PV are ~~determined~~ generated using an ensemble Kalman filter (EnKF) with simulated soil water potential and vapor pressure deficit from the DCHM-V~~outputs~~, MODIS MOD15A2H FPAR/LAI, and concurrent meteorological conditions from 2003 (DRY), 2005 (WET), and 2003-2005 (3YR). DCHM-V outputs of interest include evapotranspiration (ET), Root water uptake (RU), and gross primary productivity (GPP). Additional DCHM-PV outputs include predicted fraction of photosynthetically active radiation (FPAR) and leaf area index (LAI).

3 Results

~~We first present phenology model parameters as estimated from the data assimilation procedure. Then, we show DCHM-V (forced phenology) and DCHM-PV (predictive phenology) results.~~

3.1 Phenology

3.1.1 ~~Phenology Model Parameters~~Growth Rate Parameter

The growth rate parameter, γ, dictates how much phenological state (i.e. FPAR and LAI) can change in a given time step (Lowman and Barros, 2018; Stöckli et al., 2008). ~~Lower uncertainty in the growth rate parameter~~ The uncertainty in γ shows

the variability in vegetation responses to changing phenological states. Lower uncertainty in γ establishes the 3YR assimilation period, with a mixture of wet and dry years, as the preferred choice for running the DCHM-PV (Figure 4)~~and~~ . This finding is in agreement with Lowman and Barros (2018) who found that using assimilation periods with both wet and dry conditions has the effect of capturing adaptive plant water use strategies. This lower uncertainty propagates through the DCBP in the DCHM-PV, ~~reducing~~ leading to lower uncertainty in the predictions of FPAR and LAI (Figures 5 and 6). The values of γ vary by site ~~, and therefore plant function type(PFT~~due to a combination of local climate and vegetation type. US-KFS, modeled as a savanna, has the lowest mean and standard deviation of γ (Table 4). The smaller magnitudes of the growth parameters indicates that vegetation is less likely to make abrupt changes and exhibit more resilience when faced with extreme dry down. Other parameter estimation outputs used to generate ensembles from the 3YR assimilation period can be found in Table 4.

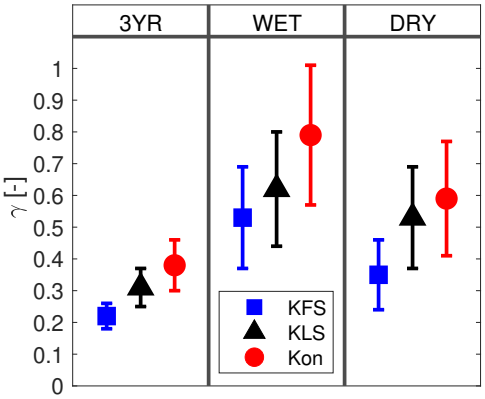

Figure 4. ~~Growth rate parameters,γ with~~ Ensemble means and one standard deviation of the growth rate parameter, γ, for each site ~~for~~ and all three data assimilation periods: 3YR (2003-2005), WET (2005), DRY (2003).

3.1.2 FPAR

Overall, DCHM-PV simulated FPAR tends to follow the same patterns as MODIS throughout the growing season, irrespective of choice of parameters. Results indicate slower senescence and reduced variance using the 3YR assimilation parameters as compared to the WET and DRY parameters during late June and early July 2012 across all three sites ~~. A decrease in FPAR can be seen in late June 2012 across all simulations~~ (Figure 5 a,d,g). This aligns with the known period of flash drought that occurred across Kansas (Lisonbee et al., 2021). ~~For each site, the simulated FPAR from the 3YR assimilation phenology parameters shows a less dramatic response in the decrease in FPAR when compared to the DCHM-PV simulations using the WET and DRY parameters.~~ The predicted values of FPAR at US-KFS and US-KLS are slightly higher than the MODIS values during the 2012 growing season. The predicted values of FPAR match well against MODIS for the US-Kon site, especially during the decline in late June through July. During the flash drought period, there is a notable decrease in variance, or uncertainty, across the Monte Carlo simulations.

Table 4. ~~Phenology~~ Ensemble mean and one standard deviation of predictive phenology model parameters from the 3YR assimilation period~~.~~

			Mean parameter estimates ± one standard deviation		
Parameter	Description	Units	US-KFS	US-KLS	US-Kon
$T_{min_{min}}$	Minimum value of daily minimum temperature	°C	-5.5 ± 3.1	0.1 ± 2.4	-2.3 ± 3.2
$T_{min_{max}}$	Maximum value of daily minimum temperature	°C	14.0 ± 1.8	16.5 ± 1.8	15.8 ± 2.0
Pht_{min}	Minimum daily exposure to sunlight	h	10.0 ± 0.4	9.8 ± 0.6	10.7 ± 0.6
Pht_{max}	Maximum daily exposure to sunlight	h	14.3 ± 0.3	14.2 ± 0.4	14.3 ± 0.4
$VPD_{avg_{min}}$	Minimum daily average vapor pressure deficit	mb	17.1 ± 1.3	16.6 ± 1.4	16.9 ± 1.4
$VPD_{avg_{max}}$	Maximum daily average vapor pressure deficit	mb	58.7 ± 2.3	55.8 ± 2.2	55.6 ± 2.3
$\psi_{soil,avg_{min}}$	Minimum daily average soil water potential	J kg^{-1}	-42.1 ± 5.6	-37.2 ± 5.8	16.9 ± 5.5
$\psi_{soil,avg_{max}}$	Maximum daily average soil water potential	J kg^{-1}	-7.4 ± 1.3	-7.0 ± 1.4	-6.9 ± 1.4
$FPAR_{min}$	Minimum fraction of photosynthetically active radiation	-	0.31 ± 0.01	0.35 ± 0.01	0.31 ± 0.01
LAI_{max}	Maximum leaf area index	m^2 m^{-2}	6.36 ± 0.15	6.51 ± 0.17	6.65 ± 0.18
γ	growth rate	day^{-1}	0.22 ± 0.04	0.31 ± 0.06	0.38 ± 0.08

For an in depth description of the predictive phenology routine within dynamic canopy biophysical properties (DCBP) model see Lowman et al. (2023) and Lowman and Barros (2018).

~~Time series of fraction of photosynthetically active radiation (FPAR) predicted from DCHM-PV for the flash drought year (2012) and an above average precipitation year (2019) for the three AmeriFlux study sites (US-KFS, US-KLS, US-Kon). The different colors represent the usage of parameters from the different data assimilation periods (yellow - 3YR (2003-2005), blue - WET (2005), red - DRY (2003), with corresponding shaded regions representing one standard deviation of model outputs from the 2000 ensemble simulations. 8 day MODIS MOD15A2H FPAR is indicated with black markers. The gray shaded region highlights the June to July decrease in FPAR during the 2012 flash drought.~~ For US-KFS across the three simulations, the simulation using the WET parameters achieves a higher FPAR during the flash drought and holds its peak throughout the month of May, with declines beginning in June and bottoming in early July before rising again in the latter part of the growing season. ~~The decrease in FPAR for the WET parameters is~~ FPAR decreases from 0.77 to 0.41 for the WET parameters while reductions from the time of peak FPAR to early July in the simulations using DRY and 3YR parameters are from 0.73 to 0.47 and 0.76 to 0.53, respectively.

The decreases in FPAR observed from mid-May to mid-July in 2012 are more pronounced than during the growing season of the drought year 2018 when fluctuations in FPAR were smaller. Results from an above average precipitation year (2019) show a steady increase, a longer peak growing season, and a decrease in line with fall senescence across all simulations~~, though~~. However, using WET and DRY parameters at US-KLS ~~both lead to a phenological response in~~ lead to ~0.2 reduction in FPAR in July 2019, opposed to ~0.1 reduction from the 3YR parameters. The larger reduction is likely due to the below average July precipitation ~~. Overall, the simulations tend to follow the same patterns as MODIS throughout the growing season, irrespective~~

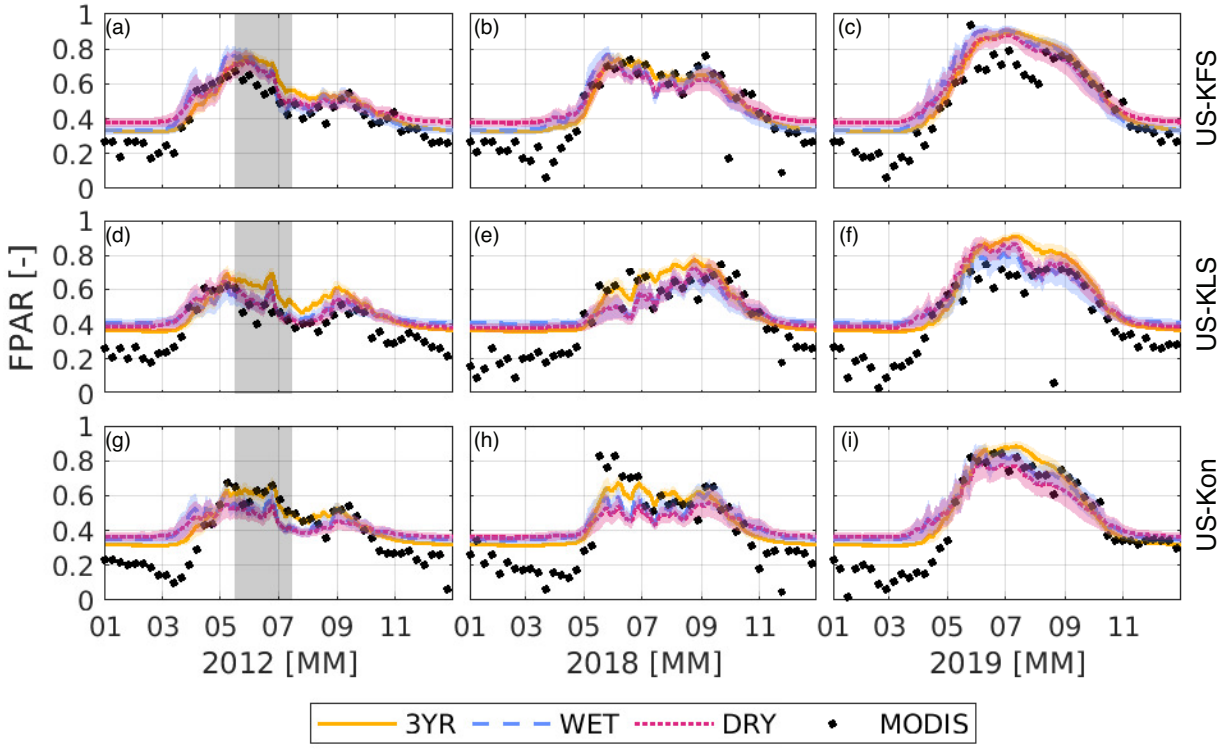

Figure 5. Fraction of photosynthetically active radiation (FPAR) predicted from the DCHM-PV for the flash drought year (2012), a drought year (2018), and a non-drought year (2019). Colors indicate the different data assimilation periods: 3YR (yellow), WET (blue), DRY (red). Corresponding shaded regions represent one standard deviation of model outputs from the 2000 ensemble members. The 8-day MODIS MOD15A2H LAI is shown as black dots. The gray shaded regions in the left most panels highlights the 2012 flash drought period.

~~of choice of parameters~~and the larger WET and DRY values of γ leading to more rapid phenological changes. Similar to the 2012 results, 2019 simulations using phenology parameters from the 3YR assimilation period showed slower late-season declines in FPAR than ~~the~~ simulations using parameters ~~derived~~ from the WET or DRY assimilation periods. This ~~behavior~~ can be seen from the 3YR parameter simulations for US-KLS and US-Kon which show higher FPAR through July. ~~At these sites, the dip in July FPAR using the WET and DRY parameters is likely due to the susceptibility of abrupt changes in response to minimal July rainfall. At US-KFS, the three different simulations vary little from one another which could be due to the savanna representation at US-KFS and its resiliency to the minimal July precipitation during 2019. Despite the minimal July rainfall, phenological stages were generally resilient due to the abundance of soil water from early precipitation.~~

3.1.3 LAI

Predicted values of LAI are similar to MODIS LAI ~~, with relative differences between DCHM-PV and MODIS similar to the FPAR results~~ with small relative differences (Figure 6). During the flash drought year of 2012, a steep decline in modeled LAI

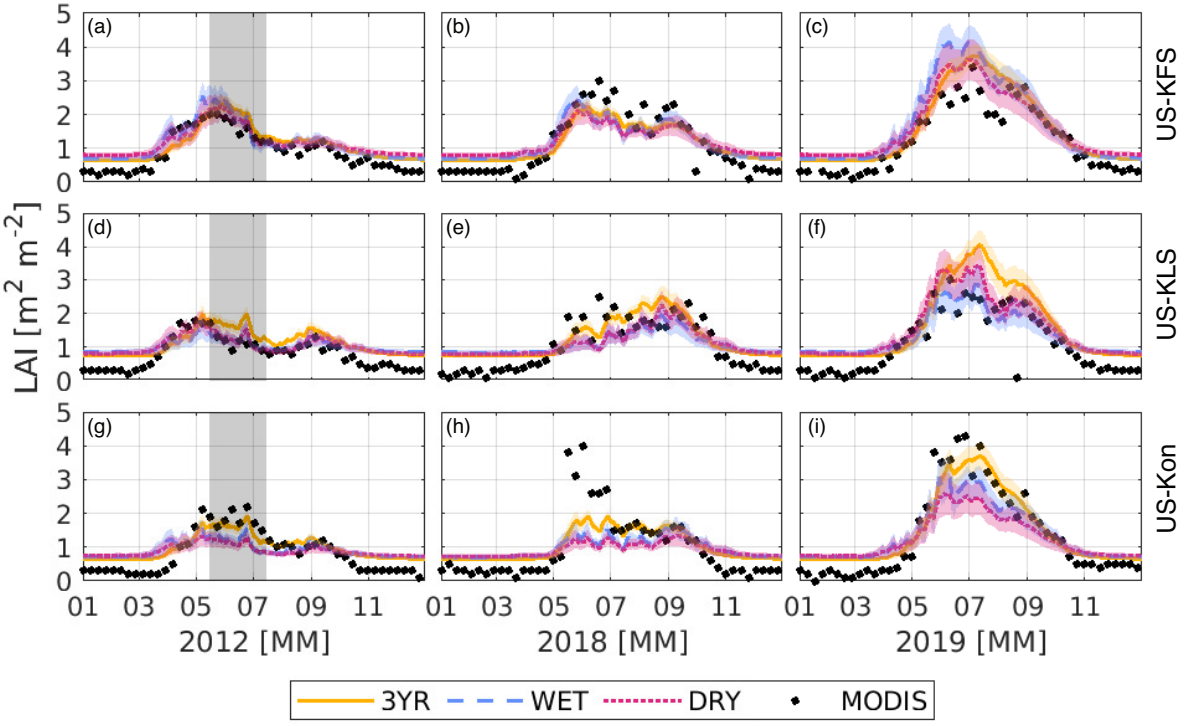

Figure 6. Leaf area index (LAI) predicted from DCHM-PV for the flash drought year (2012), a drought year (2018), and a non-drought year (2019). Colors indicate the different data assimilation periods (yellow - 3YR (2003-2005), blue - WET (2005), red - DRY (2003)), with corresponding shaded regions representing one standard deviation of model outputs from the 2000 ensemble simulations. The 8-day MODIS MOD15A2H LAI is shown in black markers. The gray shaded regions in the left most panels highlights the 2012 flash drought period.

can be seen in late June and early July across the three sites. ~~The LAI experienced declines of~~ LAI declines almost 1 m^2 m^{-2} in ~~just a few days.~~ a few weeks during summer 2012 compared to steadier values during the drought of 2018. Growing season LAI was ~0.5 m^2 m^{-2} lower in 2012 compared to 2018. DCHM-PV model outputs of LAI during 2019 match MODIS but are 1-2 m^2 m^{-2} higher during June, July, and early August at US-KFS and US-KLS, and slightly lower than MODIS at US-Kon. ~~Time series plots of leaf area index (LAI) predicted from DCHM-PV for the flash drought year (2012) and an above average precipitation year (2019) for the three AmeriFlux study sites (US-KFS, US-KLS, US-Kon). The different colors represent the usage of parameters from the different data assimilation periods (yellow - 3YR (2003-2005), blue - WET (2005), red - DRY (2003)), with corresponding shaded regions representing one standard deviation of model outputs from the 2000 ensemble simulations. 8 day MODIS MOD15A2H LAI is indicated with black markers. The gray shaded region highlights the June to July decrease in FPAR during the 2012 flash drought. Simulated LAI~~

Simulated LAI values vary slightly across the three sites. For US-KFS, simulations using the WET year parameters achieve higher values in LAI than the other two simulations (Figure 6 ~~a,b~~a-c). For US-KLS, and US-Kon, the growing season LAI has

the highest peaks in the simulations using the 3YR parameters (Figure 6 ~~c,d~~d-i). With more rainfall in May and June 2019, the simulations using the WET parameters ~~show~~ result in lower LAI than the simulations using the DRY parameters.

The most consistent similarities across the phenology results is that the simulations using the 3YR parameters generally show a slower decline in LAI in ~~both a flash drought year and a wet year~~ flash and non-flash drought years for all sites. ~~Another similarity across these figures is that~~ Additionally, the simulations using WET and DRY parameters ~~align with one another more than they match~~ are more similar to each other than to the simulations using 3YR parameters. This result is commensurate with the values of the means and variances of ~~the growth rate parameters~~ γ resulting from the different assimilation periods.

~~Differences in the growth rate parameter can also be seen in LAI outputs from the simulations of the DCHM-PV (6). During the 2012 flash drought, simulations~~ Simulations using the 3YR assimilation period ~~show LAI staying~~ result in LAI remaining high for a longer period of time ~~, and the decrease develops~~ with a decrease in response to flash drought developing slower than the other two simulations. This ~~feature~~ is also apparent ~~in the 2019 plots~~ for US-KLS and US-Kon ~~. In~~ in the 2019 ~~plots, simulations continue to show growth through June, with peaks occurring~~ 3YR simulations in which leaf growth continues through June and peaks in the middle of July, while ~~the LAI in plots of~~ in the WET and DRY simulations ~~seem to flatten their growth~~ new growth tends to slow from the beginning of June ~~to~~ through mid-July.

3.2 ~~Vegetation Responses~~

3.1.1 ~~GPP~~

Generally, the predictive phenology model compares favorably with the seasonal changes observed in MODIS FPAR and LAI (Figures 5 and 6) in both flash drought and non-flash drought periods. In the summer, at US-KFS and US-KLS during 2019, the model tends to predict FPAR and LAI values higher than MODIS. In 2019, at US-KFS, MODIS observed a steady decline in FPAR from 0.8 to 0.6 throughout July followed by an increase to 0.8 over an 8-day period at the beginning of August (Figure 5c). The DCHM-PV results do not show the same decline. Similarly, MODIS observes a drop in LAI (Figure 6c) before an abrupt increase while model estimates remain higher than MODIS. Yet, in June 2019 at US-Kon, the DCHM-PV estimates are lower than MODIS LAI.

~~Time series of yearly totals of GPP and ET for 2006-2019 at US-KFS, US-KLS, and US-Kon from DCHM-V, three DCHM-PV, AmeriFlux, and MODIS (GPP only). Yearly totals from the 2000 DCHM-PV Monte Carlo simulations are shown as ensemble means and one standard deviation indicated by error bars. Estimates of ET from AmeriFlux were generated by dividing measurements of latent heat by the coefficient of vaporization and were eliminated from the analysis if more than 20% of the yearly data was missing.~~ The bulk of the following results and analysis compares vegetation responses during flash drought and non-flash drought periods rather than an inter model comparison across the different assimilation strategies. Estimates from the WET and DRY simulations tend to be in agreement with results from the 3YR simulations. From this point forward, we only show results from the 3YR simulations.

3.2 Sub-surface Water

3.2.1 Infiltration

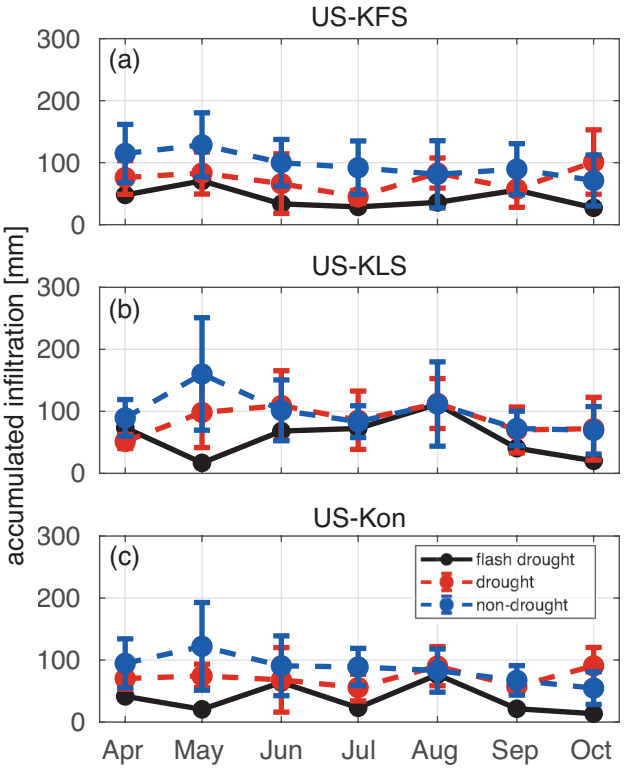

Figure 7. DCHM-PV 3YR ensemble means of monthly infiltration accumulations for drought (red dashed line) and non-drought (blue dashed line) years compared to 2012 (black solid line) for all three study sites. Monthly sums are computed from the ensemble means of the 2000 Monte Carlo simulations then averaged across drought or non-drought years. Error bars represent one standard deviation across drought and non-drought years.

~~Yearly totals (2006-2019) of GPP are shown in Figure ?? a-c for each site. The points used in the yearly time series represent the ensemble means from DCHM-PV and yearly totals from DCHM-V, MODIS, and AmeriFlux tower records. The DCHM-PV yearly totals of GPP at~~ During non-drought years, monthly infiltration accumulations are above or near 100 mm per month, on average, from April to July with the highest amounts in May (Figure 7). During drought years, infiltration between April-July is less than non-drought years. Furthermore, monthly accumulated infiltration is lower during the flash drought year compared to both drought and non-drought years, suggesting there is less water available for plant use during the growing season. At US-KFS from April-October of 2012, monthly infiltration is slightly below that observed during drought years. A large decline in May infiltration at US-KLS and US-Kon ~~are similar to totals estimated for the same sites in another study which updated LAI and vegetation cover dynamically using Noah-MP (Hosseini et al., 2022). Ameriflux tower yearly totals were discarded from~~

~~the analysis if more than 20% of the data were missing for the year. The error bars on the DCHM-PV plots show one standard deviation from the mean for the 2000 ensemble members. Carbon uptake during water stress years is about~~ led to infiltration accumulations that are 1-2 standard deviations below average drought conditions. All sites had infiltration rates below 100 mm for all months during 2012 with the exception of US-KLS in August 2012.

Low monthly infiltration amounts during the flash drought year are likely due to lower precipitation accumulations (Figure A4) coupled with an increase in the number of days between precipitation events (Figure 8) and an increase in atmospheric demand for water (Figure A). During drought and non-drought years, the average number of days between rainfall events within a month ranges from 1 ~~$kgCm^{-2}$ less than during years experiencing above average precipitation. The DCHM-V, which uses MODIS to update vegetation state indices (FPAR and LAI), compares well in magnitude to MODIS GPP yearly assimilation rates. In periods where there is no water stress (~~to 7 days, while the lower end for the flash drought year is higher at 2.5 days. Additionally, during drought and non-drought years, monthly infiltration exceeds 150 mm, but in 2012 remains at or below 75 mm for all sites aside from August 2012 at US-KLS where monthly infiltration is ~110 mm. In 2012, all three sites averaged over four days between rainfall events during May, June, and July with US-KFS averaging over six days between rainfall events during both May and June and more than five days in July (Figure 8a). Across all three sites from April-October 2012, there were more than four days between precipitation events 80% percent of the time compared to just 20% of the time in non-flash drought years.

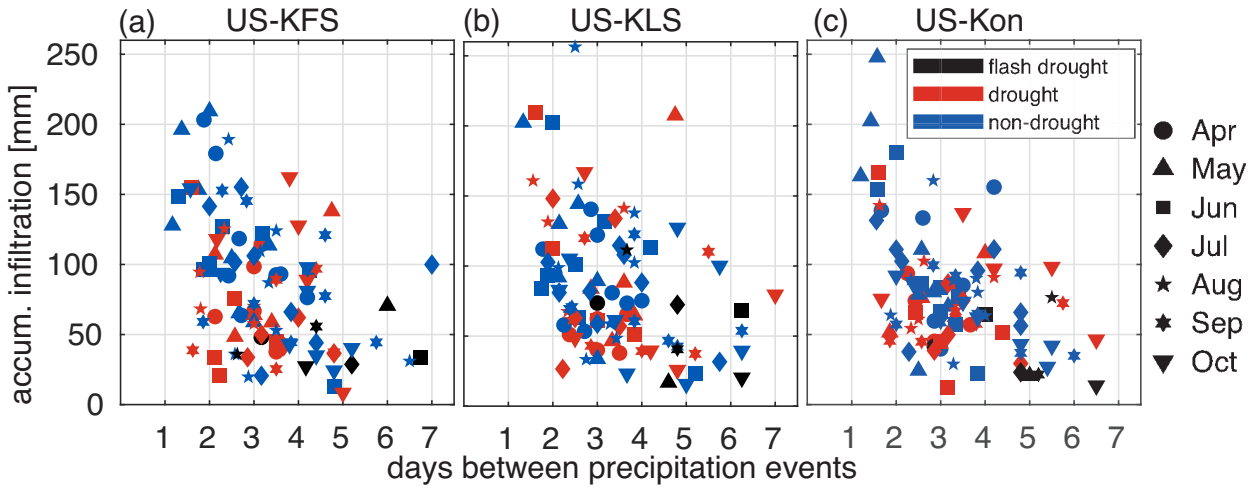

Figure 8. Monthly infiltration accumulation vs average days between precipitation events within a single month for (a) US-KFS, (b) US-KLS, and (c) US-KON. Each shape indicates one month over which the averaging occurred and colors distinguish flash drought (black) from drought (red) and non-drought (blue) years.

3.2.2 Soil Moisture

Soil moisture analysis and comparison to other soil moisture products is similar for all three study sites. Figures for soil moisture at US-KFS for all three soil layers are available in supplemental material. Top layer soil moisture reaches the wilting point several times throughout the flash drought period of 2012 (Figure Aa). During peak flash drought, at the end of June and beginning of July, moisture content remains at wilting point for many days. Daily soil moisture agrees with AmeriFlux soil moisture observations in the top layer during 2012 at US-KFS. Discrepancies exist in 2018 when AmeriFlux observations fall to levels just above 0 m^3 m^{-3}. ~~g.~~

Fluctuations in soil moisture match favorably with NLDAS-2 estimates across the top two layers in 2012, 2018, and 2019. However, middle layer soil moisture from DCHM estimates is about 0.05 m^3 m^{-3} higher than NLDAS-2 and SMERGE by the late growing season of the flash drought year (Figure A2). DCHM estimates remain fairly steady in the deep layer during 2012, while NLDAS-2 soil moisture estimates continue to fall throughout the rest of the growing season (Figure A3). The steady DCHM soil moisture levels during flash drought may be indicative of the modeling stunting root water uptake during the same time, preserving soil water content.

3.2.3 Root Water Uptake

Root water uptake is above non-flash drought levels in 2012 before the onset of flash drought in June. Then it remains lower than non-flash drought levels for the remainder of the growing season (Figure A6). The middle soil layer is responsible for up to four times more root water uptake than the other layers. Thus, a major decline in root water uptake through the middle layer is informative of how plant water use is altered during drought. While root water uptake starts out in 2012 at levels above average non-drought years, it falls to more than one standard deviation below drought averages by July. This drastic shift is likely due to lower infiltration (Figure 7) and drives down rates of transpiration within the DCHM-V and -PV over the same period.

3.3 Plant-Atmosphere Interactions

3.3.1 Sub-daily Stomatal Conductance

Sub-daily estimates of stomatal conductance highlight how VPD can drive stomatal activity within the DCHM. In 2012, stomatal conductance in the first week of May was as high or higher than in 2019~~), the~~ , a non-drought year at US-KFS (Figure 9). But by July, major differences in 2012 and 2019 stomatal conductance coincide with changes to VPD. In July 2012, high VPD shuts down midday stomatal conductance whereas lower values of VPD allow for higher rates of stomatal conductance during the same time in 2019. The large reduction in stomatal conductance from the first week of May to the first week of July during the flash drought year of 2012 is unlike that seen in a drought year like 2018 where stomatal conductance rates are similar in May and July.

3.3.2 GPP

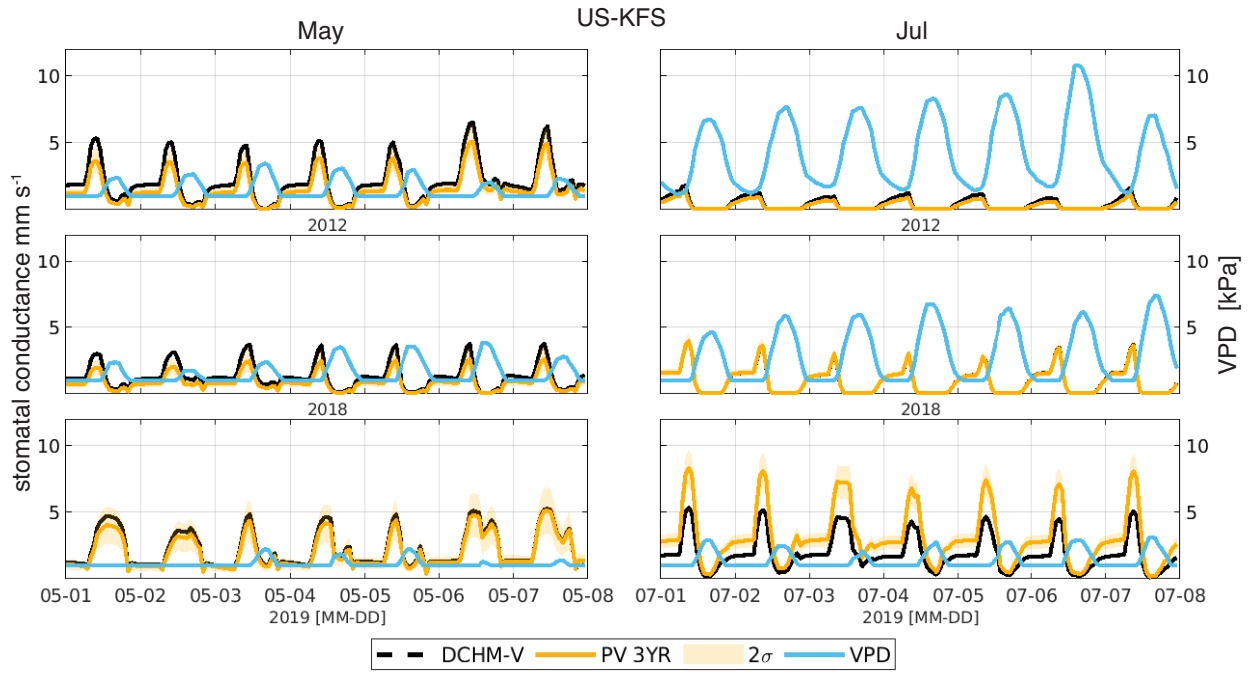

Figure 9. Stomatal conductance [mm s^{-1}] and vapor pressure deficit (VPD, kPa) for one week in May and July of 2012, 2018, and 2019 for US-KFS.

Monthly averages of GPP accumulations from DCHM-PV ~~predicts more carbon assimilation than DCHM-V and MODIS. All simulations show major declines in net carbon assimilation during the~~ ensemble means throughout the water year (April - October) indicate that carbon uptake falls below drought averages from May to June during the flash drought year of 2012 ~~flash drought~~ (Figure 10 a,c,e). Flash drought carbon assimilation amounts remain below drought levels before converging to average drought/non-drought levels by the end of October. GPP amounts are up to 50% lower in drought years compared to non-drought years. During the flash drought, GPP monthly totals in June through August 2012 are at least one standard deviation lower than drought years averaged over the 2006-2019 simulation period. June 2012 GPP accumulations are half that of drought years and less than 30% of non-drought years. An even greater discrepancy is apparent in July with carbon assimilation amounts less than 30% of drought levels and 15% of non-drought levels. Despite increased GPP from July to August in 2012, accumulations are still one standard deviation below drought levels.

~~We highlight the seasonal variation~~ Seasonal variations of GPP at US-KFS (~~Figures 11, A15, A16~~Figure 11) for simulations from the DCHM-V and -PV (3YR) with observations from MODIS and AmeriFlux for the flash drought year (2012)~~and an above average precipitation~~ , a drought year (2018), and a non-drought year (2019) ~~. We observe that during the growing season of 2019, the simulations all predict GPP on par with MODIS, but during~~ can also be explored at the daily scale. Daily GPP is lower in drought versus non-drought years between April and October. During the flash drought ~~of 2012, the DCHM simulations (both -V~~ year, there is a decline in GPP from 10 gC m^2 d^{-1} in early May, above what was observed in 2018 and

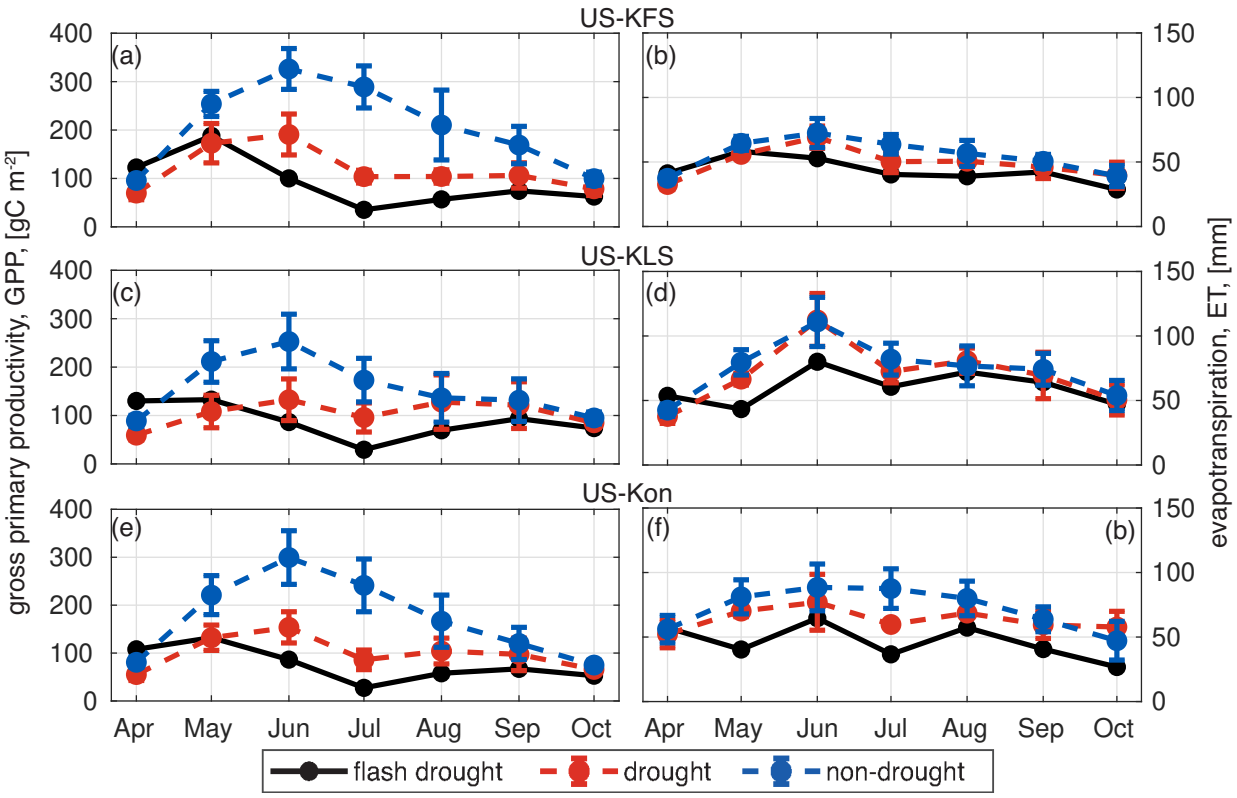

Figure 10. DCHM-PV 3YR monthly totals of GPP (a,c,e) and ET (b,d,f) for drought (red) and non-drought (blue) years compared to flash drought (black) for US-KFS, US-KLS, and US-Kon AmeriFlux sites. Monthly totals are computed from the ensemble means of the 2000 Monte Carlo simulations then averaged across drought or non-drought years. Error bars represent one standard deviation across drought and non-drought years, respectively.

~~-PV)respond to the dry down earlier than either MODIS or the tower. In particular, in late June to early July~~ 2019, to near zero by July in 2012 (Figure 11,A15,A16). During the drought year (2018), daily GPP remains low throughout the growing season, but never decreases to below 1.2 gC m^2 d^{-1} at US-KFS. From June to July in 2012, carbon uptake ~~decreases from 5.0 to 0.7 gCm~~decreased from more than 5 to less than 1 gC m^{-2} ~~day~~d^{-1}. ~~From these plots, we can also notice that uncertainties from the ensemble runs are largest during the green up period, but are generally smaller in the flash drought year than in the above average precipitation year.~~ This type of decline is not observed in a drought year (e.g., 2018). The rapid decline in GPP from May to July is what distinguishes the 2012 flash drought as a period of time where land-atmosphere interactions switch from resembling conditions wetter than an average wet year to drier than an average dry year. The DCHM-PV GPP results are similar to MODIS GPP in most cases, except that it tends to underestimate GPP compared to MODIS in a drought year, which aligns with the higher MODIS estimates of FPAR and LAI during the same periods (Figure 6). Simulated GPP tends to underestimate flux tower GPP during June and July in 2012 and 2018, but overestimate in 2019.

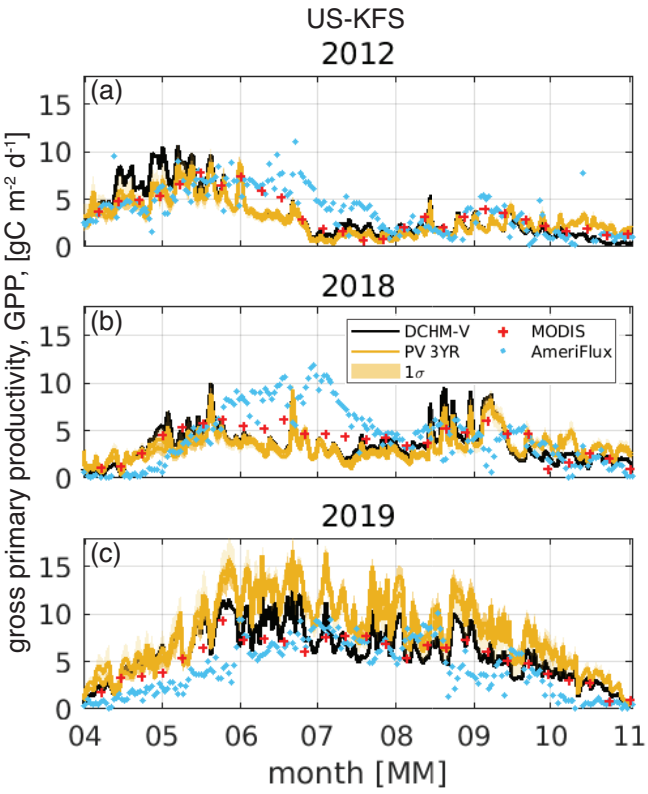

Figure 11. ~~Time series from the DCHM-V~~Daily gross primary productivity, ~~DCHM-PV three year assimilation period, 8 day MODIS, and daily AmeriFlux totals of~~ GPP, at US-KFS for (a) 2012 ~~,~~ flash drought~~year and~~ , (b) 2018 drought and (c) 2019 ~~, an above average precipitation~~ a non-drought year. One standard deviation is shown as a shaded region for the DCHM-PV simulations. MODIS GPP are shown as red crosses and AmeriFlux GPP as blue dots.

3.4 ET

~~Yearly ET totals for 2012 are approximately 0.1 m yr^{-1} less than maximum at US-KFS (Figure ?? d) and 0.2 m yr^{-1} at the other~~ We consider monthly accumulations of ET for the flash drought year and averaged across non-flash drought years for the three study sites (Figure ~~??~~ e,10 b,d,f). ~~DCHM-PV simulations (using WET, DRY, and 3YR) tend to estimate higher ET than the DCHM-V and lower ET than that observed by AmeriFlux (Figure 13 with other sites in appendix, Figures A17 and A18). The Monte Carlo simulations indicate uncertainty is smaller during the~~ ET accumulations are lower in the flash drought year starting in May, particularly at US-KLS and US-Kon. Monthly ET during drought periods are slightly lower, but generally similar to non-drought at US-KFS and US-KLS, indicating that ET may not be a strong indicator of drought. However, parsing ET into its components of evaporation and transpiration offers a different perspective. Simulated monthly transpiration accumulations follow trajectories similar to GPP during flash drought (Figure ~~13). Overall uncertainty in ET increases during the green up period at the beginning~~ 12 a,c,e). Transpiration amounts during flash drought exceed non-drought years in April, match what is

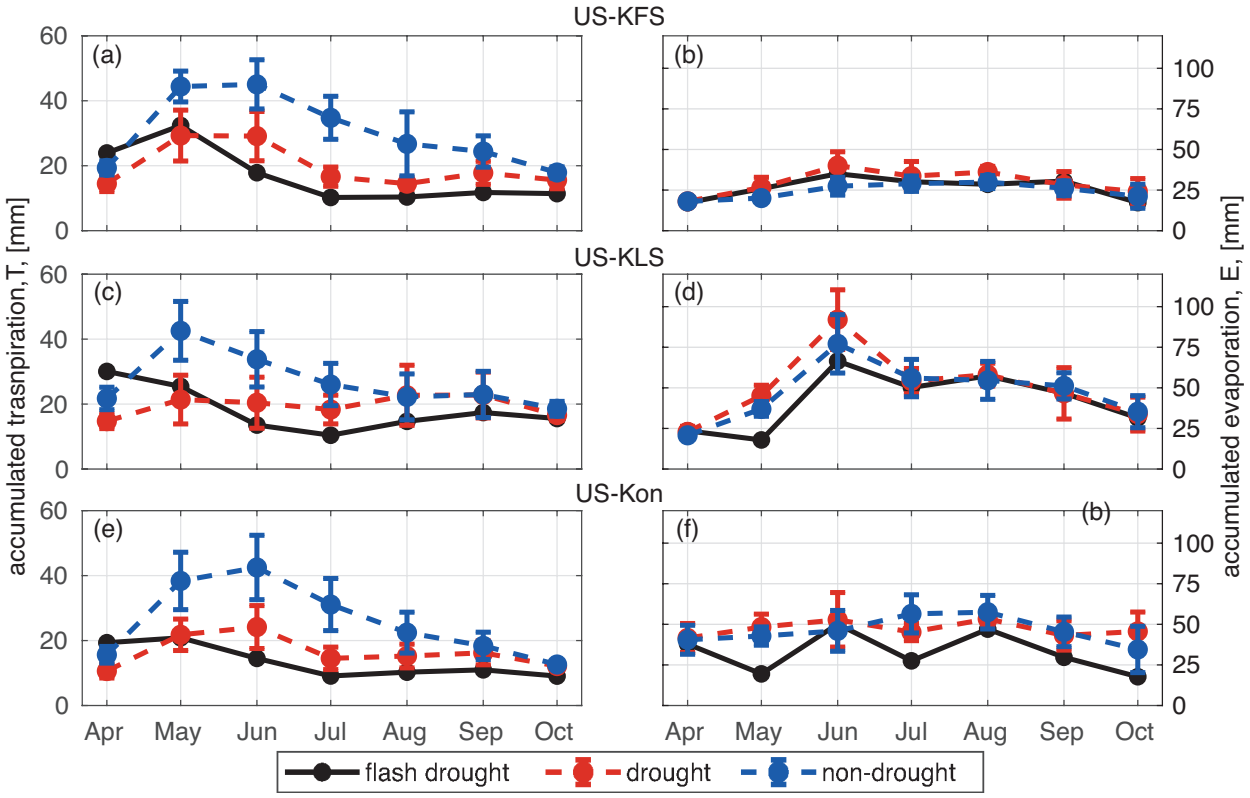

Figure 12. ~~Time series~~ DCHM-PV 3YR monthly totals of ~~ET at US-KFS for~~ transpiration, T, (a,c,e) ~~2012~~and evaporation, ~~flash~~ E, (b,d,f) for drought ~~year~~ (red) and non-drought (~~b~~blue) ~~2019~~years compared to flash drought (black) for US-KFS, ~~wet year from DCHM-V~~ US-KLS, and ~~three different DCHM-PV simulations~~US-Kon AmeriFlux sites. ~~Two standard deviations~~ Monthly totals are ~~shown for DCHM-PV~~ computed from the ensemble means of the 2000 Monte Carlo simulations then averaged across drought or non-drought years. ~~AmeriFlux ET is showing with the blue markers~~Error bars represent one standard deviation across drought and non-drought years,respectively.

observed during drought years in May, and decline to levels below drought years through the rest of the growing season~~(April). The differences in simulated ET among the different assimilation strategies are most apparent during the early months of the~~ . Transpiration in July 2012 falls below one standard deviation of the drought years. At all sites, evaporation rates for drought and non-drought years are similar. At US-KFS, monthly evaporation is comparable to both drought and non-drought years throughout the entire growing season (~~April - May)with the WET assimilation showing highest rates of ET. During the 2012 flash drought from June through August, outputs of ET were similar across simulations with different phenology model parameters. Peaks in ET occur after precipitation events with extended declines and troughs between rain events. The amount of troughs and the corresponding ET rates are indicative of slowed vegetation activity in response to the water stress.~~ Figure 12b). At US-KLS, May and June evaporation totals are lower during the flash drought than drought and non-drought years. At US-Kon, May and July evaporation falls below drought and non-drought years.

When ET was partitioned into evaporation and transpiration during During the flash drought, transpiration gradually declined . Resulting large from May to July (Figures A19a, 12). The fluctuations in total ET are a starting in June 2012 are the result of evaporation in response to precipitation (Figure A19a)small precipitation events. This suggests water evaporated before it had a chance to infiltrate the soils and be absorbed by the vegetation root systems. Since we compute transpiration that following precipitation events during flash drought onset, ET is dominated by evaporation. Reduced infiltration limits water available for root water uptake (Figures 7, A6). As transpiration is computed from root water uptake through across the three soil layers, the observation that transpiration decreases but still maintains a small consistent rate through the flash drought is indicative of vegetation indicates that vegetation is extracting water from the deeper soil layersas it undergoes stress. ET never completely shuts down because there is always a small in 2012 because of the low rate of transpiration. Evaporation reaches zero However, evaporation completely halts during early July 2012, which is the peak of the flash drought period. Similar to flash drought, during drought in 2018, ET is dominated by evaporation (Figure A19 b). But in the non-drought year 2019, transpiration makes up more than 50% of ET throughout the entire growing season except for short periods in July and August (Figure A19c).

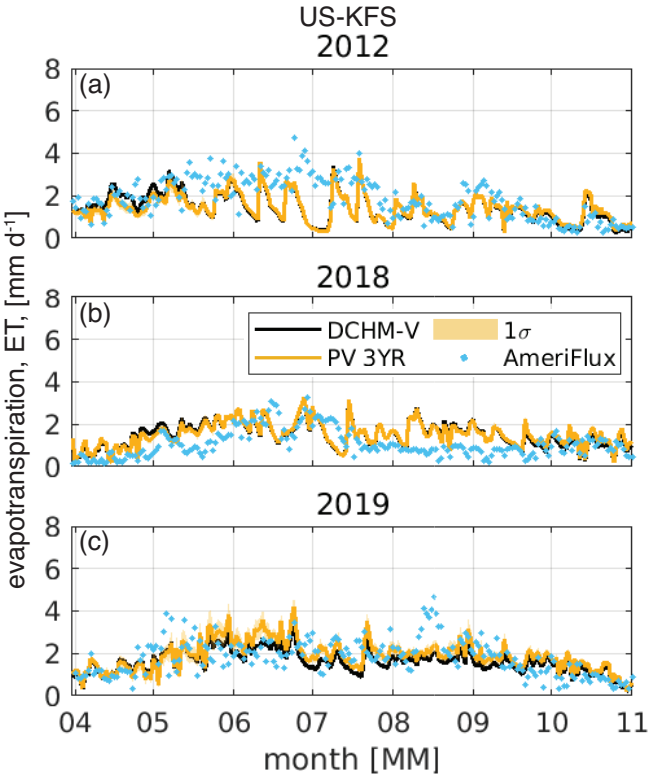

Figure 13. Ensemble means of simulated Daily evapotranspirationpartitioned into evaporation (E) and transpiration (T) for , ET, [mm d^{-1}], at US-KFS in for (a) 2012 , flash droughtand , (b) 2018 drought and (c) 2019 , wet a non-drought year. Transpiration totals Two standard deviations are in DCHM from total root uptake across shown for the three soil layersDCHM-PV simulations. The top axis AmeriFlux ET is daily StageIV precipitation totalsderived from latent heat measurements and shown as blue dots.

~~In contrast to~~ Daily ET estimated by the DCHM-PV matches well against AmeriFlux estimates at US-KFS during the flash-drought, and non-flash drought years (Figure 13). In 2012, ~~during~~ DCHM-PV ET agrees with AmeriFlux through mid-May. From late May through July the model results tend to fall below AmeriFlux until August when they once again agree. In the drought (2018) and non-drought (2019~~there was ample rainfall and water available for plant use~~) years, DCHM-PV ET appears to align with AmeriFlux throughout most of the season (Figure 13b,c). While model estimates of ET are higher than flux tower measurements in 2019 at US-KLS, they compare favorably in 2012 and 2018 (Figure A17). In contrast to model and flux tower comparisons at US-KFS and US-KLS, at US-Kon modeled ET (Figure A18) agrees with AmeriFlux in 2019 (non-drought), but underestimates during the summer months in 2012 (flash drought) and 2018 (drought). One explanation for the differences between model and tower ET data could be that water use by vegetation during flash drought is highly variable across sites, and the model is not able to represent all possible responses. Additionally, it is difficult for the DCHM and other Earth system models to account for plant access to deep water stores (Giardina et al., 2023).

4 Discussion

4.1 Mechanisms Controlling Plant Responses to Drought

4.1.1 Stomatal and Non-stomatal Regulation of GPP

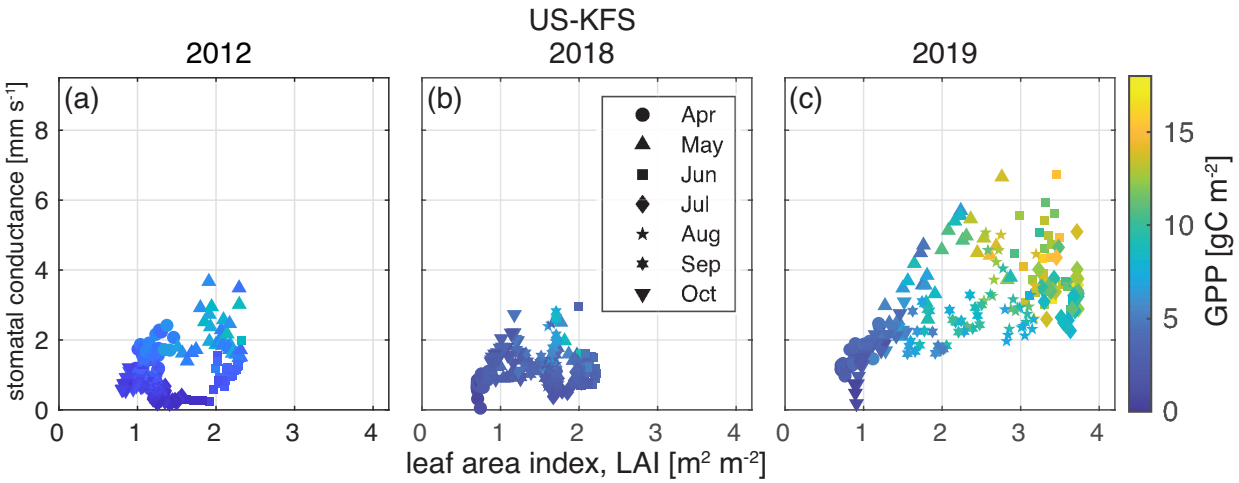

Figure 14. Stomatal conductance [mm s^{-1}] vs leaf area index, LAI [m^2 m^{-2}] for US-KFS for a flash drought year (2012), a drought year (2018), and a non-drought year (2019). Marker shapes indicate individual days between April 1 - October 31. Each month is given a unique shape whose color reflects daily accumulations of gross primary productivity [gC m^{-2}].

An objective of this work is to evaluate whether changes in phenology versus changes in stomatal conductance have a stronger control on carbon uptake during flash drought (H2, H3). We consider how GPP covaries during flash drought,

drought, and non-drought years with sub-seasonal changes in LAI and stomatal conductance at US-KFS (Figure 14). During a non-drought year (2019), there exists a wider range of values of stomatal conductance, LAI, and GPP throughout the growing season ~~. Despite minimal rainfall in early July~~ (Figure 14c). There is also a clear seasonal cycle in the clockwise movement through the stomatal conductance-LAI parameter space. Stomatal conductance increases faster than LAI in the early season before reaching maximum values around June. After LAI peaks, there is first a reduction in stomatal conductance and GPP at higher LAI before LAI decreases through August and September.

In contrast, during flash drought (2012) and drought (2018), peak stomatal conductance, LAI, and GPP values at US-KFS are approximately half of 2019 ~~, we observe~~ values. Both stomatal conductance and LAI remain low throughout the growing season and GPP is below 10 gC m^{-2} at all sites in 2012 (Figure A7). Stomatal conductance and LAI are highest in May 2012 as opposed to June and July 2019. While both 2012 and 2018 have low values of stomatal conductance, LAI, and GPP, an important difference is the near-zero stomatal conductance during June and July 2012 for a range of LAI values (1-2 m^2 m^{-2}, Figure 14) that is not observed in 2018 and other drought years (Figure A11).

The relationship between stomatal conductance, LAI, and GPP is similar across all three sites when considering flash drought (Figure A7), drought (Figure A11), or non-drought periods (Figures A8, A9, A10). The observable clockwise movement through parameter space is not as clear in flash drought and drought as compared to non-drought. In drought years, stomatal conductance from April-October averages 1.4 mm s^{-1} across all sites (Figure A11) compared to 2.3 mm s^{-1} in non drought years (Figures A8, A9, A10) and 1.1 mm s^{-1} in flash drought (Figure A7). Peak LAI is approximately 1-2 m^2 m^{-2} higher in non-drought years compared to flash drought and other drought years. Similarly, non-drought GPP levels are approximately 6-8 gC m^{-2} higher than flash drought and non-drought periods.

Prior work linked phenological responses to drought to changes in vegetation-atmosphere interactions (Lowman and Barros, 2018; Cui et . Dynamically estimated FPAR and LAI tend to exert strong controls on the resulting GPP (Lowman and Barros, 2018). By updating phenological states using the phenology model rather than forcing phenology with remotely sensed values, we were able to capture the plant growth response to water availability. When more water is available, DCHM-PV simulation predicts higher values of FPAR, LAI, and thus higher values of GPP. At the onset of flash drought, DCHM-V and -PV respond faster to changes in LAI and FPAR than MODIS whose affects were also seen in differences in modeled and remotely sensed GPP (Figure 11). Moreover, regardless of the simulation, the rapidness of the change in LAI and FPAR is indicative of flash drought (Figures 5 and 6) and in agreement with Zhang et al. (2020). Decreases in phenological state due to the lack of soil water available to plants affected carbon and water exchanges, suggesting support for the third hypothesis (H3), however, decreases in stomatal conductance driven by increased VPD may compound the detrimental phenological effects.

4.1.2 VPD Dependence

While phenology is an important component to consider when computing changes to transpiration and carbon uptake (Lowman and Barros, , our results indicate that stomatal conductance is also critical for accurately representing these fluxes. Plants adaptively regulate their stomata during periods of water stress (Guo et al., 2020), and some have been demonstrated to maintain open stomata or even increase stomatal conductance under high VPD conditions (Urban et al., 2017). Stomatal conductance shuts down under

high VPD in the DCHM (Figure 9), which does not account for the possibility of an adaptive stomatal regulation strategy. Since GPP is directly dependent on stomatal conductance (Farquhar and Sharkey, 1982), DCHM estimates of sub-daily GPP decrease in response to elevated VPD (Figure A22). Moreover, changes in phenological growth state (i.e. LAI) occur across longer (i.e. seasonal) time scales (Katul et al., 2001) than stomatal regulation, which controls carbon and water exchange at sub-daily timescales (Guo et al., 2020).

The differences between modeled and observed GPP and ET (Figures 11, 13) suggest that there are mechanisms controlling plant responses to drought stress not accounted for within the DCHM. For example, the DCHM could be too strict in representing the sensitivity of stomatal closure to elevated VPD for the Kansas study sites. There could be plant or climate specific VPD dependence (Grossiord et al., 2020), plants could have access to stores of water not accounted for (Giardina et al., 2023), or both. Guo et al. (2020) showed that isohydricity (i.e. stomatal regulation) exists on a spectrum and that some plants are able to move along that spectrum at sub-daily time-scales with varying environmental conditions, such as higher VPD. Given the high VPD in 2012 at our study sites (Figures A, A28, A29, A30), we expect the DCHM to estimate low stomatal conductance, and thus low GPP relative to AmeriFlux observations when under atmospheric water stress. Additionally, VPD estimated by the DCHM using the NLDAS-2 Forcing File A atmospheric variables is higher during 2012 and 2018 and lower in 2019 than the AmeriFlux observations (Figure A28), explaining in part the discrepancies between model and AmeriFlux GPP. As stomatal response to increasing VPD and resulting impacts on land-atmosphere water fluxes is more complex than how it is represented in LSMs (Vargas Zeppetello et al., 2023), future modeling studies should focus on how rising VPD drives stomatal closure across different vegetation types Grossiord et al. (2020).

4.2 Surface and Sub-surface Water Movement

4.2.1 Infiltration and Evaporation

At the onset of flash drought there is an increase in evaporative demand for water which leads to a temporary increase in surface evaporation (Lowman et al., 2023; Otkin et al., 2018) until the soil and canopy reservoirs no longer contain enough water to evaporate. Then evaporation shuts down. Despite evaporation tapering to zero during June and July of 2012 (~~3YR)model predictions of decreased ET in response to the lower rainfall, but transpiration rates were still higher than evaporation rates throughout the growing season (~~Figure A19), pulses of rainfall lead to temporary rapid increases in rates of evaporation. Increased surface evaporation may reduce water infiltrating the soils. In May of 2012 at US-KFS there was 70 mm of water infiltrating the soils (Figure 7) with 35 mm of evaporation (Figure 12b). ~~During the~~ But in June and July total infiltration was 61 mm with 65 mm of evaporation over the two months. Similar comparisons can be found at US-KLS and US-Kon (Figures 7, 10). In contrast, at US-KFS, during non-drought years, June averages of infiltration are in excess of 100 mm with 41 mm of evaporation. Average drought years have 66 mm of infiltration with 47 mm of evaporation (Figure 7a). Since infiltration usually exceeds evaporation in the growing season, ~~transpiration rates usually comprise~~ infiltration accumulations of similar magnitude to evaporation totals may indicate flash drought.

4.2.2 The Partitioning of ET

In this study, from 2006-2019, excluding 2012, growing season transpiration rates averaged more than 50% of total ET at US-KFS~~, a finding that aligns with~~ . This finding aligns with prior results from Hosseini et al. (2022) who used the Noah-MP ~~Land Surface Model which~~ LSM that also computes transpiration from root water uptake (Li et al., 2021). However, during the flash drought year~~of 2012~~, transpiration rates fell below 35% of overall ET at US-KFS (Figure ??15a). ~~Partitioned transpiration~~ Transpiration decreases approximately 40% from May to June at US-KLS (Figure ??15b), and 20% at US-Kon (Figure ??15c). The rapid decline in transpiration rates can be attributed to the slowing of root water uptake due to the lack of available water ~~.~~ ~~The transpiration rates follow changes in GPP during the flash drought of 2012 (Figure A23a). However~~and decreased stomatal conductance (Figures A6, A7). In contrast, ET decreases at US-KFS during July 2019 while experiencing a brief period of low rainfall (Figure A19b), yet ~~is~~ plants are able to maintain rates of GPP during this period due to the amount of available water in soils from the excessive precipitation during May and June (Figures ??, ??, ??Ac, A2c, A3c).

5 ~~Discussion~~

4.1 ~~Vegetation Responses to Flash Drought~~

Accumulated monthly averages of transpiration as a fraction of evapotranspiration (T/ET) show a transition from at or above non-drought levels to at or below drought levels (Figure 15). At US-KFS drought years have a lower fraction of transpiration throughout the growing season whereas drought and non-drought values are similar from July-October at US-KLS and US-Kon. US-Kon experiences larger fluctuations in the fraction of transpiration through the early and middle parts of the growing season (April - July). It is possible that the fluctuating T/ET at US-Kon, modeled as a grassland, is indicative of an adaptation to the water stresses.

~~Vegetation responses to water stress can be seen through fluctuations in GPP (Zhang and Yuan, 2020; Jin et al., 2019) and ET (Chen et al., 2019). Decreases in GPP occur when plants close their stomata. With the stomata closed, plants will not undergo normal gas exchange through photosynthesis and decrease their transpiration rates. Transpiration is only one part of ET, so we must be careful not to directly link fluctuations in GPP with fluctuations in ET. Evaporation can still be high when there is little to no transpiration , but GPP tend to follow the same trajectories as transpiration (Beer et al., 2009). The DCHM accounts for evaporation of water intercepted by the canopy, water that has ponded on the ground, and water in the top soil layer. At the onset of flash drought there is an increase in evaporative demand for water which leads to a temporary increase in surface evaporation (?Otkin et al., 2018) until the soil and canopy reservoirs no longer contain enough water to evaporate. Then evaporation shuts down. With small rates of transpiration still occurring, small rates of GPP are maintained (i.e. carbon uptake drastically slows, but it does not stop, Figure A23a) which affects plant WUE (Figure A24a). These results align with our initial hypotheses (H1, H2). However, we did find that even during the peak flash drought ,~~

4.1 Linking Carbon and Water Fluxes

Despite major reductions in infiltration and fluctuations in top layer soil moisture during flash drought onset, modeled root water uptake indicates that plants were still pulling small amounts of water ~~from deep soil layers, allowing for transpiration and carbon exchanges, preventing plants from complete shut down.~~

~~Computed growing season water use efficiency (WUE=GPP/ET) from DCHM-V, DCHM-PV (3YR), and AmeriFlux for (a) 2012, flash drought and (b) 2019, wet year at US-KFS. AmeriFlux WUE computed by converting latent heat into ET by dividing by the coefficient of vaporization.~~

~~We compare simulated and observed data to determine how vegetation regulates its water use, either pulling water from deeper or shutting down transpiration. We compare the timing of fluctuations in GPP and ET by combining previous plots together on the same axes (Figure A23).~~ through their roots, preventing them from completely shutting down. With the ability to tap into water stores from deeper layers (Giardina et al., 2023) and small rates of transpiration still occurring, modeled carbon uptake is still maintained (Figure 11a, A15a, A16a). Although GPP drastically slows, it does not stop. During the flash drought of 2012 (mid May - early July), we estimated steady declines in rates of GPP ~~with~~ despite bursts in ET ~~corresponding~~ in response to rain recharge events ~~. This implies evaporation may~~ (Figure A23a). We found evaporation to be the main contributor to total ET ~~during the flash drought since GPP is decreasing (Figures 11aand A23a~~and the decreases in GPP followed changes in transpiration during flash drought (Figure A19a). The decreases in simulated GPP due to flash drought during June and July 2012 are consistent in terms of magnitude ~~withdecreases~~ with decreases found in recent studies (Yao et al., 2022; Poonia et al., 2022; Zhang et al., 2020). ~~These decreases are attributed to changes in transpiration during flash drought (Figure A19a). We also find that when plants are transpiring more , they~~

Plants are more efficient during non-drought periods, and are less efficient during flash drought onset (Figure 15). Ratios of T/ET also indicate plants that transpire more are more efficient in their water use~~(Figure **??**).~~

~~2012-2019 growing season time series transpiration as a fraction of ET (a-c) and WUE (d-f) for all three study sites.~~

~~Future studies would benefit from improved estimates of root water uptake since it is directly linked to the amount of available water for transpiration. Vegetation types have distinct root characteristics leading to differences in hydraulic tendencies under variable water regimes. Species specific hydraulic strategies may differ in a single location (Liu et al., 2020) so generalization of water use by PFT in hydrologic models would represent the average tendency of vegetation to regulate water. It is also possible that the changing phenological state of root systems plays an important role in root water uptake. Thus, researchers should ensure parameterizations of plant functions are accurately representing vegetation state and heterogeneity of the study area.~~

~~We find noteworthy differences when we consider the contrasting conditions in July~~ . WUE is similar at US-KFS in August-October regardless in drought and non-drought years which might be attributed the site being modeled as a cropland. WUE at all sites started off in 2012 ~~and 2019. During both years , minimal rainfall occurred in late June into early July, but rates of ET did not decline as much in 2019 as they did in 2012. When US-KFS received rain in July~~ with above average non-drought levels and an increase from April to May. However, from May-July WUE at all sites fell from above non-drought years to more than one standard deviation below drought years. With GPP differences being more substantial than ET between flash drought and non-flash drought periods (Figure 10), subseasonal reductions in WUE can be attributed to the losses in GPP. Reductions

in WUE from above non-drought conditions to below drought conditions (e.g., the 60%-70% reduction from May to July in 2012~~, there were immediate increases in rates of ET (Figure 13). This is likely due to the size of the rain events (Figure A19 coupled with the evaporative demand of the atmosphere. It is important to examine the coupling of ET and GPP since plants transpire as they process carbon. We do not observe changes in GPP during July 2012 corresponding to the increased ET, indicating the main driver or ET during this time is the evaporation component and not transpiration. Alternatively, GPP levels off in July 2019, and does not follow the 2012 decline as a result of little rainfall. This is indicative of the vegetation remaining healthy during a period of low rainfall in a year experiencing otherwise above average rainfall. The continued carbon cycling is likely due to the soil moisture available to the plants during this time (Figure **??**).~~

~~The modeled vegetation responses are likely linked to the predictive phenological responses to drought (Lowman and Barros, 2018; Cui e . As in Lowman and Barros (2018), the modeled FPAR and LAI were directly linked to the resulting GPP . By updating phenological states using the phenology model rather than forcing phenology with remotely sensed values, we are able to capture the direct vegetation response to water availability. When more water is available, DCHM-PV simulation predicts higher values of FPAR, LAI, and thus higher values of GPPthan MODIS. Decreases in phenological state due to the lack of soil water available to plants affected carbon and water exchanges, validating our third hypothesis (H3).At the onset of flash drought, DCHM-V and -PV respond faster to changes in LAI and FPAR than MODIS whose affects were also seen in differences in modeled and remotely sensed GPP (Figure 11). Moreover, regardless of the simulation, the rapidness of the change in LAI and FPAR is indicative of flash drought (Figures 5 and 6) and in agreement with (Zhang et al., 2020)~~, Figure 15 d,e,f), appear to be a feature of flash drought onset.

4.2 Uncertainty in Vegetation Responses

We implemented three different assimilation strategies to prepare ensemble parameters to be used in the predictive phenology routine in the DCHM-PV. The 2003-2005 period represented "average" conditions as it spanned periods of below and above average precipitation. Compared to the single year assimilation periods (WET and DRY), the uncertainty ranges in model parameters were smaller in the 3YR assimilation period. The results are consistent with ~~(Lowman and Barros, 2018)~~ Lowman and Barros (2018) in that uncertainty in phenology shrinks during dry periods. Daily standard deviations in LAI across simulations are approximately 0.5 m^2 m^{-2} during the growing season of a wet year but shrink to values of 0.2 at the onset of flash drought and less than 0.1 during peak flash drought. The lower ensemble spread during the flash drought period corresponds with winter phenological variability when plants are dormant. Similarly, decreases in uncertainty in estimates of GPP and ET during the flash drought period fall to winter levels implying variability in plant life stage and functionality are similar in drought periods and dormant months.

The ~~growth parameters, which drives the plant activity~~γ parameter values, which drive plant growth in the DCHM-PV, were all smaller in the 3YR assimilation period for all three test sites when compared to simulations from drought and wet years. Vegetation leaf out occurs later in the simulations from the 3YR assimilations (Figures 5 and 6). However, the more notable effects of the smaller growth parameters, with regards to flash drought, can be seen through the delayed phenology responses in the 3YR assimilations compared to the WET/DRY assimilations. Across the three test sites, the FPAR and LAI decreases

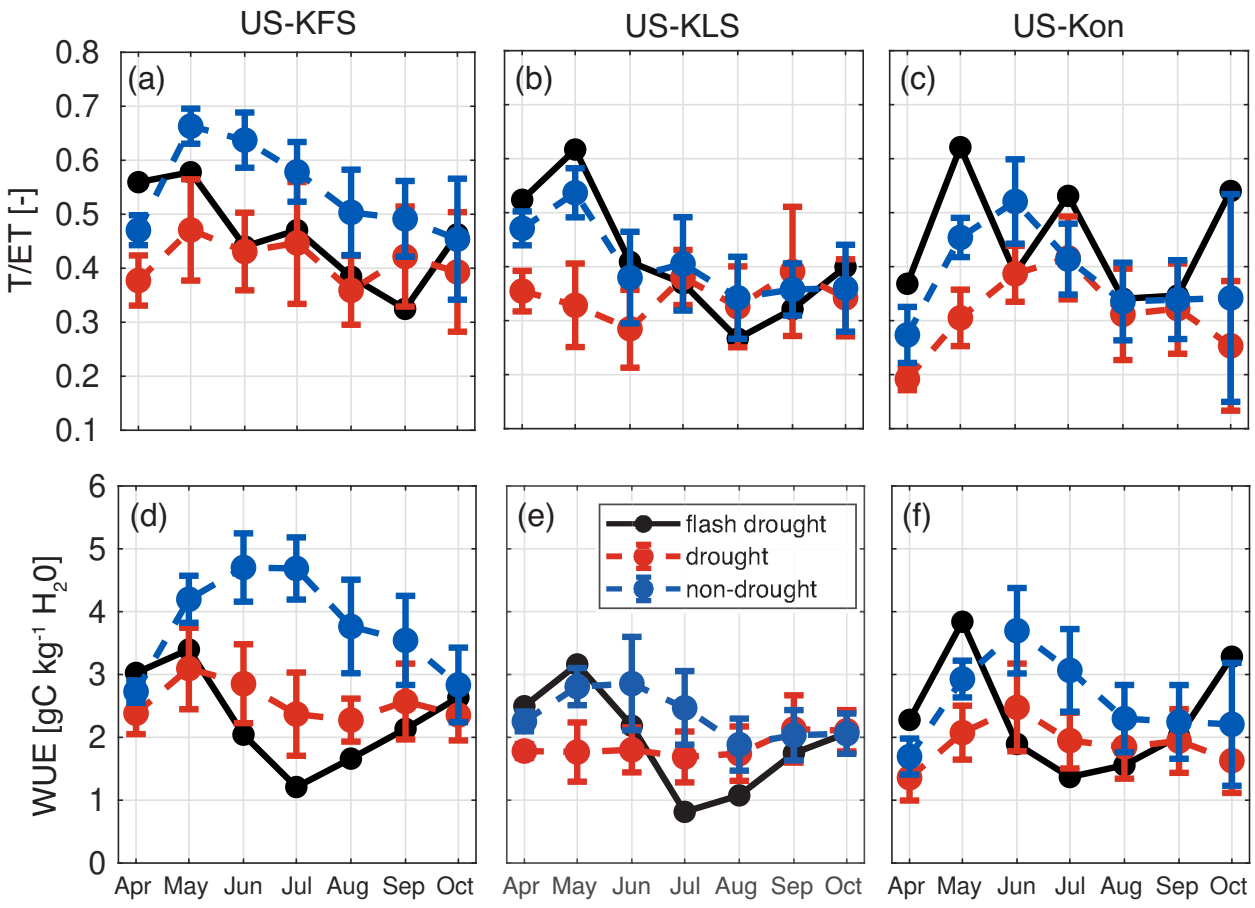

Figure 15. Ratio of transpiration to evapotranspiration, T/ET, and water use efficiency, WUE, for for drought (red) and non-drought (blue) years compared to flash drought (black) for US-KFS, US-KLS, and US-Kon.

were slower in the simulations that used the 3YR assimilation period. The vegetation that was trained using average conditions was slower to change when faced with the abrupt decrease in water availability. Although it was an above average year for precipitation, there was little rainfall in early July 2019 at our Kansas sites. At US-KLS and US-Kon, there was a rapid decrease in LAI during this time (Figure 6d,f) with some recovery in August. Moreover, the ~~resiliency to the abrupt change is apparent in the maintenance of season~~ slower changes in seasonal LAI and FPAR dynamics from the 3YR ~~assimilation simulations~~ simulations show the resiliency to abrupt phenological changes.

Future studies should use an assimilation period encompassing multiple ~~wetness~~ precipitation regimes (i.e. multi year inference period) to best represent the ~~variety and~~ variability of climatological conditions ~~, and~~ because it leads to ~~less abrupt changes to extreme stress~~reduced uncertainty in model outputs. However, if the intent of a future study is to investigate vegetation responses to extreme events in a changing climate (Kirono et al., 2020; Pearson et al., 2013, e.g.,), it may be appropriate to use inference periods encompassing ~~only~~ extreme wet or dry conditions. For example, ~~researchers~~ one could fit parameters

to a dry regime ~~if they want~~ to investigate how plants ~~used to wetter~~ accustomed to today's average conditions will function in a future ~~regime where more drought is~~ climate where drier conditions are expected.

4.3 ~~Kansas Site Comparisons during 2012 Flash Drought~~Land Cover Influences

The seasonal dynamics of FPAR, LAI, and GPP from the simulations match well against the remotely sensed observations from MODIS regardless of vegetation type. Effects of water stress on infiltration, stomatal conductances, and WUE are similar across all three sites and help to distinguish flash drought conditions from non-flash droughts. However, there are subtle differences in vegetation responses to water stress across all three sites. As seen in Figures 5 and 6, the phenological responses to flash drought at US-KLS (cropland) and US-Kon (grassland) follow a similar trajectory throughout the growing season. The savanna at US-KFS (note - AmeriFlux classifies US-KFS as a grassland~~but the MODIS pixel (500m) containing US-KFS reports a savanna terrain)~~) suggests more resilience to flash drought at first when compared to croplands and grasslands in that values of FPAR and LAI are maintained for a longer period before tapering in late June. This can also be seen in the slow reductions in GPP during May and June 2012 before reaching a minimum near the beginning of July marking stomatal closure and a shift toward more isohydric behavior (Meinzer, 2002). ~~The slower reduction, driven by the lower growth rate parameter (γ), indicates that the vegetation is responding to the initial water stress, but also maintaining some activity.~~

~~The vegetation at US-KLS and US-Kon show an earlier response to the water stress in 2012 by slowing phenology (FPAR, Figure 5; LAI, Figure 6) at the beginning of May. Both sites experience another decrease in activity by the beginning of July. These conservative strategies indicate that the vegetation is more isohydric at these locations. Interestingly, when the phenology model parameters are generated from observations from a year of above average precipitation, the vegetation responds even faster to the stress of water. It is likely that the water use characteristics defined in~~ When analyzing DCHM outputs against remotely sensed and eddy covariance measurements, we are comparing data across temporal and spatial scales. The flux towers exist within a 4 km by 4 km region defined by the Stage-IV spatial grid cell used in the DCHM. Flux tower spatial extents range from a couple hundred meters to a few kilometers (Baldocchi, 2003; Schmid, 1994) making the 4 km grid cell near the maximum range. Sub-grid scale heterogeneity can lead to considerable discrepancies between parameterized and actual fluxes (Schmid, 1994). One explanation for why flux tower data differs from model output is that the flux tower estimates incorporate a variety of vegetation types within the fetch contributing to the vertical fluxes, rather than the single vegetation type used within the model. Additionally, the size and orientation of the contributing fetch varies in time depending on measurement height and turbulent fluxes (Chu et al., 2021).

Differences in land cover classification could be another reason for discrepancies between modeled and observed FPAR and LAI. Though we use MODIS to determine the land cover type, we first interpolated the 500 m data to determine the value of the 4 km grid cell used in the DCHM. After upscale, the pixel at US-KFS is labeled as a savanna, but the 500 m MODIS grid cell containing US-KFS is classified as grassland. Regardless of the classification differences, the spectral reflectance method used by MODIS is inherently different from the predictive phenology routine used in the DCHM-PV~~(Lowman and Barros, 2016; Garcia-Quijano based on PFT cause the model to be more conservative in its water use strategies. Another explanation could be the deep soil layers (1.83 m, 72 in) (Soil Survey Staff) allowing for deep root the deep soils of the Kansas Plains and to allow the model to~~

~~account for deeper root water uptake (Lowman and Barros, 2016).~~ , specifically in that it cannot account for how soil water availability influences vegetation growth (Lowman and Barros, 2018).

4.4 ~~Implications~~

~~The coupling of the land-surface-subsurface hydrology model to the predictive phenology model allows for dynamic updates of vegetation growth states (Lowman and Barros, 2018). By updating phenology, we are able to better capture vegetation responses to water stress events through water use efficiency (Figure A24), indicating plants that transpire more are more efficient in their water use. Vegetation activity is directly linked to the coupling of the water and carbon cycling through photosynthesis (Farquhar et al., 1980) and assimilating plant phenology into land-surface models (e.g., DCHM-V or Noah-MP) can improve estimates of GPP and ET (Hosseini et al., 2022; Xu et al., 2021; Mocko et al., 2021; Kumar et al., 2019).~~

4.4 Model Performance and Limitations

4.4.1 Model vs Observations

This study allows us to investigate how vegetation responses can be used to study the effects of flash droughts on the total carbon ~~budget~~and water budgets. Our modeling approach permits direct comparisons of remotely sensed observations to physically derived estimates. Generally, MODIS overestimates GPP compared to EC flux tower data (Heinsch et al., 2006; Running et al., 2004)~~and our model underestimates MODIS and flux tower GPP during droughtperiods and aligns more with MODIS~~ . Daily GPP from the DCHM tends to match the magnitude of MODIS and AmeriFlux GPP at US-KFS throughout much of the growing season but underestimates June and July observations in 2012 (flash drought) and 2018 (drought). The DCHM-PV tends to overestimate during 2019 (non-drought) while the DCHM-V more closely aligns with observations. Large discrepancies are also apparent in hourly estimates of GPP at US-KFS (Figure A22). The DCHM halts midday GPP in July 2018, but AmeriFlux values remain high. The differences are smaller in 2012, where AmeriFlux observed carbon assimilation rates of 1 gC m^{-2} s^{-1} throughout the daytime and the DCHM shut down carbon assimilation due to elevated VPD (Figure A22).

The DCHM-PV compares favorably against MODIS LAI during flash drought and non-drought at US-KFS and ~~flux tower estimates during high precipitation years. By explicitly considering plant tendencies, we can dynamically account for current meteorological conditions~~ US-KLS (Figure 6a,c,d,f) and underestimate those sites during drought (Figure 6 b,e). At US-Kon, MODIS LAI during May, June, and July tends to be above DCHM-PV estimates. The higher DCHM-PV model estimates of FPAR and LAI during summer 2019 could be due to the model accounting for excess water availability and other meteorological conditions favorable for growth (temperature, VPD, etc.). MODIS estimates of FPAR and LAI are based on radiative transfer models using bidirectional reflectance of incoming radiation from the red and near infrared bands (Myneni et al., 2015; Yan et al., 2016) . MODIS GPP is directly dependent on observations of FPAR (Running et al., 2015). This difference is apparent in DCHM-PV estimates of GPP exceeding estimates from the DCHM-V and MODIS GPP during the same period where the DCHM-PV predicts larger values of FPAR and LAI during 2019 (Figure 11). Our model performance against MODIS is similar to that

found in Hosseini et al. (2022), who used a predictive phenology model coupled with Noah-MP. Across all 11 years in that study, their dynamic vegetation models tended to underestimate June and July LAI at US-Kon and slightly overestimate at US-KFS.

AmeriFlux estimates of GPP during June and early July of 2012 and ~~thus use physical principles to capture vegetation-atmosphere interactions. Moving forward, improvements made to phenological states of the entire plants (i. e. root systems included)rather than just the leaf phenology might better capture water movement through plants under water stress conditions.~~

4.5 ~~Limitations~~

2018 are also above estimates from MODIS. This suggests that during drought and flash drought, plants are able to maintain higher levels of GPP than what can be recreated in land surface models and satellite remote sensing. Differences in DCHM-PV and AmeriFlux GPP cannot be fully attributed to carbon reallocation since the Noah-MP model accounts for carbon reallocation and similarly underestimated GPP compared to flux tower data (Hosseini et al., 2022). Even while accounting for carbon movement, they found that during June, July, and August they underestimated tower data by 100 gC m^{-2} at US-Kon while overestimating by the same amount at US-KFS in April, May, and June (averaged across an 11-year study period encompassing wet and dry periods). The DCHM-PV, which does not account for carbon reallocation, responds to drought and flash drought differently than what is observed at flux tower sites. It matches better with AmeriFlux data during 2012, the flash drought year, at US-KFS and US-KLS compared to 2018, a drought year (Figure 11, A15).

Another difference between modeled and flux tower data could be that models may not be able to fully represent how vegetation can maintain ET by accessing groundwater or deep soil moisture, ultimately biasing models towards more severe effects of drought on vegetation (Giardina et al., 2023). DCHM has similar soil moisture profiles to NLDAS-2, derived from Noah-LSM, and Hosseini et al. (2022) who used Noah-MP configurations, for both the 2012 flash drought and the 2018 drought. The DCHM also follows trends similar to AmeriFlux in 2012, but AmeriFlux top layer soil moisture values are much smaller from May to October of 2018, often under 0.1 m^3 m^{-3} during that time (Figure A). Despite extremely low top layer soil moisture in 2018, AmeriFlux GPP reaches levels above 10 gC m^{-2} d^{-1} coinciding with a brief recharge in soil moisture at the end of June. The DCHM estimates of GPP are often less than 50 % of AmeriFlux GPP in 2012 and 2018. The model results from the Noah-MP similarly underestimate GPP and overestimate soil moisture during these drought periods (Hosseini et al., 2022) suggesting that access to deep water reserves are responsible for these differences (Giardina et al., 2023) .

4.4.1 Implications for LSMs

Capturing phenological responses and subsequent changes to carbon and water fluxes within a physically based model is not without its limitations. As we update phenological states during the DCHM-PV simulations, forced atmospheric conditions from NLDAS-2 and ~~StageIV~~ Stage-IV variables are the same as in the DCHM-V simulations. We continue to use these conditions to force the model, so it is possible that the meteorological observations are already accounting for some vegetation-atmosphere interactions. ~~When analyzing DCHM outputs against remotely sensed and eddy covariance measurements, we are~~

~~comparing data across temporal and spatial scales. For example, the DCHM takes in one value for soil texture and porosity and land cover type, and uses these values to define how water moves through soils and root systems across the 4 km grid cell. Vegetation at AmeriFlux tower sites differs from the interpolated MODIS land cover type used in the DCHM in some instances. Other challenges arise throughout the analysis with missing tower data, and data at different scales, units, and measurement locations. Here, the DCHM is operating at a 4 km grid scale, so representing vegetation as one PFT does not capture the landscape heterogeneity below the grid scale even if it does match AmeriFlux . Soil moisture measurements from SMERGE, Noah-LSM, and Ameriflux (Figures ??-??) are all at varying depths that may differ from, but most closely align with, the soil layers we defined. We derive evapotranspiration using latent heat fluxes from AmeriFlux towers and recognize that the energy balance may not be closed in doing this (Wilson et al., 2002), while the DCHM forces energy balance closure.To get past the limitations, the ensemble Monte Carlo simulations help capture model uncertainty, incorporated throughout the results as ensemble means and standard deviations.~~ But, by explicitly considering plant tendencies, we can dynamically account for current meteorological conditions and thus use physical principles to capture vegetation-atmosphere interactions.

Vegetation responses to water stress are apparent through fluctuations in GPP (Zhang and Yuan, 2020; Jin et al., 2019) and ET (Chen et al., 2019). Decreases in GPP occur when plants close their stomata. With the stomata closed, plants will limit gas exchange affecting both photosynthesis and transpiration rates. Transpiration is only one part of ET, so we must be careful not to directly link fluctuations in GPP with fluctuations in ET. Evaporation can still be high when there is little to no transpiration, but GPP tend to follow the same trajectories as transpiration (Figures 10, 12, Beer et al., 2009). In some cases, vegetation can reallocate already processed carbon to their roots when under drought stress mitigating GPP losses (Ingrisch et al., 2020). However, modeled GPP losses are likely a result of modeled stomatal behavior, as the model does not account for reallocation of carbon stores within the plants. Sub-daily scale stomatal conductance reduces to zero in response to increased VPD (Figure 9) leading to similar reductions in modeled GPP (Figure A22). This limitation of the DCHM could explain why AmeriFlux GPP tends to be higher than the modeled GPP.

Vegetation activity is directly linked to the coupling of the water and carbon cycling through photosynthesis (Farquhar et al., 1980) and assimilating plant phenology into land-surface models (e.g., DCHM-V or Noah-MP) can improve estimates of GPP and ET (Hosseini et al., 2022; Xu et al., 2021; Mocko et al., 2021; Kumar et al., 2019). However, our findings also indicate that improved phenology cannot alone account for vegetation adaptations to water stress and ability to access water in ways that current LSMs cannot account for (Giardina et al., 2023). Future studies should focus on improving our understanding how how plants are able to tap into different stores of water to continue exchanging water and carbon despite lower precipitation or increased VPD. Additionally, as stomata control the movement of water and carbon, affecting GPP and water use efficiency (Lawson and Vialet-Chabrand, 2019), accounting for plant adaptations that adaptively regulate stomatal sensitivity to drought stress, especially VPD, may improve model accuracy.

Moving forward, improvements made to phenological states of the entire plants (i.e. root systems included) rather than just the leaf phenology might better capture water movement through plants under water stress conditions. Future studies would benefit from improved estimates of root water uptake since it is directly linked to the amount of available water for transpiration. Vegetation types have distinct root characteristics leading to differences in hydraulic tendencies under variable

water regimes and atmospheric conditions which distinguish vegetation that is more likely to survive or recover from drought (McDowell et al., 2008; Martínez-Vilalta et al., 2002). Species specific hydraulic strategies may differ in a single location (Liu et al., 2020) so generalization of water use by PFT in hydrologic models would represent the average tendency of vegetation to regulate water. It is also possible that the changing phenological state of root systems plays an important role in root water uptake (McCormack et al., 2014). Moreover, models that can account for different vegetation behavior such as the reallocation of carbon storage and below ground respiration during drought may provide a better understanding of mechanisms driving drought resiliency and changes to carbon uptake during drought (Ingrisch et al., 2020; Sanaullah et al., 2012). These types of mechanisms could explain how a warm and wet spring mitigated the effects of the 2012 flash drought on GPP losses (Wolf et al., 2016).

5 Conclusions

~~Changes in vegetation phenology, or growth stage, drive water use strategies and have implications on the carbon and water budgets (H3).~~

To address how water stresses affect carbon and water cycling, we implemented a one-dimensional version of the DCHM-V coupled to a predictive phenology model and analyzed ~~vegetation water use strategies during drought and non drought~~vegetation-atmosphere water and carbon exchanges during flash drought, drought, and non-drought periods. The modeling procedure first required running the DCHM-V with phenology updates from remotely sensed observations of FPAR and LAI. ~~In order to couple~~ Coupling the predictive phenology model to the DCHM-V, we generated ensembles of model parameters ~~from the outputs of the DCHM-V~~ and ran Monte Carlo simulations of the DCHM-PV with concurrent meteorological conditions. We ran three simulations using three distinct assimilation periods for three different sites in Kansas. Uncertainty in model parameters and outputs is reduced when a three year assimilation period (covering net-average conditions) is used. ~~Decreases in predicted FPAR and LAI and reductions in their uncertainty ranges aligned with periods of known flash drought . These proxies for vegetation state influence rates of ET and GPP and thus WUE as seen through the partitioning of ET and the near shutdown of transpiration~~

Our findings indicate that both phenology and stomatal conductance play an important role controlling vegetation responses to extreme drought (H2, H3). Decreased infiltration due to increased days between precipitation during flash drought resulted in less new water available for plant use (H1,H2). High vapor pressure led to stomatal closure within the model. With stomata closed, root uptake, transpiration, and carbon assimilation reduced to dormant levels which led to reductions in WUE during flash drought to levels more than one standard deviation below other drought periods (H2)~~during the summer of 2012 (Figure A24a), while evaporation continued in response to precipitation and atmospheric demand for water (H1).~~ . FPAR and LAI also reduced during flash drought, but did not exert as strong of a control on reductions in GPP as did changes to stomatal conductance due to increased VPD.

The seasonal timing of the flash drought ~~likely~~ had larger impacts ~~since~~ as the rapid dry down occurred during the peak growing season (Yuan et al., 2019). The amount of ~~available water is~~ water available during the growing season has a major in-

fluence on vegetation activity (H1). In this region of the United States, droughts can reduce ~~yearly~~ monthly carbon assimilation by ~~50% compared to periods of average or above average precipitation (Figure ??a-c)~~ half compared to non-drought periods (Figure 10) while flash droughts are even more detrimental to the overall carbon budget. This has major implications for the annual crop yield as well as the carbon uptake capacity for the grasslands and savannas that cover ~~most~~ much of the Mid-western US. Future modeling studies should investigate how different vegetation types ~~change~~ alter their water use strategies in response to different water stresses by ~~focusing on~~ including (1) ~~expanding this modeling framework to include seasonal variations in the representation of root distributions which can affect subsurface responses to water stresses and (2) exploring a wider range of plant function~~ adaptive stomatal regulation under elevated VPD, (2) access deep stores of water in soils and (3) wider ranges of plant functional types and climatological regimes.

Appendix A: ~~Additional~~ Supplemental Figures

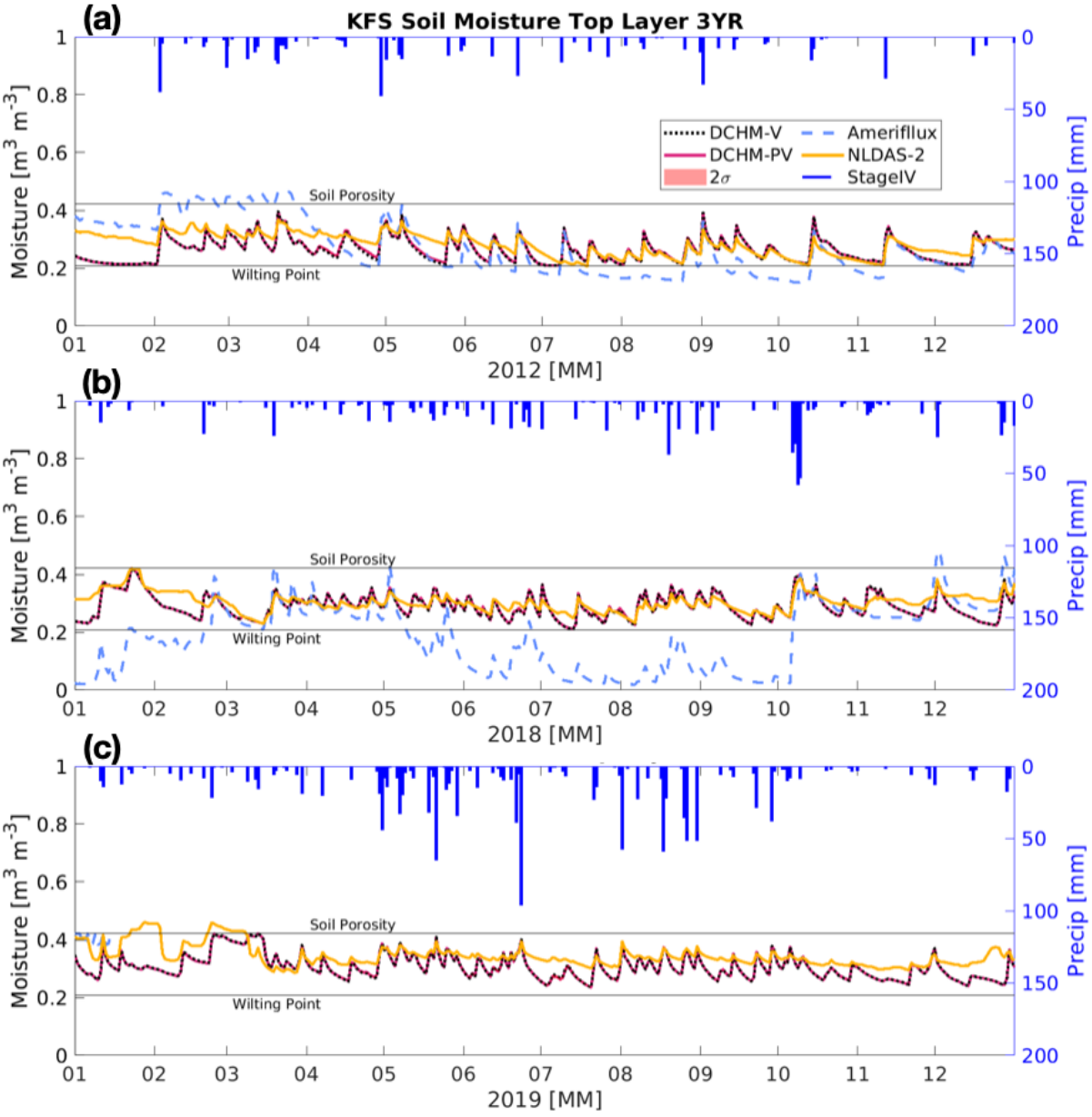

~~Top layer soil moisture for the non flash~~ , (b) 2018 drought and (c) 2019 a non-drought year ~~2019.~~using the DCHM-V (black dotted line), the DCHM-PV with two standard deviations (red), AmeriFlux (blue dashed line), NLDAS-2 derived from Noah-LSM (yellow) and Stage IV precipitation on the top and right axes (blue).

~~Top layer soil moisture for the non flash~~ , (b) 2018 drought and (c) 2019 a non-drought year ~~2019.~~using the DCHM-V (black dotted line), the DCHM-PV with two standard deviations (red), AmeriFlux (blue dashed line), NLDAS-2 derived from Noah-LSM (yellow) and Stage IV precipitation on the top and right axes (blue).

Figure A1. Top layer soil moisture at US-KFS for ~~the~~ (a) 2012, flash drought~~year 2012.~~

~~Top layer soil moisture for the non flash~~ , (b) 2018 drought and (c) 2019 a non-drought year ~~2019.~~using the DCHM-V (black dotted line), the DCHM-PV with two standard deviations (red), AmeriFlux (blue dashed line), NLDAS-2 derived from Noah-LSM (yellow) and Stage IV precipitation on the top and right axes (blue).

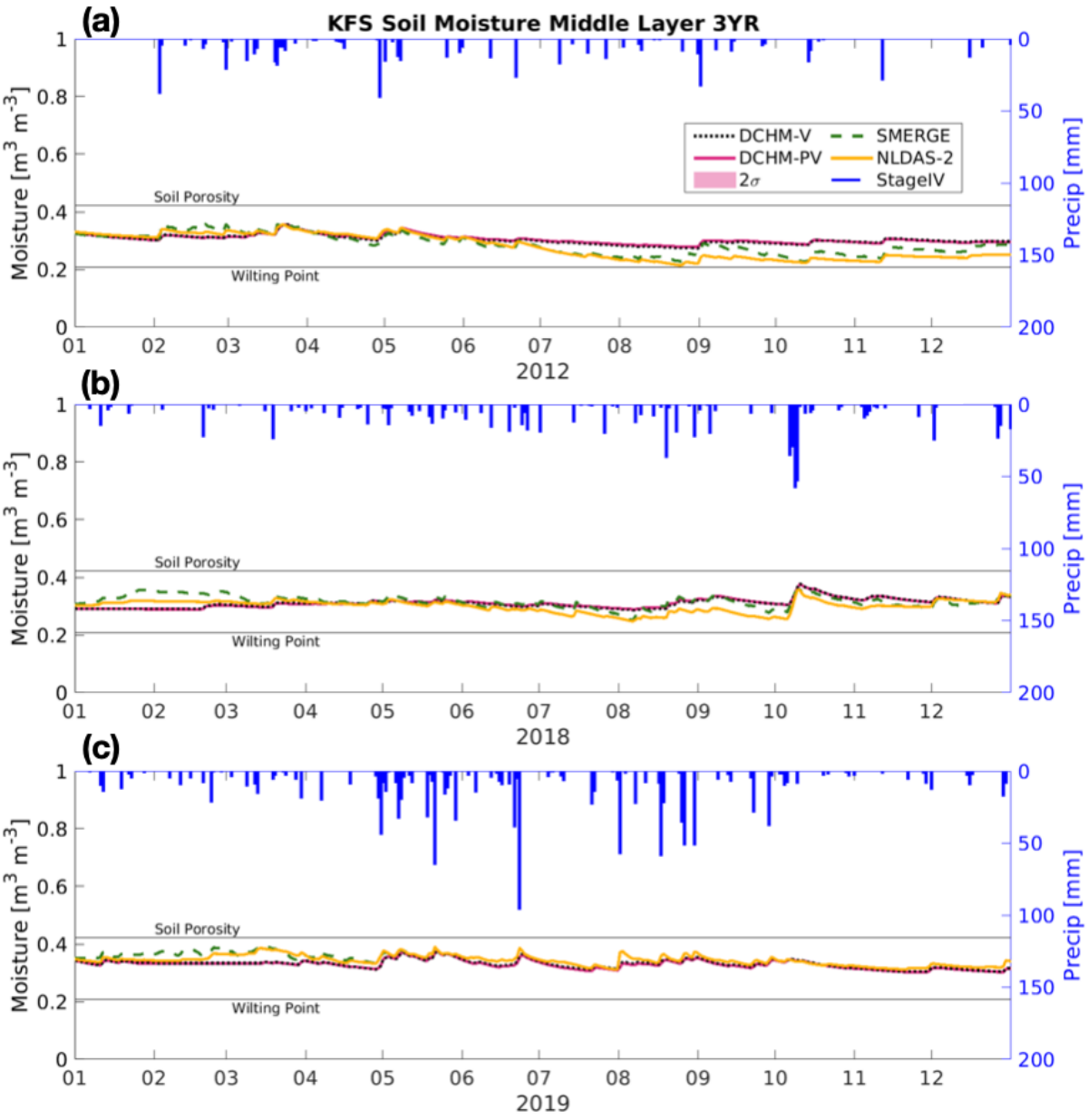

Figure A2. Middle ~~layer~~ soil moisture at US-KFS for ~~the~~ (a) 2012, flash drought, (b) 2018 drought and (c) 2019 a non-drought year ~~2012.~~using the DCHM-V (black dotted line), the DCHM-PV with two standard deviations (red), AmeriFlux (blue dashed line), NLDAS-2 derived from Noah-LSM (yellow) and Stage IV precipitation on the top and right axes (blue).

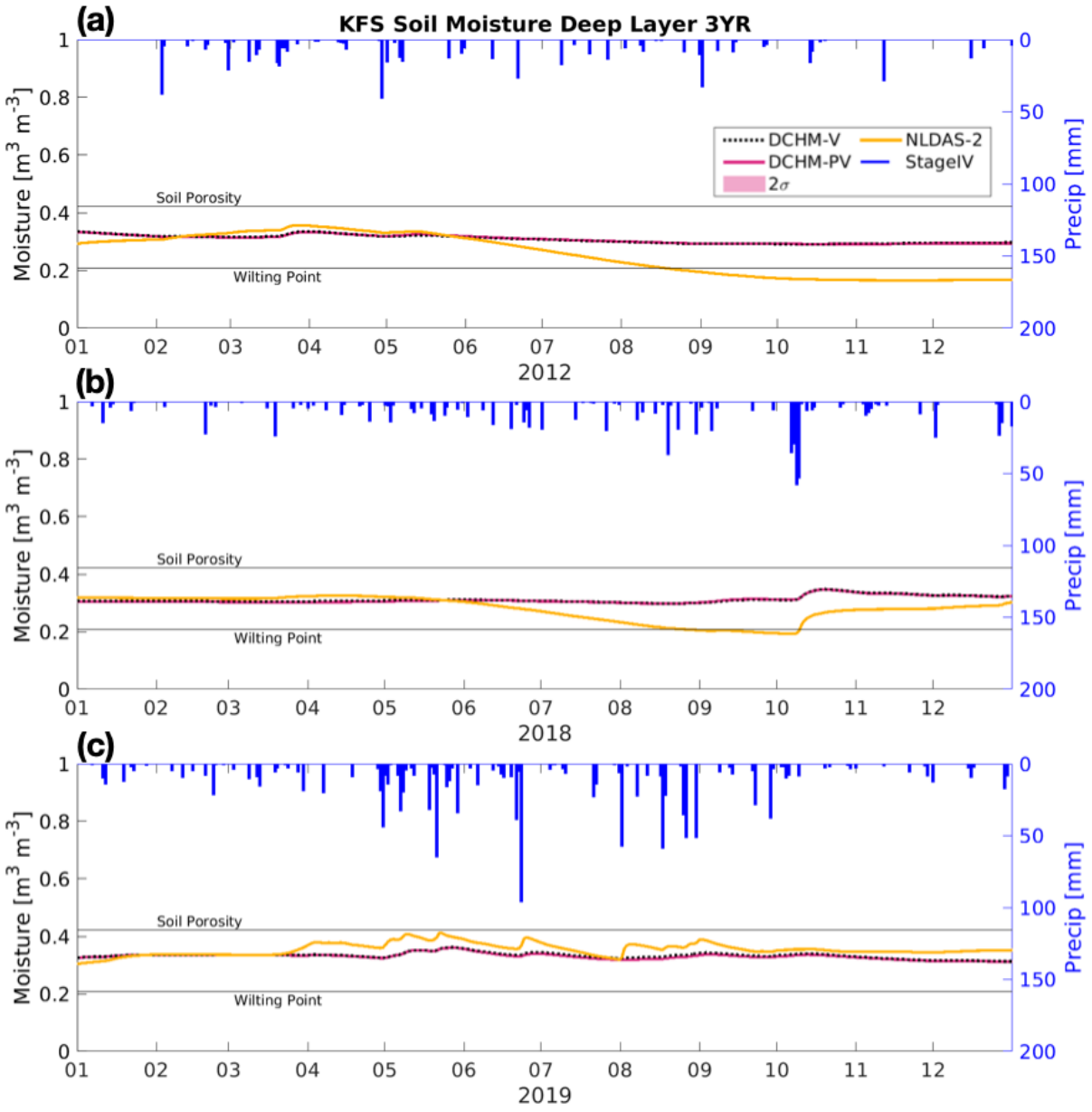

Figure A3. ~~Middle layer~~ Deep soil moisture at US-KFS for ~~the non~~ (a) 2012, flash drought, (b) 2018 drought and (c) 2019 a non-drought year ~~2019~~ using the DCHM-V (black dotted line), the DCHM-PV with two standard deviations (red), AmeriFlux (blue dashed line), NLDAS-2 derived from Noah-LSM (yellow) and Stage IV precipitation on the top and right axes (blue).

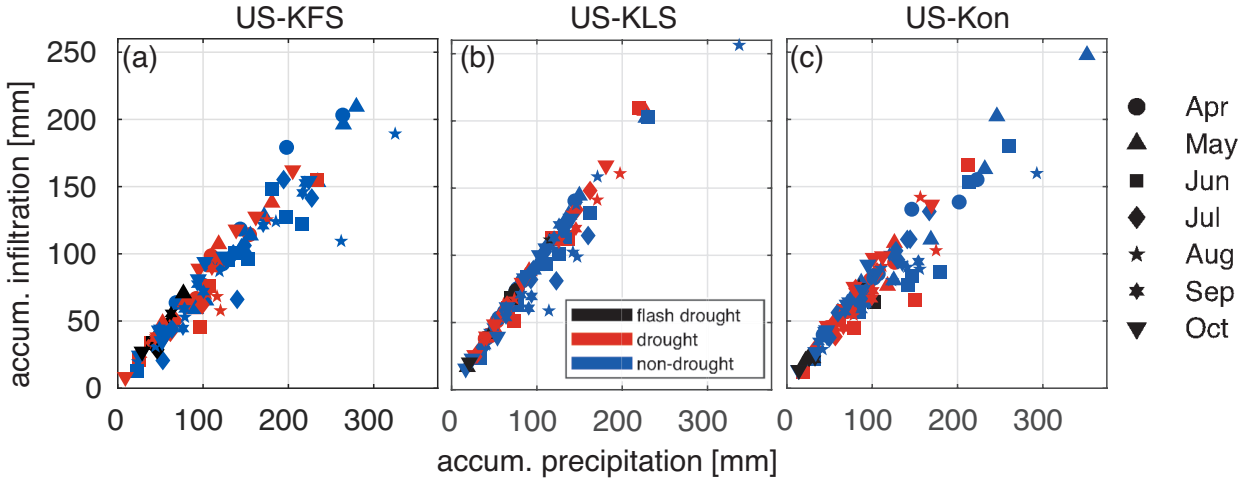

Figure A4. ~~Deep layer soil moisture for~~ Monthly accumulation of infiltration versus precipitation. Each shape indicates one month over which the averaging occurred and colors distinguish flash drought ~~year 2012.~~(black) from drought (red) and non-drought years (blue)

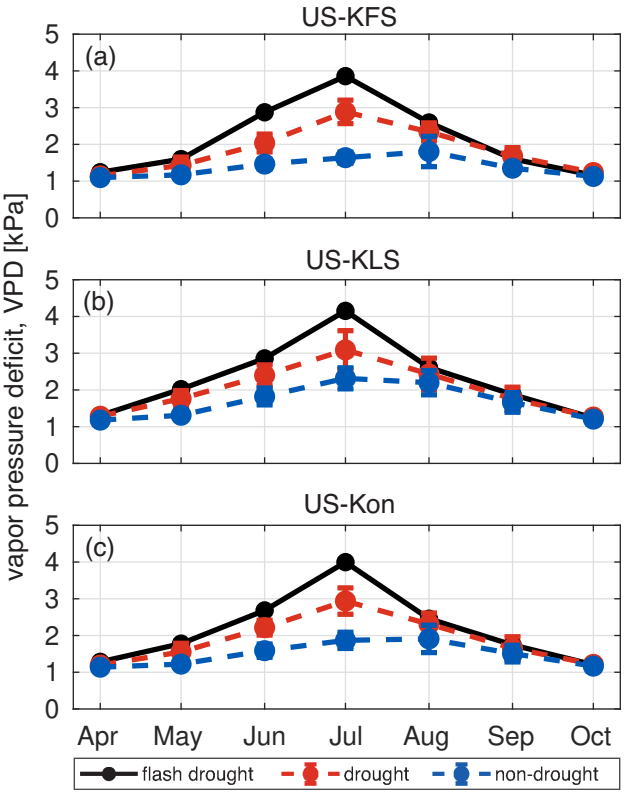

~~Root water uptake through three soil layers throughout~~ 2012 ~~using the DCHM-V~~ (black), drought (red), and ~~DCHM-PV 3YR~~non-drought (blue). The error bar represents one standard deviation across drought and non-drought years, respectively.

~~Root water uptake through three soil layers throughout~~ 2012 ~~using the DCHM-V~~ (black), drought (red), and ~~DCHM-PV 3YR~~non-drought (blue). The error bar represents one standard deviation across drought and non-drought years, respectively.

Figure A5. ~~Deep layer soil moisture~~ Monthly average vapor pressure deficit [kPa] for the ~~non~~ three AmeriFlux sites from April - October for the flash drought year ~~2019.~~

~~Root water uptake through three soil layers throughout~~ 2012 ~~using the DCHM-V~~ (black), drought (red), and ~~DCHM-PV 3YR~~non-drought (blue). The error bar represents one standard deviation across drought and non-drought years, respectively.

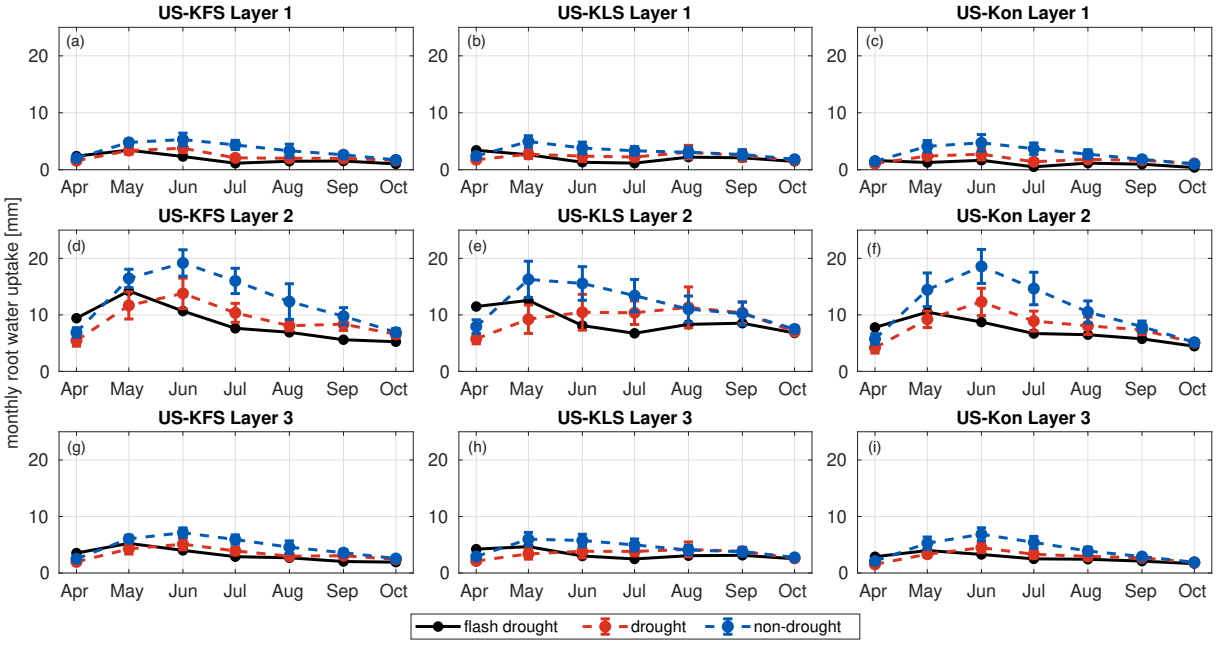

Figure A6. ~~Root~~ DCHM-PV 3YR monthly root water uptake ~~through~~ totals for drought (red) and non-drought (blue) years compared to flash drought (black) across three soil layers ~~throughout 2019 using~~ for our three study sites. Monthly sums are computed from the ~~DCHM-V~~ ensemble means of the 2000 Monte Carlo simulations then averaged across drought or non-drought years. Error bars represent one standard deviation across drought and ~~DCHM-PV 3YR~~non-drought years, respectively. Drought years are 2006, 2011, 2013, 2014, 2018 and non-drought years are 2007-2010, 2015-2017, 2019.

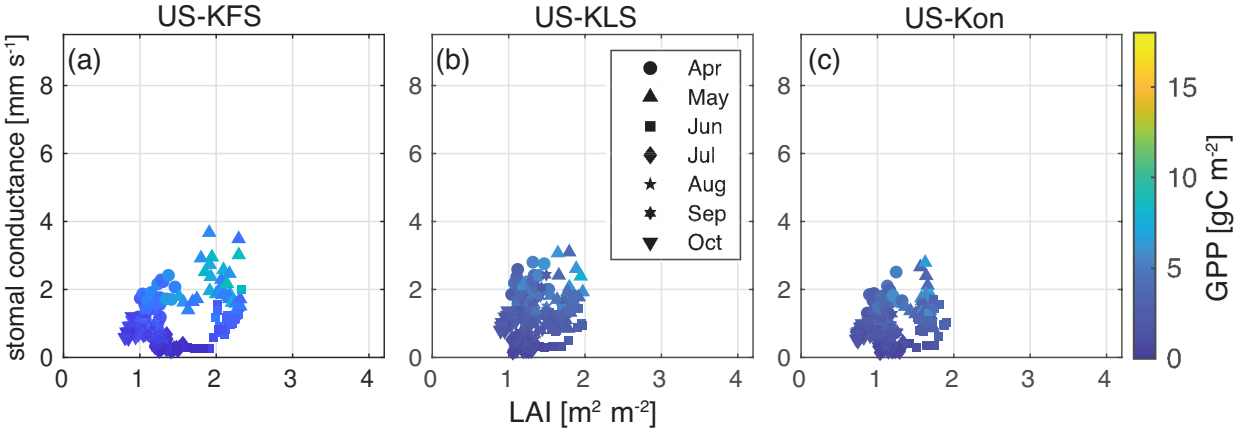

Figure A7. ~~MODIS (MOD17A2H)~~ Daily stomatal conductance [mm s^{-1}] vs ~~DCHM-PV (DRY~~leaf area index, ~~WET, and 3YR)~~ LAI [m^2 m^{-2}] for all three sites during the flash drought of 2012. Marker shapes indicate individual days from April 1 - October 31 from the selected year. Each month is given a unique shape and daily totals of gross primary productivity [gC m^{-2}] are indicated by color.

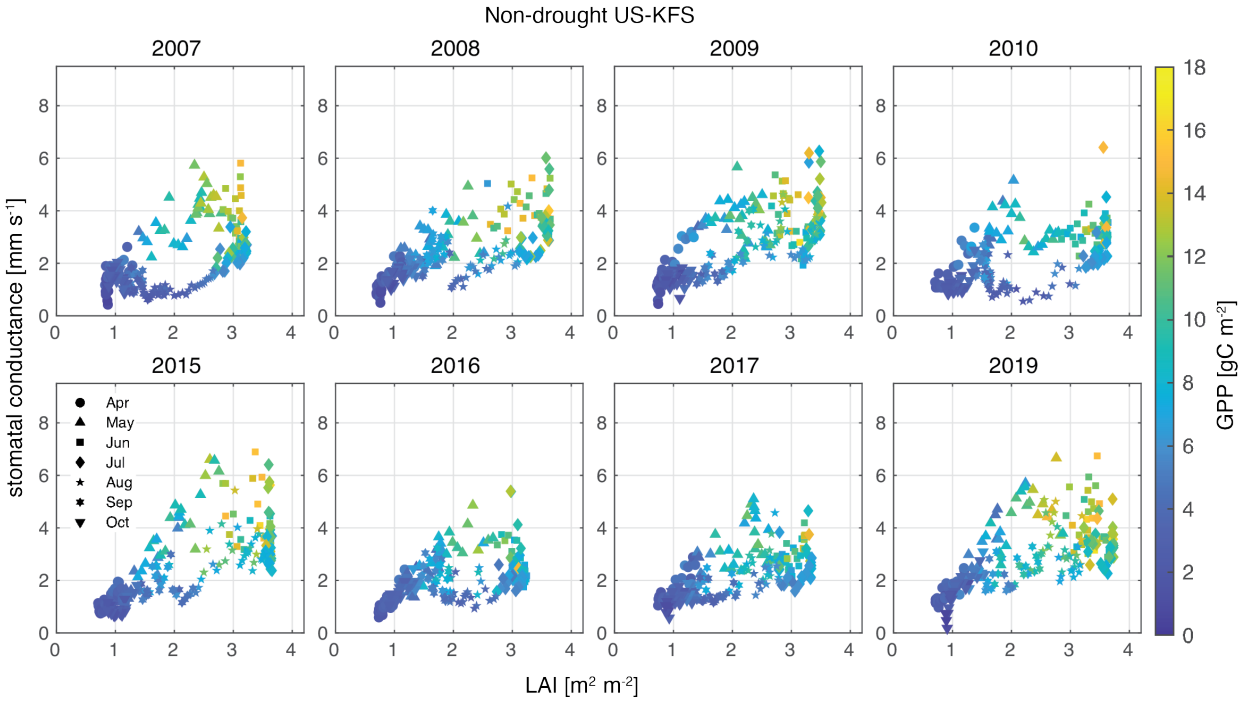

Figure A8. Daily stomatal conductance [mm s^{-1}] vs leaf area index, LAI [m^2 m^{-2}] for US-KFS for selected non-drought years. Marker shapes indicate individual days from April 1 - October 31 from the selected drought year. Each month is given a unique shape and daily totals of gross primary productivity [gC m^{-2}] are indicated by color.

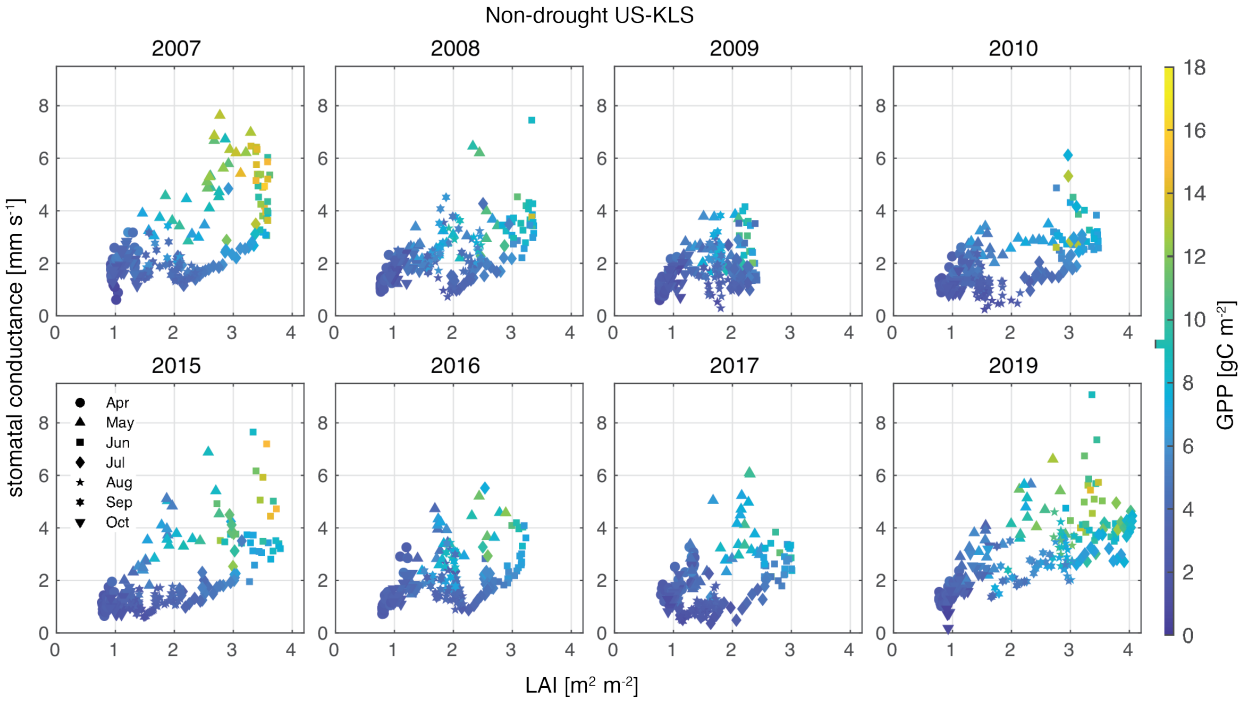

Figure A9. ~~MODIS (MOD17A2H)~~ Daily stomatal conductance [mm s^{-1}] vs ~~DCHM-PV (DRY~~leaf area index, ~~WET~~LAI [m^2 m^{-2}] for US-KLS for selected non-drought years. Marker shapes indicate individual days from April 1 - October 31 from the selected drought year. Each month is given a unique shape and daily totals of gross primary productivity [gC m^{-2}] are indicated by color.

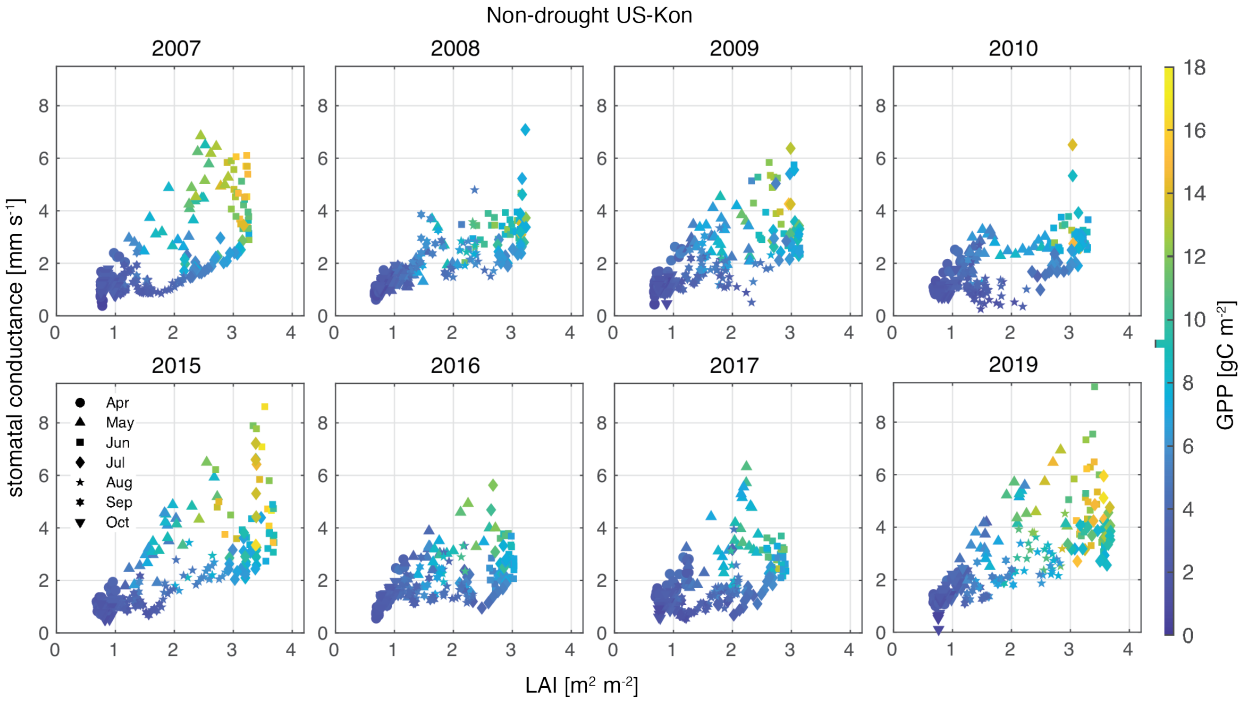

Figure A10. Daily stomatal conductance [mm s^{-1}] vs leaf area index, LAI [m^2 m^{-2}] for US-Kon for selected non-drought years. Marker shapes indicate individual days from April 1 - October 31 from the selected drought year. Each month is given a unique shape and ~~3YR)~~ daily totals of gross primary productivity [gC m^{-2}] are indicated by color.

Figure A11. Daily stomatal conductance [mm s^{-1}] vs leaf area index, LAI [m^2 m^{-2}] for all three study sites ~~during 2012.~~for selected drought years. Marker shapes indicate individual days from April 1 - October 31 from the selected drought year. Each month is given a unique shape and daily totals of gross primary productivity [gC m^{-2}] are indicated by color.

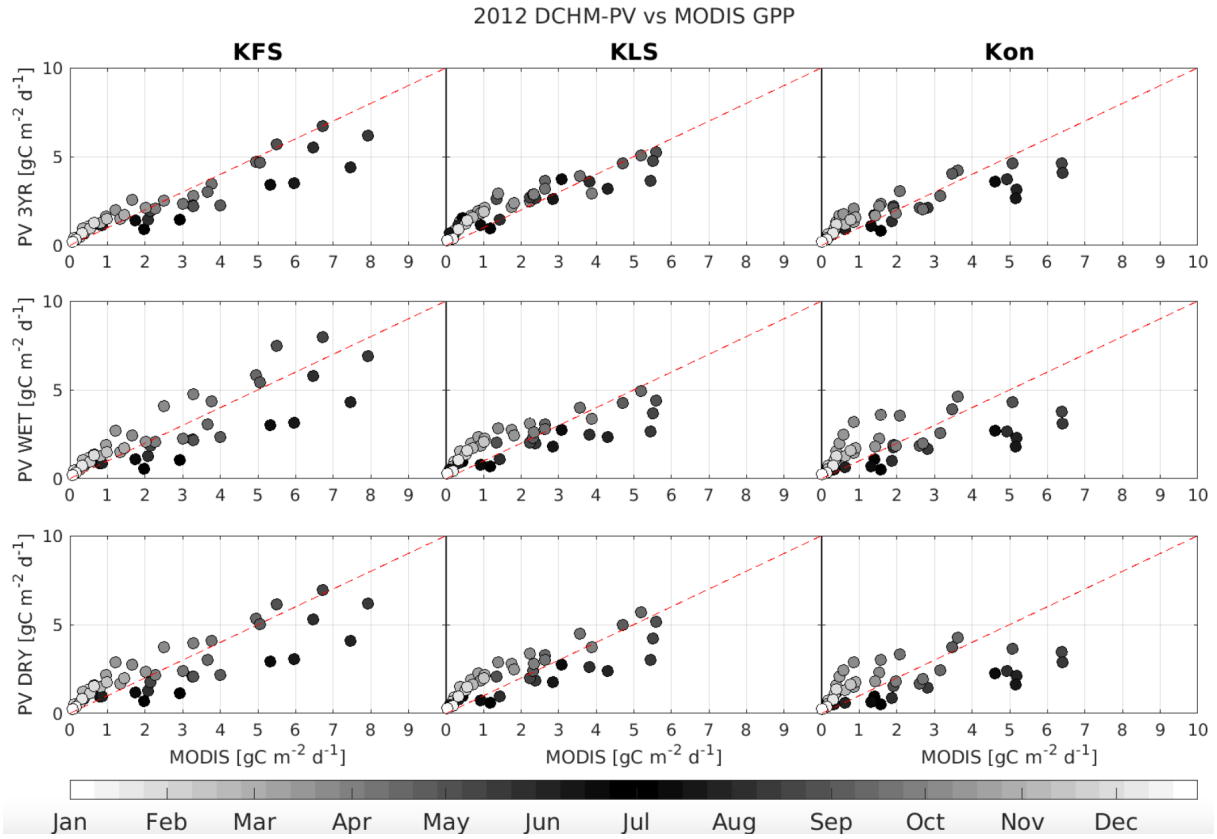

Figure A12. MODIS (MOD17A2H) vs DCHM-PV 3YR, WET, and DRY for all three sites during 2012.

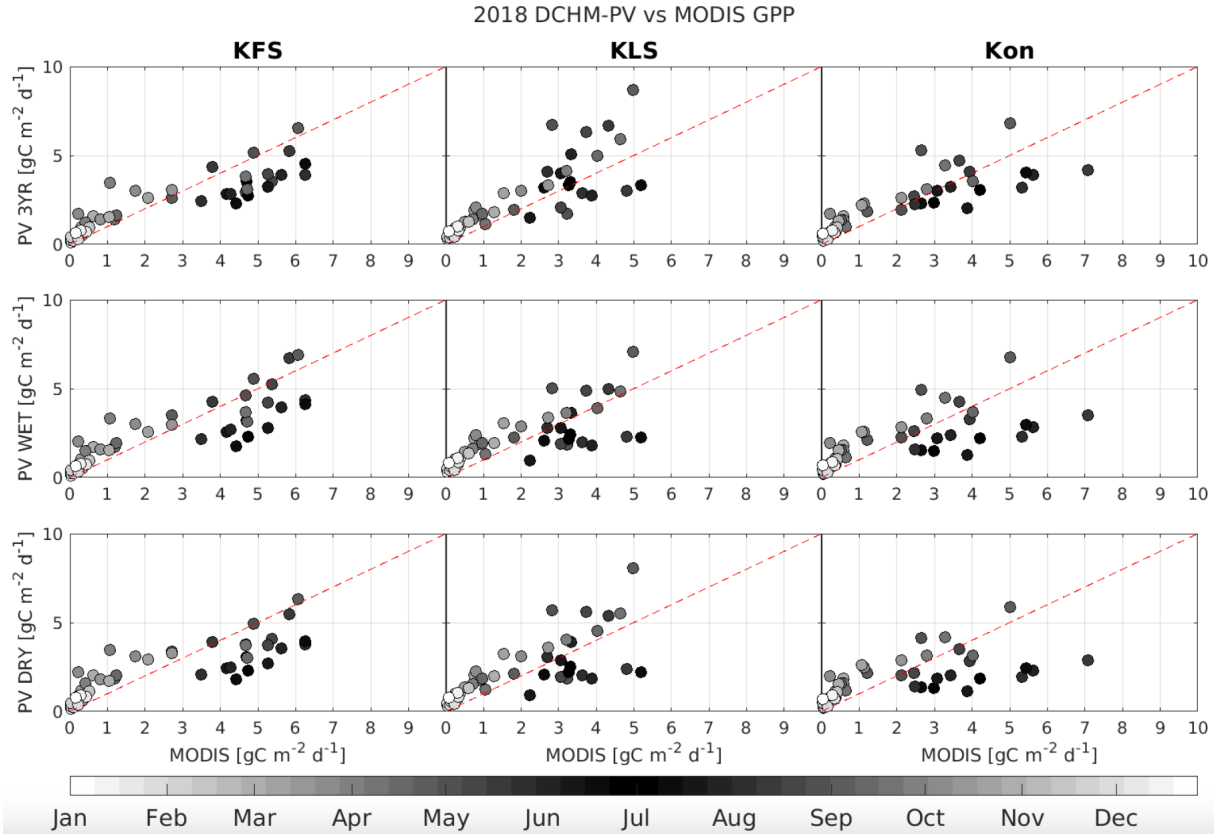

Figure A13. MODIS (MOD17A2H) vs DCHM-PV 3YR, WET, and DRY for all three sites during 2018.

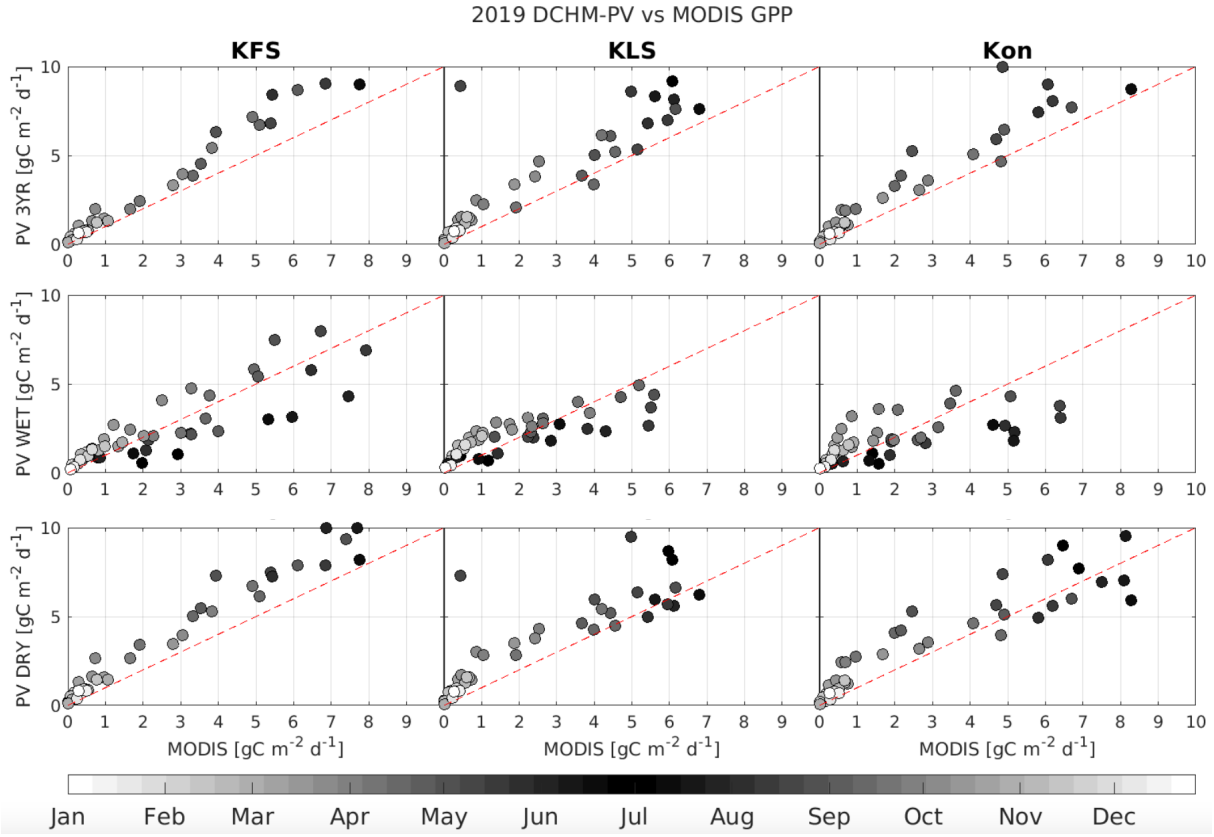

Figure A14. MODIS (MOD17A2H) vs DCHM-PV 3YR, WET, and DRY for all three sites during 2019.

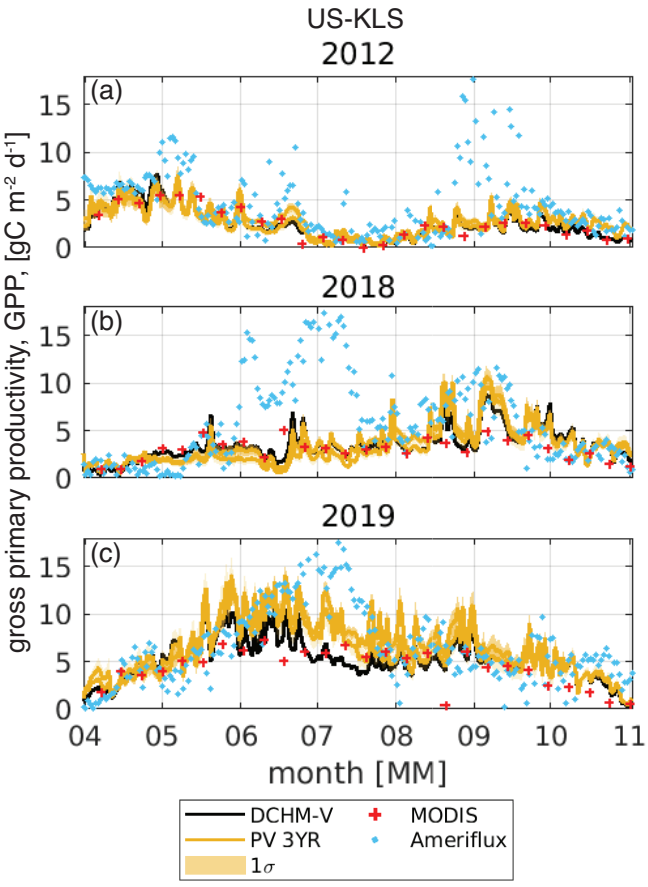

Figure A15. ~~Time series from the DCHM-V~~Daily gross primary productivity, ~~DCHM-PV three year assimilation period~~GPP, ~~8 day MODIS~~at US-KLS for (a) 2012 flash drought, (b) 2018 drought and ~~daily~~ (c) 2019 a non-drought year. One standard deviation is shown as a shaded region for the DCHM-PV simulations. MODIS GPP are shown as red crosses and AmeriFlux ~~totals~~ GPP as blue dots. series of gross primary productivity, GPP, at US-KLS for (a) 2012, flash drought~~year and~~ , (b) 2018 drought and (c) 2019 ~~, an above average precipitation~~ a non-drought year. One standard deviation is shown for the DCHM-PV simulations. MODIS GPP are shown as red crosses and AmeriFlux GPP as small dots.

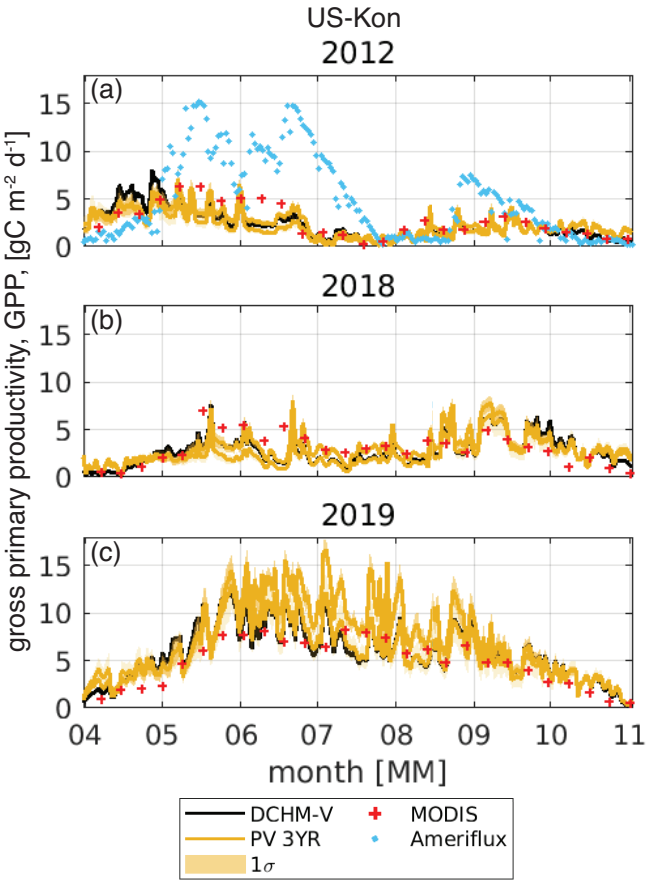

Figure A16. ~~Time series from the DCHM-V~~Daily gross primary productivity, ~~DCHM-PV three year assimilation period, 8 day MODIS, and daily AmeriFlux totals of~~ GPP, at US-Kon for (a) 2012 ~~,~~ flash drought~~year and~~ , (b) 2018 drought and (c) 2019 ~~, an above average precipitation~~ a non-drought year. One standard deviation is shown as a shaded region for the DCHM-PV simulations. MODIS GPP are shown as red crosses and AmeriFlux GPP as blue dots.

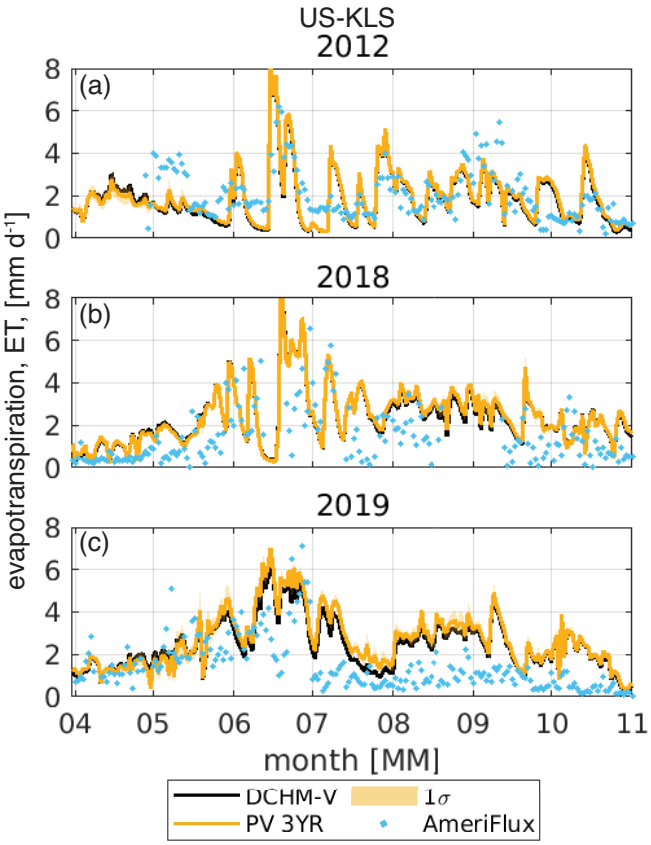

Figure A17. ~~Time series of~~ Daily evapotranspiration, ET, [mm d^{-1}], at US-KLS for (a) 2012 ~~,~~ flash drought~~year and ,~~ (b) 2018 drought and (c) 2019 ~~, wet~~ a non-drought year~~from DCHM-V and three different DCHM-PV simulations~~. Two standard deviations are shown for the DCHM-PV simulations. AmeriFlux ET is ~~showing with the~~ derived from latent heat measurements and shown as blue ~~markers~~dots.

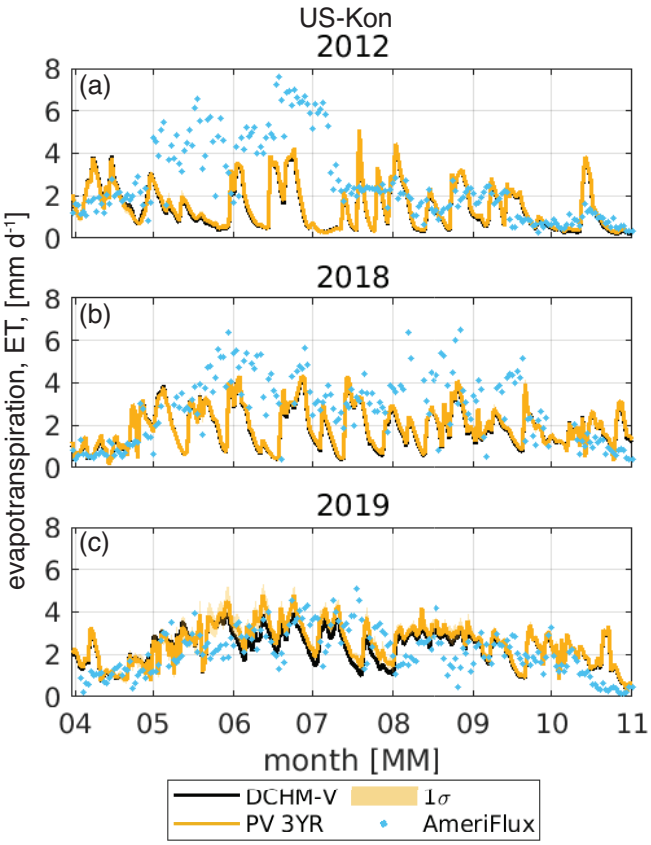

Figure A18. ~~Time series of~~ Daily evapotranspiration, ET, [mm d^{-1}], at US-Kon for (a) 2012 ~~,~~ flash drought~~year and ,~~ (b) 2018 drought and (c) 2019 ~~, wet~~ a non-drought year~~from DCHM-V and three different DCHM-PV simulations~~. Two standard deviations are shown for the DCHM-PV simulations. AmeriFlux ET is ~~showing with the~~ derived from latent heat measurements and shown as blue ~~markers~~dots.

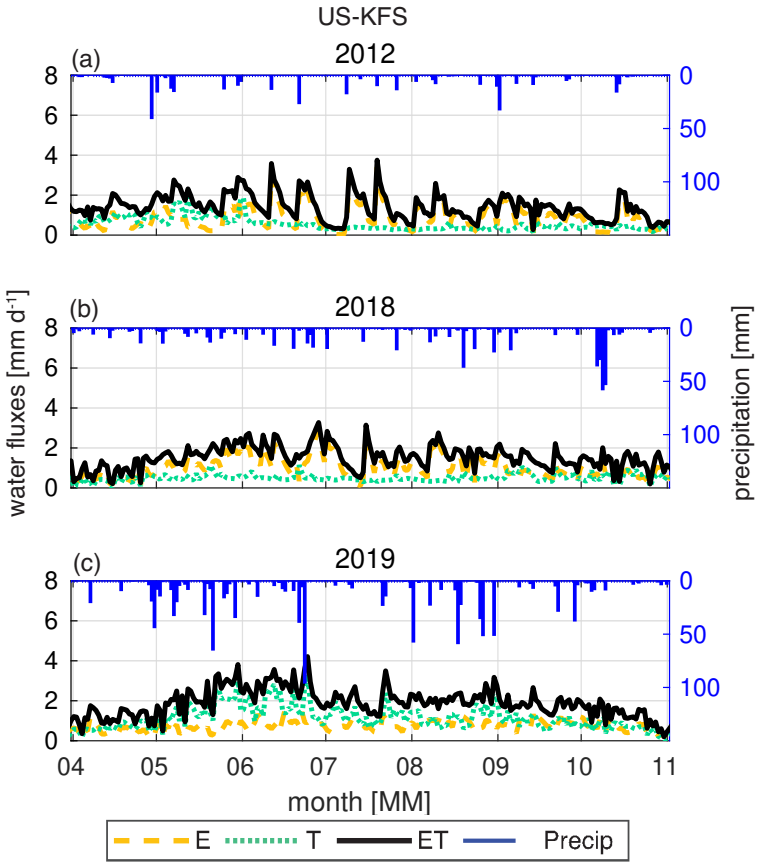

Figure A19. ~~Simulated~~ Daily evapotranspiration, ET, partitioned into evaporation~~(~~, E~~)~~, and transpiration~~(~~, T~~) for US-KLS~~, in mm d^{-1} at US-KFS for (a) 2012 ~~,~~ flash drought~~and~~, (b) ~~2019~~2018 drought, ~~wet~~ and (c) a 2019 non-drought year. ~~Transpiration totals are in DCHM~~ The curves represent ensemble means from ~~total root uptake across~~ the ~~three soil layers~~DCHM-PV 3YR. ~~The top axis is daily StageIV~~ Daily precipitation ~~totals~~accumulation is shown on the right axis.

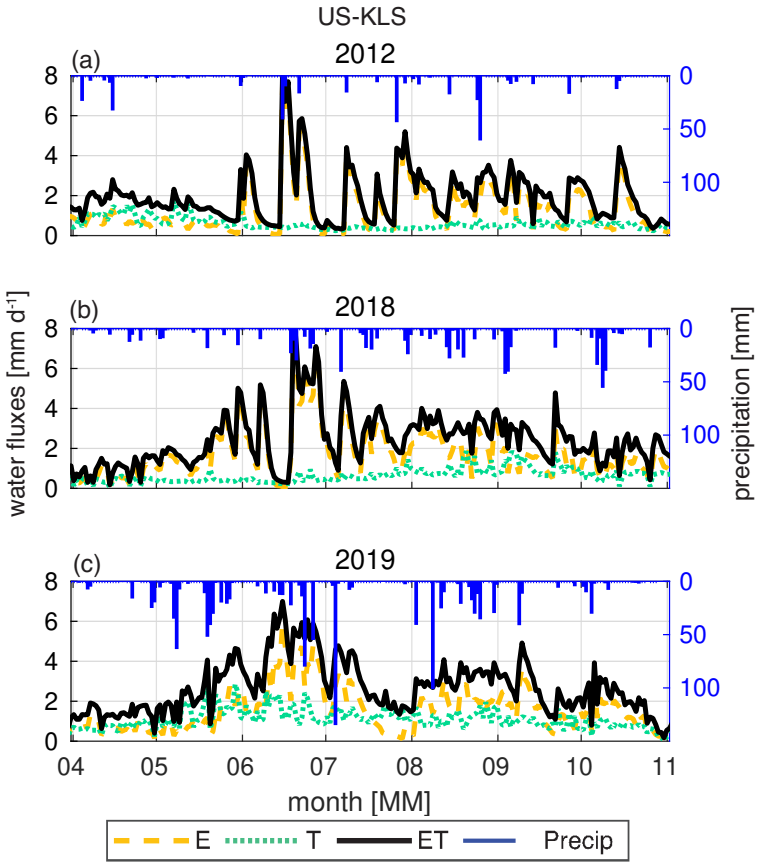

Figure A20. Daily evapotranspiration, ET, partitioned into evaporation, E, and transpiration, T, in mm d^{-1} at US-KLS for (a) 2012 flash drought, (b) 2018 drought, and (c) a 2019 non-drought year. The curves represent ensemble means from the DCHM-PV 3YR. Daily precipitation accumulation is shown on the right axis.

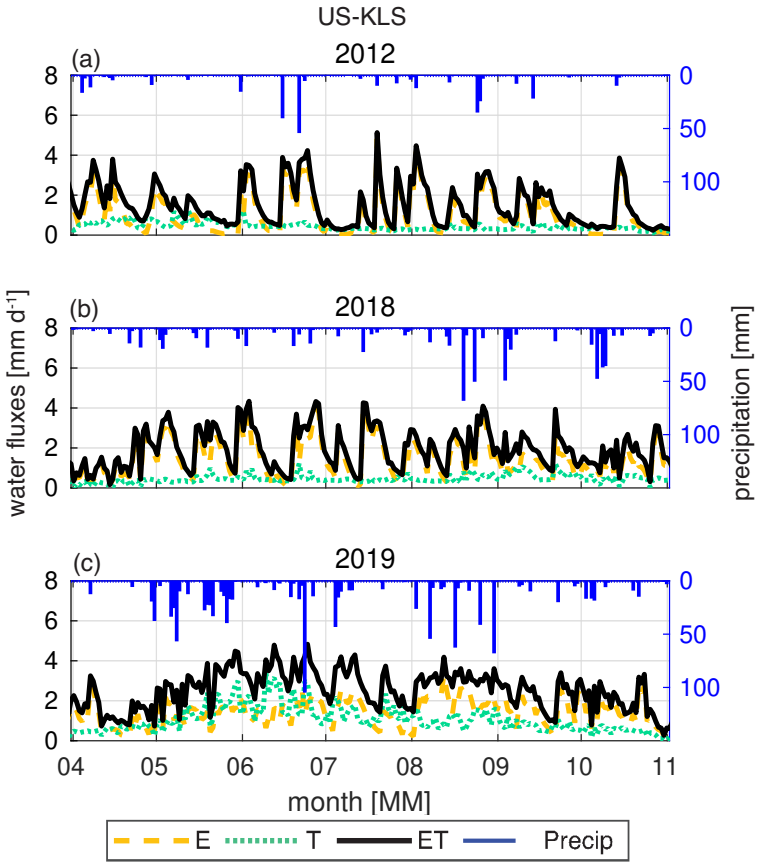

Figure A21. ~~Simulated~~ Daily evapotranspiration, ET, partitioned into evaporation~~(~~, E~~)~~, and transpiration~~(~~, T~~) for US-Kon ~~, in mm d^{-1} at US-Kon for (a) 2012 ~~,~~ flash drought~~and~~ , (b) ~~2019~~2018 drought, ~~wet~~ and (c) a 2019 non-drought year. ~~Transpiration totals are in DCHM~~ The curves represent ensemble means from ~~total root uptake across~~ the ~~three soil layers~~DCHM-PV 3YR. ~~The top axis is daily StageIV~~ Daily precipitation ~~totals~~accumulation is shown on the right axis.

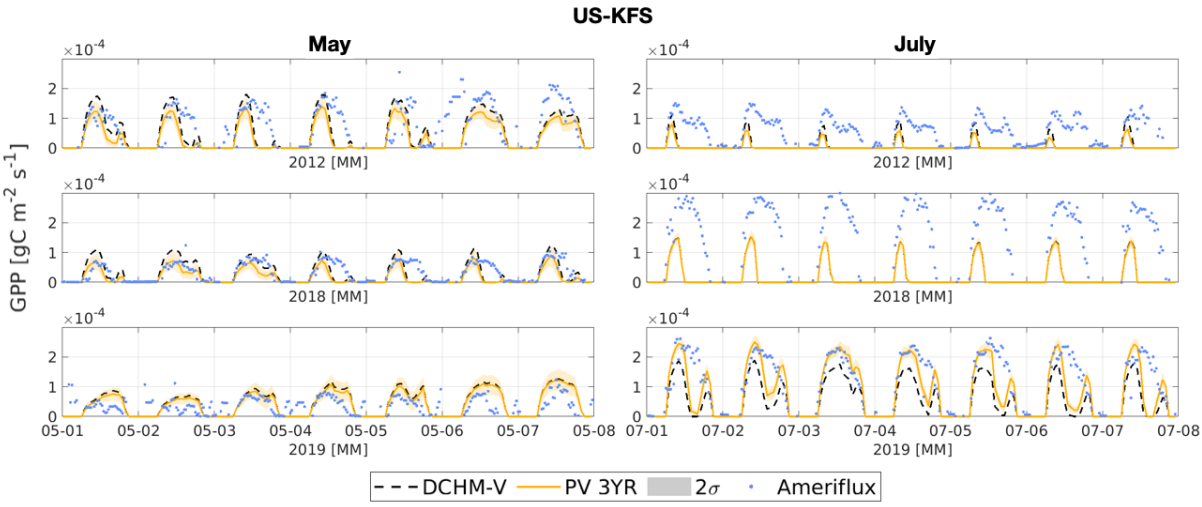

Figure A22. Hourly gross primary productivity [gC m^{-2} s^{-1}] from the DCHM-V and DCHM-PV shown against AmeriFlux 30-minute estimates for one week in May, July, and August of 2012, 2018, and 2019 at US-KFS.

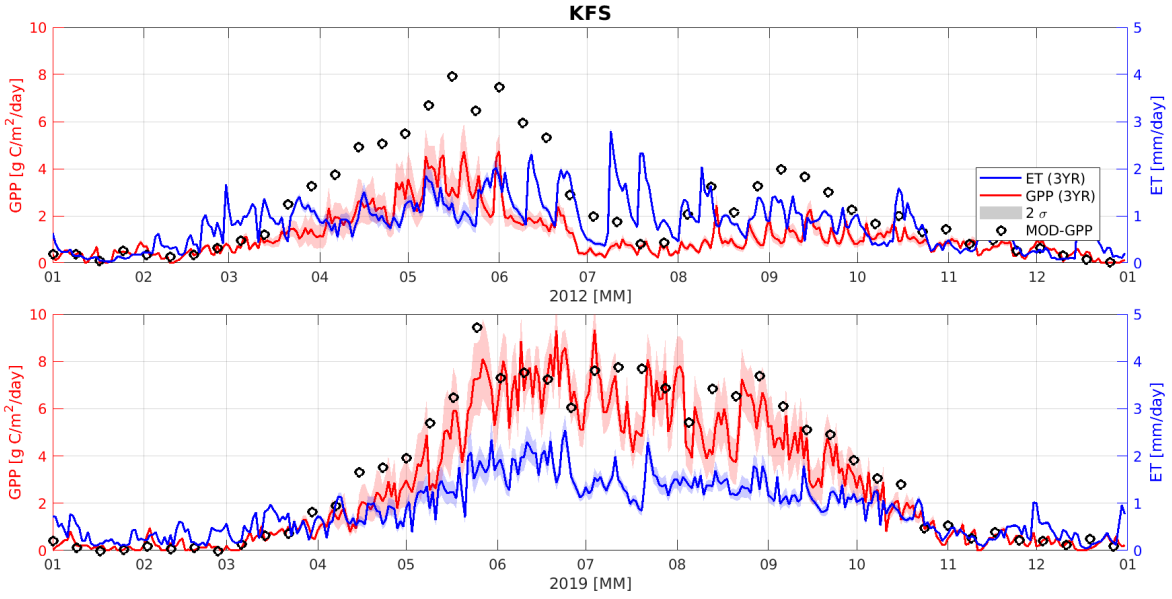

Figure A23. Simulated daily totals of GPP and ET from the DCHM-PV 3YR assimilation period for (a) 2012, flash drought year and (b) 2019, wet year.

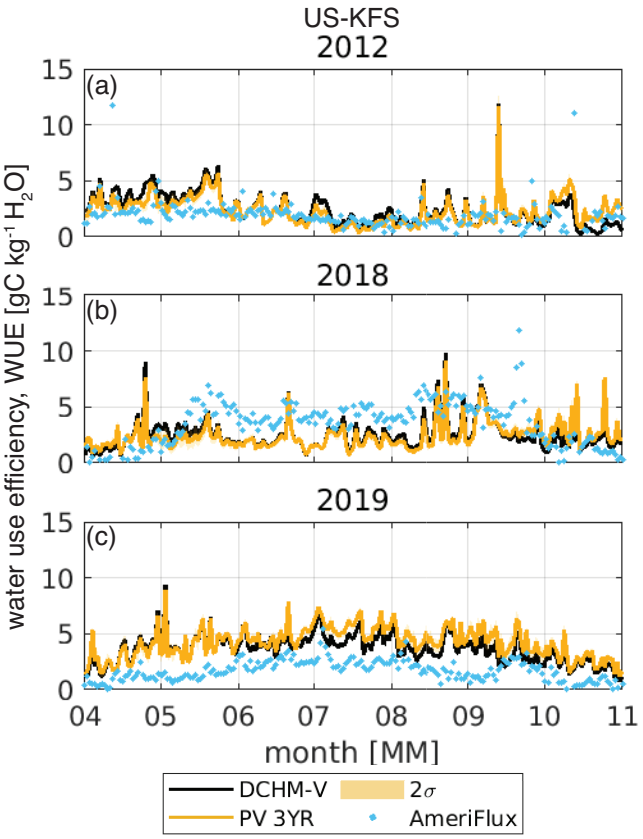

Figure A24. ~~2012 and 2019~~ Growing season water use efficiency (WUE=GPP/ET) from DCHM-V, DCHM-PV (3YR), and AmeriFlux for ~~US-KLS~~(a) 2012 flash drought, (b) 2018 drought, and (c) 2019 non-drought at US-KFS. Ensemble means shown for DCHM-PV with 2 standard deviations (shaded).

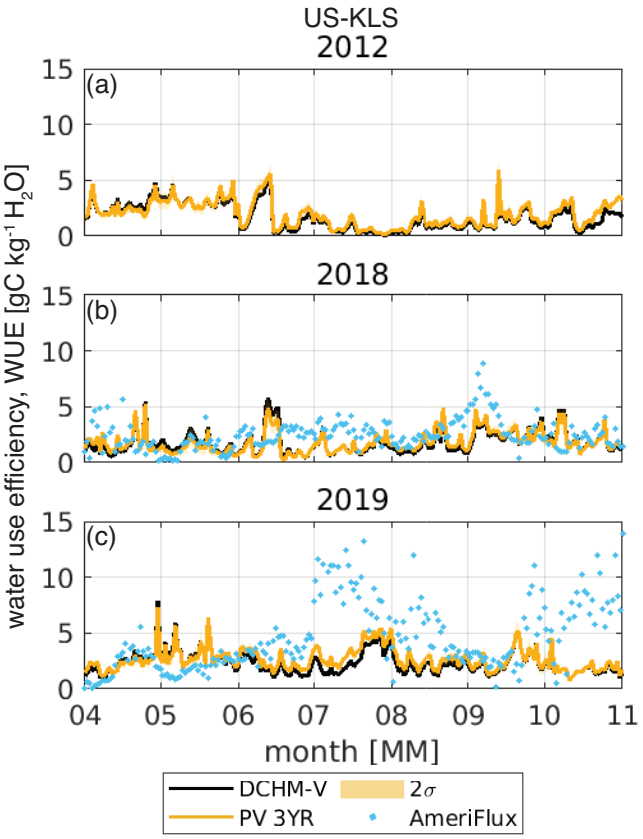

Figure A25. Growing season water use efficiency (WUE=GPP/ET) from DCHM-V, DCHM-PV (3YR), and AmeriFlux for (a) 2012 flash drought, (b) 2018 drought, and (c) 2019 non-drought at US-KLS. Ensemble means shown for DCHM-PV with 2 standard deviations (shaded).

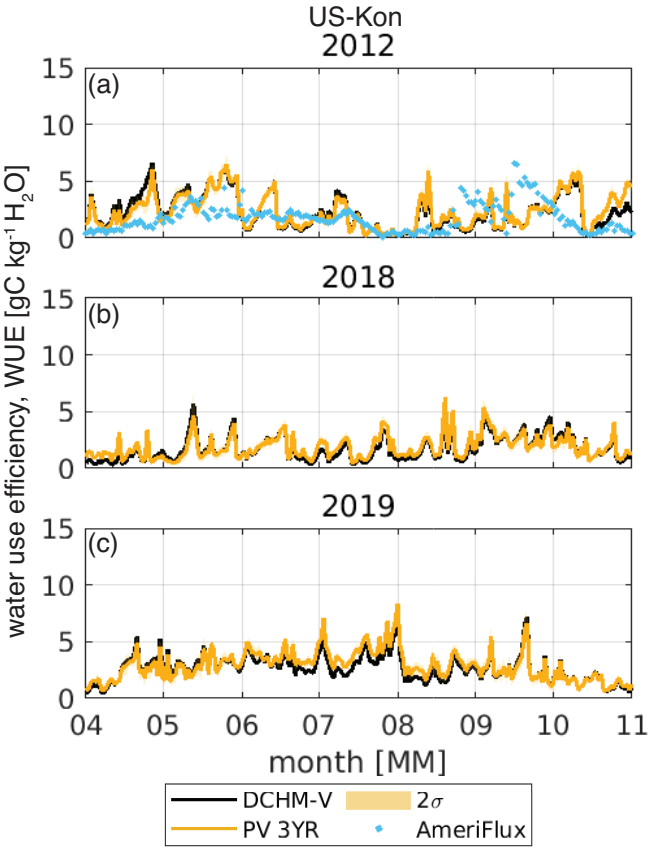

Figure A26. ~~2012 and 2019~~ Growing season water use efficiency (WUE=GPP/ET) from DCHM-V, DCHM-PV (3YR), and AmeriFlux for (a) 2012 flash drought, (b) 2018 drought, and (c) 2019 non-drought at US-Kon. Ensemble means shown for DCHM-PV with 2 standard deviations (shaded).

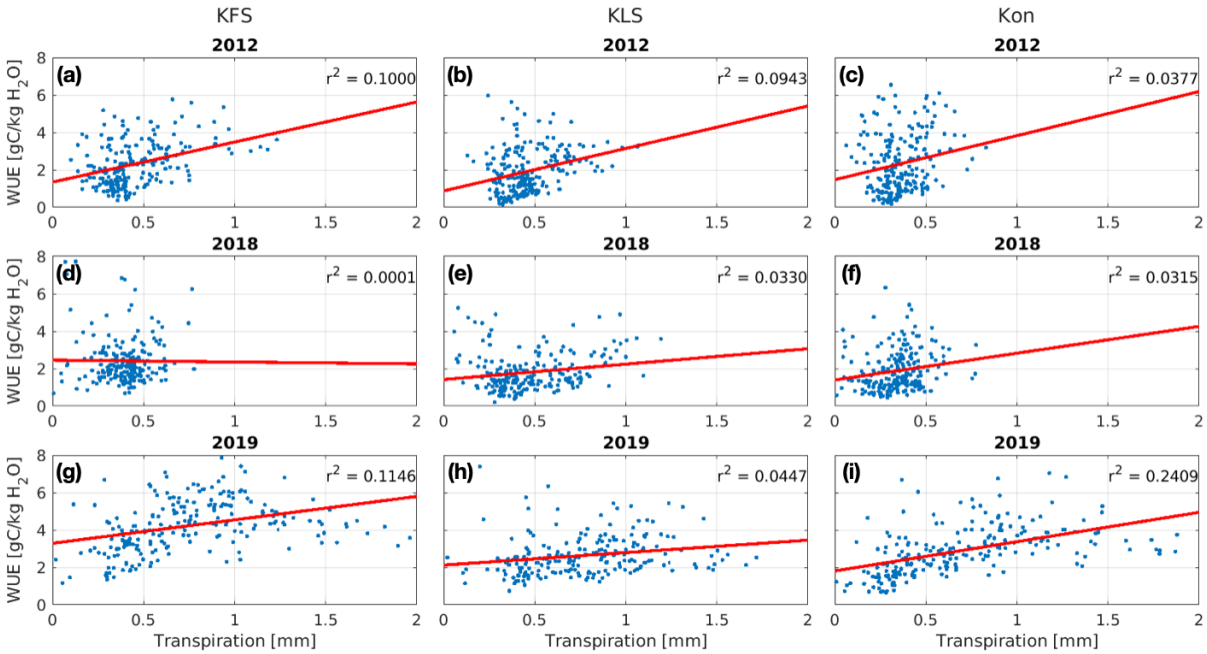

Figure A27. Daily averages of water use efficiency versus transpiration for 2012, 2018, and 2019.

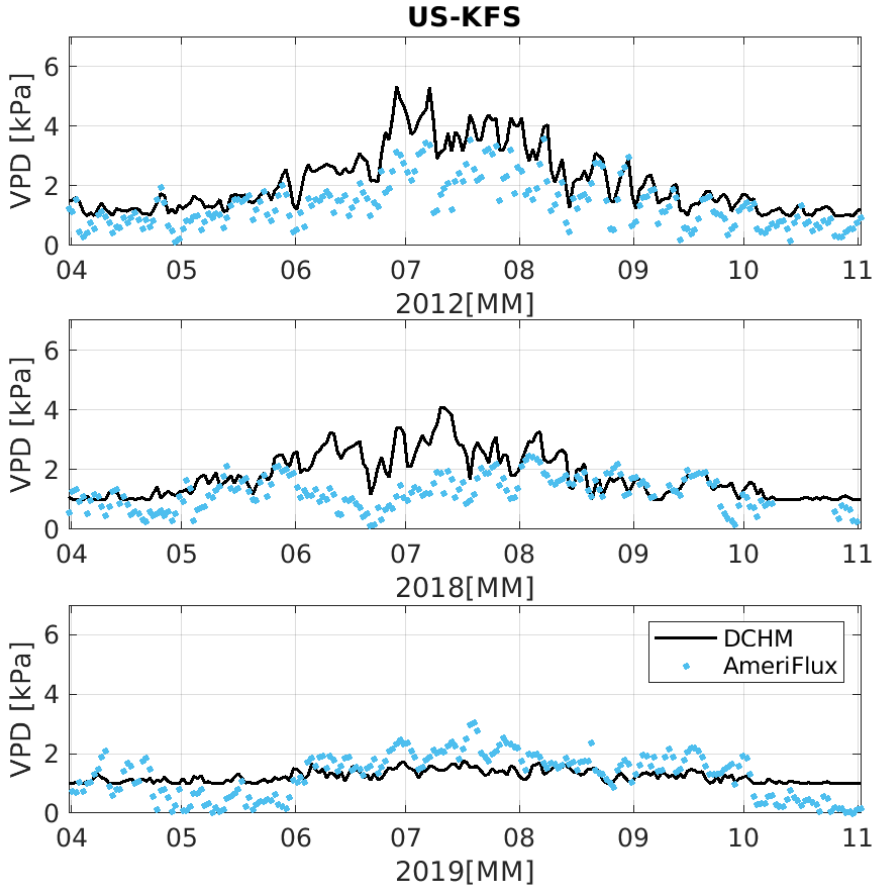

Figure A28. Daily vapor pressure deficit at US-KFS for (a) 2012 - flash drought, (b) 2018 - drought and (c) 2019 - non-drought. The DCHM computes VPD using air temperature and vapor pressure from NLDAS-2 Forcing File A.

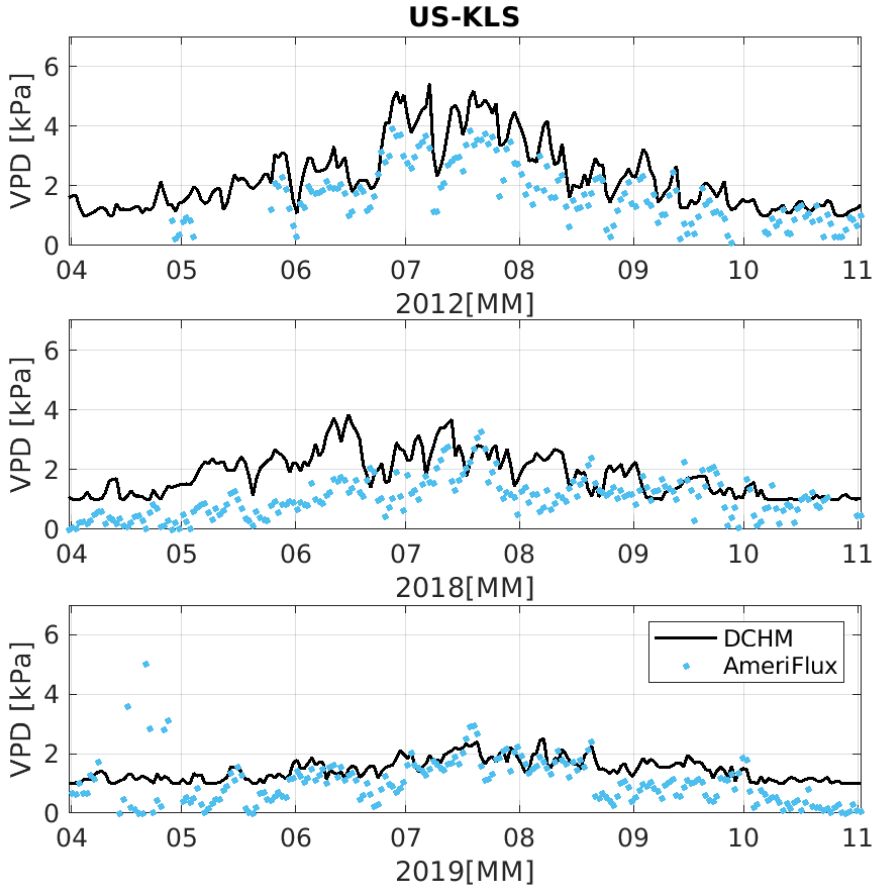

Figure A29. Daily vapor pressure deficit at US-KLS for (a) 2012 - flash drought, (b) 2018 - drought and (c) 2019 - non-drought. The DCHM computes VPD using air temperature and vapor pressure from NLDAS-2 Forcing File A.

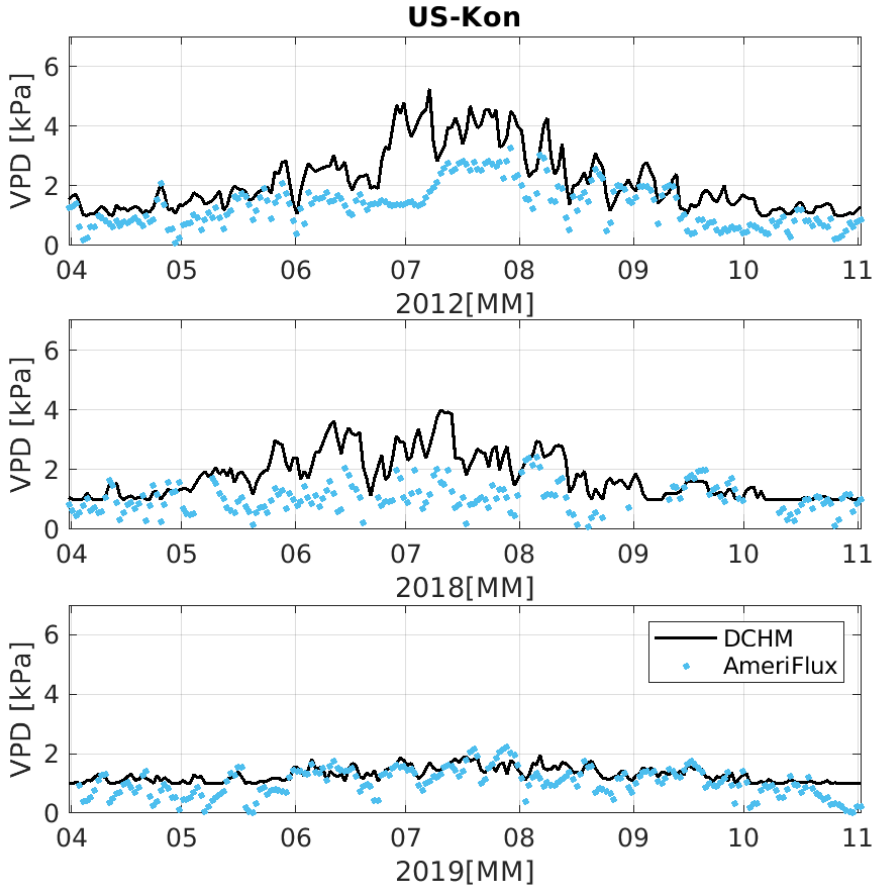

Figure A30. Daily vapor pressure deficit at US-Kon for (a) 2012 - flash drought, (b) 2018 - drought and (c) 2019 - non-drought. The DCHM computes VPD using air temperature and vapor pressure from NLDAS-2 Forcing File A.

Data availability. Results from model simulations are available for download at *****.

Author contributions. TF, JO, and LL conceived the idea for this paper. LL designed the methodology and supervised implementation by NC. NC and LL analyzed results. NC wrote the original draft and prepared the submission. All authors contributed to reviewing and editing the original draft.

Competing interests. The authors declare that no competing interests exist.

Acknowledgements. The forcing data used in this study are available from a variety of sources. The NCEP/EMC Stage IV data were acquired from UCAR/NCAR - Earth Observing Laboratory and are avaiable at https://data.eol.ucar.edu/. NLDAS Phase 2, Noah-MP, and SMERGE data used in this study were acquired as part of the mission of NASA's Earth Science Division and archived and distributed by the Goddard Earth Sciences (GES) Data and Information Services Center (DISC). The MODIS MOD15A2H data were retrieved online from Appeears and distibuted by NASA Land Processes Distributed Active Archive Center (LP DAAC), http://appeears.earthdatacloud.nasa.gov/. Computations were performed using the Wake Forest University (WFU) High Performance Computing Facility, a centrally managed computational resource available to WFU researchers including faculty, staff, students, and collaborators (Information Systems and Wake Forest University, 2021). We acknowledge the following AmeriFlux sites for their data records: US-KFS, US-KLS, US-Kon. In addition, funding for AmeriFlux data resources was provided by the ~~U.S.~~ US Department of Energy's Office of Science. Maps were generated using data from the ~~U.S.~~ US Drought Monitor which is jointly produced by the National Drought Mitigation Center at the University of Nebraska-Lincoln, the United States Department of Agriculture, and the National Oceanic and Atmospheric Administration. This material is based upon work supported by the National Science Foundation under Award Number 2228047.

References

Baldocchi, D., Falge, E., Gu, L., Olson, R., Hollinger, D., Running, S., Anthoni, P., Bernhofer, C., Davis, K., Evans, R., et al.: FLUXNET: A new tool to study the temporal and spatial variability of ecosystem-scale carbon dioxide, water vapor, and energy flux densities, Bulletin of the American Meteorological Society, 82, 2415–2434, 2001.

Baldocchi, D. D.: Assessing the eddy covariance technique for evaluating carbon dioxide exchange rates of ecosystems: past, present and future, Global change biology, 9, 479–492, 2003.

Baldwin, M. and Mitchell, K.: Progress on the NCEP hourly multi-sensor US precipitation analysis for operations and GCIP research, WORLD METEOROLOGICAL ORGANIZATION-PUBLICATIONS-WMO TD, pp. 1–7, 1998.

Barros, A. P.: Adaptive multilevel modeling of land-atmosphere interactions, Journal of climate, 8, 2144–2160, 1995.

Basara, J. B., Christian, J. I., Wakefield, R. A., Otkin, J. A., Hunt, E. H., and Brown, D. P.: The evolution, propagation, and spread of flash drought in the Central United States during 2012, Environmental Research Letters, 14, 084 025, 2019.

Beer, C., Ciais, P., Reichstein, M., Baldocchi, D., Law, B., Papale, D., Soussana, J.-F., Ammann, C., Buchmann, N., Frank, D., et al.: Temporal and among-site variability of inherent water use efficiency at the ecosystem level, Global biogeochemical cycles, 23, 2009.

Brunsell, N.: AmeriFlux BASE US-KFS Kansas Field Station, Ver. 7-5, AmeriFlux AMP, (Dataset), https://doi.org/10.17190/AMF/1246132, 2020a.

Brunsell, N.: AmeriFlux BASE US-Kon Konza Prairie LTER (KNZ), Ver. 5-5, AmeriFlux AMP, (Dataset), https://doi.org/10.17190/AMF/1246068, 2020b.

Brunsell, N.: AmeriFlux BASE US-KLS Kansas Land Institute, Ver. 2-5, AmeriFlux AMP, (Dataset), https://doi.org/10.17190/AMF/1498745, 2021.

Caldararu, S., Purves, D., and Palmer, P.: Phenology as a strategy for carbon optimality: a global model, Biogeosciences, 11, 763–778, 2014.

Chen, J., Jönsson, P., Tamura, M., Gu, Z., Matsushita, B., and Eklundh, L.: A simple method for reconstructing a high-quality NDVI time-series data set based on the Savitzky–Golay filter, Remote sensing of Environment, 91, 332–344, https://doi.org/10.1016/j.rse.2004.03.014, 2004.

Chen, L., Ford, T. W., and Yadav, P.: The Role of Vegetation in Flash Drought Occurrence: A Sensitivity Study Using Community Earth System Model, Version 2, Journal of Hydrometeorology, 22, 845–857, https://doi.org/10.1175/JHM-D-20-0214.1, 2021.

Chen, L. G., Gottschalck, J., Hartman, A., Miskus, D., Tinker, R., and Artusa, A.: Flash drought characteristics based on US drought monitor, Atmosphere, 10, 498, 2019.

Christian, J. I., Basara, J. B., Lowman, L. E., Xiao, X., Mesheske, D., and Zhou, Y.: Flash drought identification from satellite-based land surface water index, Remote Sensing Applications: Society and Environment, 26, 100 770, 2022.

Christian, J. I., Minor, E. R., Basara, J. B., , Furtado, J. C., , Otkin, J. A., Lowman, L. E. L., Hunt, E. D., Mishra, V., and Xiao, X.: Global projections of flash drought show increased risk in a warming climate, Communications Earth and Environment, 4, 165, https://doi.org/10.1038/s43247-023-00826-1, 2023.

Chu, H., Luo, X., Ouyang, Z., Chan, W. S., Dengel, S., Biraud, S. C., Torn, M. S., Metzger, S., Kumar, J., Arain, M. A., et al.: Representativeness of Eddy-Covariance flux footprints for areas surrounding AmeriFlux sites, Agricultural and Forest Meteorology, 301, 108 350, 2021.

Cihlar, J., Ly, H., Li, Z., Chen, J., Pokrant, H., and Huang, F.: Multitemporal, multichannel AVHRR data sets for land biosphere studies—artifacts and corrections, Remote sensing of environment, 60, 35–57, https://doi.org/10.1016/S0034-4257(96)00137-X, 1997.

Clausnitzer, V. and Hopmans, J.: Simultaneous modeling of transient three-dimensional root growth and soil water flow, Plant and soil, 164, 299–314, 1994.

Cui, T., Martz, L., and Guo, X.: Grassland phenology response to drought in the Canadian prairies, Remote Sensing, 9, 1258, 2017.

Dai, A.: Increasing drought under global warming in observations and models, Nature climate change, 3, 52–58, 2013.

Dai, S., Shulski, M. D., Hubbard, K. G., and Takle, E. S.: A spatiotemporal analysis of Midwest US temperature and precipitation trends during the growing season from 1980 to 2013, International Journal of Climatology, 36, 517–525, 2016.

Devonec, E. and Barros, A. P.: Exploring the transferability of a land-surface hydrology model, Journal of Hydrology, 265, 258–282, 2002.

Dietze, M. C.: Prediction in ecology: A first-principles framework, Ecological Applications, 27, 2048–2060, 2017.

Dietze, M. C., Lebauer, D. S., and Kooper, R.: On improving the communication between models and data, Plant, Cell & Environment, 36, 1575–1585, 2013.

Dingman, S. L.: Physical hydrology, Waveland press, 2015.

Du, J.: NCEP/EMC 4KM Gridded Data (GRIB) Stage IV Data. Version 1.0, https://doi.org/10.5065/D6PG1QDD, 2011.

Farquhar, G. D. and Caemmerer, S. v.: Modelling of photosynthetic response to environmental conditions, in: Physiological plant ecology II, pp. 549–587, Springer, 1982.

Farquhar, G. D. and Sharkey, T. D.: Stomatal conductance and photosynthesis, Annual review of plant physiology, 33, 317–345, 1982.

Farquhar, G. D., von Caemmerer, S. v., and Berry, J. A.: A biochemical model of photosynthetic CO2 assimilation in leaves of C3 species, planta, 149, 78–90, 1980.

Flack-Prain, S., Meir, P., Malhi, Y., Smallman, T. L., and Williams, M.: The importance of physiological, structural and trait responses to drought stress in driving spatial and temporal variation in GPP across Amazon forests, Biogeosciences, 16, 4463–4484, 2019.

Ford, T. W. and Labosier, C. F.: Meteorological conditions associated with the onset of flash drought in the eastern United States, Agricultural and forest meteorology, 247, 414–423, https://doi.org/10.1016/j.agrformet.2017.08.031, 2017.

Friedl, M. and Sulla-Menashe, D.: MCD12Q1 MODIS, Terra+ Aqua Land cover type yearly L3 global 500m SIN grid, 6, 2015.

Garcia-Forner, N., Biel, C., Savé, R., and Martínez-Vilalta, J.: Isohydric species are not necessarily more carbon limited than anisohydric species during drought, Tree physiology, 37, 441–455, 2017.

Garcia-Quijano, J. F. and Barros, A. P.: Incorporating canopy physiology into a hydrological model: photosynthesis, dynamic respiration, and stomatal sensitivity, Ecological Modelling, 185, 29–49, 2005.

Gebremichael, M. and Barros, A. P.: Evaluation of MODIS gross primary productivity (GPP) in tropical monsoon regions, Remote Sensing of Environment, 100, 150–166, 2006.

Gerken, T., Bromley, G. T., Ruddell, B. L., Williams, S., and Stoy, P. C.: Convective suppression before and during the United States Northern Great Plains flash drought of 2017, Hydrology and Earth System Sciences, 22, 4155–4163, 2018.

Giardina, F., Gentine, P., Konings, A. G., Seneviratne, S. I., and Stocker, B. D.: Diagnosing evapotranspiration responses to water deficit across biomes using deep learning, New Phytologist, 2023.

Grossiord, C., Buckley, T. N., Cernusak, L. A., Novick, K. A., Poulter, B., Siegwolf, R. T., Sperry, J. S., and McDowell, N. G.: Plant responses to rising vapor pressure deficit, New Phytologist, 226, 1550–1566, 2020.

Guo, J. S., Hultine, K. R., Koch, G. W., Kropp, H., and Ogle, K.: Temporal shifts in iso/anisohydry revealed from daily observations of plant water potential in a dominant desert shrub, New Phytologist, 225, 713–726, 2020.

He, M., Kimball, J. S., Yi, Y., Running, S., Guan, K., Jensco, K., Maxwell, B., and Maneta, M.: Impacts of the 2017 flash drought in the US Northern plains informed by satellite-based evapotranspiration and solar-induced fluorescence, Environmental Research Letters, 14, 074 019, https://doi.org/10.1088/1748-9326/ab22c3, 2019.

He, W., Ju, W., Schwalm, C. R., Sippel, S., Wu, X., He, Q., Song, L., Zhang, C., Li, J., Sitch, S., et al.: Large-scale droughts responsible for dramatic reductions of terrestrial net carbon uptake over North America in 2011 and 2012, Journal of Geophysical Research: Biogeosciences, 123, 2053–2071, https://doi.org/10.1029/2018JG004520, 2018.

Heinsch, F. A., Zhao, M., Running, S. W., Kimball, J. S., Nemani, R. R., Davis, K. J., Bolstad, P. V., Cook, B. D., Desai, A. R., Ricciuto, D. M., et al.: Evaluation of remote sensing based terrestrial productivity from MODIS using regional tower eddy flux network observations, IEEE transactions on geoscience and remote sensing, 44, 1908–1925, 2006.

Hochberg, U., Rockwell, F. E., Holbrook, N. M., and Cochard, H.: Iso/anisohydry: a plant–environment interaction rather than a simple hydraulic trait, Trends in plant science, 23, 112–120, 2018.

Hosseini, A., Mocko, D. M., Brunsell, N., Kumar, S. V., Mahanama, S. P., Arsenault, K., and Roundy, J.: Understanding the Impact of Vegetation Dynamics on the Water Cycle in the Noah-MP Model, Frontiers in Water, p. 136, 2022.

Hu, Z., Yu, G., Fu, Y., Sun, X., Li, Y., Shi, P., Wang, Y., and Zheng, Z.: Effects of vegetation control on ecosystem water use efficiency within and among four grassland ecosystems in China, Global Change Biology, 14, 1609–1619, 2008.

Hunt, E. D., Svoboda, M., Wardlow, B., Hubbard, K., Hayes, M., and Arkebauer, T.: Monitoring the effects of rapid onset of drought on non-irrigated maize with agronomic data and climate-based drought indices, Agricultural and Forest Meteorology, 191, 1–11, 2014.

Information Systems and Wake Forest University: WFU High Performance Computing Facility, https://doi.org/10.57682/G13Z-2362, 2021.

Ingrisch, J., Karlowsky, S., Hasibeder, R., Gleixner, G., and Bahn, M.: Drought and recovery effects on belowground respiration dynamics and the partitioning of recent carbon in managed and abandoned grassland, Global Change Biology, 26, 4366–4378, 2020.

Jackson, R. B., Canadell, J., Ehleringer, J. R., Mooney, H., Sala, O., and Schulze, E.-D.: A global analysis of root distributions for terrestrial biomes, Oecologia, 108, 389–411, 1996.

Jin, C., Luo, X., Xiao, X., Dong, J., Li, X., Yang, J., and Zhao, D.: The 2012 flash drought threatened US Midwest agroecosystems, Chinese Geographical Science, 29, 768–783, https://doi.org/10.1007/s11769-019-1066-7, 2019.

Jolly, W. M., Nemani, R., and Running, S. W.: A generalized, bioclimatic index to predict foliar phenology in response to climate, Global Change Biology, 11, 619–632, 2005.

Kannenberg, S. A., Guo, J. S., Novick, K. A., Anderegg, W. R., Feng, X., Kennedy, D., Konings, A. G., Martínez-Vilalta, J., and Matheny, A. M.: Opportunities, challenges and pitfalls in characterizing plant water-use strategies, Functional Ecology, 36, 24–37, 2022.

Katul, G., Lai, C.-T., Schäfer, K., Vidakovic, B., Albertson, J., Ellsworth, D., and Oren, R.: Multiscale analysis of vegetation surface fluxes: from seconds to years, Advances in Water Resources, 24, 1119–1132, 2001.

Kim, Y., Moorcroft, P., Aleinov, I., Puma, M., and Kiang, N.: Variability of phenology and fluxes of water and carbon with observed and simulated soil moisture in the Ent Terrestrial Biosphere Model (Ent TBM version 1.0. 1.0. 0), Geoscientific Model Development, 8, 3837–3865, 2015.

Kimball, J. S., Jones, L., Jensco, K., He, M., Maneta, M., and Reichle, R.: SMAP L4 assessment of the US northern plains 2017 flash drought, in: IGARSS 2019-2019 IEEE International Geoscience and Remote Sensing Symposium, pp. 5366–5369, IEEE, 2019.

Kirono, D. G., Round, V., Heady, C., Chiew, F. H., and Osbrough, S.: Drought projections for Australia: Updated results and analysis of model simulations, Weather and Climate Extremes, 30, 100 280, 2020.

Konings, A. G. and Gentine, P.: Global variations in ecosystem-scale isohydricity, Global change biology, 23, 891–905, 2017.

Kumar, S. V., Mocko, D. M., Wang, S., Peters-Lidard, C. D., and Borak, J.: Assimilation of remotely sensed leaf area index into the Noah-MP land surface model: Impacts on water and carbon fluxes and states over the continental United States, Journal of Hydrometeorology, 20, 1359–1377, 2019.

Lai, C.-T. and Katul, G.: The dynamic role of root-water uptake in coupling potential to actual transpiration, Advances in Water Resources, 23, 427–439, 2000.

Lawson, T. and Vialet-Chabrand, S.: Speedy stomata, photosynthesis and plant water use efficiency, New Phytologist, 221, 93–98, 2019.

Li, L., Yang, Z.-L., Matheny, A. M., Zheng, H., Swenson, S. C., Lawrence, D. M., Barlage, M., Yan, B., McDowell, N. G., and Leung, L. R.: Representation of plant hydraulics in the Noah-MP land surface model: Model development and multiscale evaluation, Journal of Advances in Modeling Earth Systems, 13, e2020MS002 214, 2021.

Lisonbee, J., Woloszyn, M., and Skumanich, M.: Making sense of flash drought: Definitions, indicators, and where we go from here, J. Appl. Serv. Climatol, 2021, 1–19, https://doi.org/10.46275/JOASC.2021.02.001, 2021.

Liu, Y., Kumar, M., Katul, G. G., Feng, X., and Konings, A. G.: Plant hydraulics accentuates the effect of atmospheric moisture stress on transpiration, Nature Climate Change, 10, 691–695, 2020.

Lowman, L. E. and Barros, A. P.: Interplay of drought and tropical cyclone activity in SE US gross primary productivity, Journal of Geophysical Research: Biogeosciences, 121, 1540–1567, https://doi.org/10.1002/2015JG003279, 2016.

Lowman, L. E. and Barros, A. P.: Predicting canopy biophysical properties and sensitivity of plant carbon uptake to water limitations with a coupled eco-hydrological framework, Ecological Modelling, 372, 33–52, 2018.

Lowman, L. E., Christian, J. I., and Hunt, E. D.: How land surface characteristics influence the development of flash drought through the drivers of soil moisture and vapor pressure deficit, Journal of Hydrometeorology, 2023.

Martínez-Vilalta, J., Piñol, J., and Beven, K.: A hydraulic model to predict drought-induced mortality in woody plants: an application to climate change in the Mediterranean, Ecological Modelling, 155, 127–147, 2002.

McCormack, M. L., Adams, T. S., Smithwick, E. A., and Eissenstat, D. M.: Variability in root production, phenology, and turnover rate among 12 temperate tree species, Ecology, 95, 2224–2235, 2014.

McDowell, N., Pockman, W. T., Allen, C. D., Breshears, D. D., Cobb, N., Kolb, T., Plaut, J., Sperry, J., West, A., Williams, D. G., et al.: Mechanisms of plant survival and mortality during drought: why do some plants survive while others succumb to drought?, New phytologist, 178, 719–739, 2008.

Meinzer, F. C.: Co-ordination of vapour and liquid phase water transport properties in plants, Plant, Cell & Environment, 25, 265–274, 2002.

Miller, D. A. and White, R. A.: A conterminous United States multilayer soil characteristics dataset for regional climate and hydrology modeling, Earth interactions, 2, 1–26, 1998.

Mitchell, K. E., Lohmann, D., Houser, P. R., Wood, E. F., Schaake, J. C., Robock, A., Cosgrove, B. A., Sheffield, J., Duan, Q., Luo, L., et al.: The multi-institution North American Land Data Assimilation System (NLDAS): Utilizing multiple GCIP products and partners in a continental distributed hydrological modeling system, Journal of Geophysical Research: Atmospheres, 109, 2004.

Mocko, D. M., Kumar, S. V., Peters-Lidard, C. D., and Wang, S.: Assimilation of vegetation conditions improves the representation of drought over agricultural areas, Journal of Hydrometeorology, 22, 1085–1098, 2021.

Moradkhani, H., Sorooshian, S., Gupta, H. V., and Houser, P. R.: Dual state–parameter estimation of hydrological models using ensemble Kalman filter, Advances in water resources, 28, 135–147, https://doi.org/10.1016/j.advwatres.2004.09.002, 2005.

Myneni, R., Knyazikhin, Y., and Park, T.: MOD15A2H MODIS/Terra leaf area Index/FPAR 8-Day L4 global 500m SIN grid V006, NASA EOSDIS Land Processes DAAC, 2015.

Novick, K. A., Ficklin, D. L., Stoy, P. C., Williams, C. A., Bohrer, G., Oishi, A. C., Papuga, S. A., Blanken, P. D., Noormets, A., Sulman, B. N., et al.: The increasing importance of atmospheric demand for ecosystem water and carbon fluxes, Nature climate change, 6, 1023–1027, 2016.

Otkin, J. A., Anderson, M. C., Hain, C., Svoboda, M., Johnson, D., Mueller, R., Tadesse, T., Wardlow, B., and Brown, J.: Assessing the evolution of soil moisture and vegetation conditions during the 2012 United States flash drought, Agricultural and forest meteorology, 218, 230–242, https://doi.org/10.1016/j.agrformet.2015.12.065, 2016.

Otkin, J. A., Svoboda, M., Hunt, E. D., Ford, T. W., Anderson, M. C., Hain, C., and Basara, J. B.: Flash droughts: A review and assessment of the challenges imposed by rapid-onset droughts in the United States, Bulletin of the American Meteorological Society, 99, 911–919, https://doi.org/10.1175/BAMS-D-17-0149.1, 2018.

Otkin, J. A., Woloszyn, M., Wang, H., Svoboda, M., Skumanich, M., Pulwarty, R., Lisonbee, J., Hoell, A., Hobbins, M., Haigh, T., et al.: Getting ahead of Flash Drought: From Early Warning to Early Action, Bulletin of the American Meteorological Society, 103, E2188–E2202, 2022.

Pastorello, G., Trotta, C., Canfora, E., Chu, H., Christianson, D., Cheah, Y.-W., Poindexter, C., Chen, J., Elbashandy, A., Humphrey, M., et al.: The FLUXNET2015 dataset and the ONEFlux processing pipeline for eddy covariance data, Scientific data, 7, 1–27, 2020.

Pearson, R. G., Phillips, S. J., Loranty, M. M., Beck, P. S., Damoulas, T., Knight, S. J., and Goetz, S. J.: Shifts in Arctic vegetation and associated feedbacks under climate change, Nature climate change, 3, 673–677, 2013.

Poonia, V., Goyal, M. K., Jha, S., and Dubey, S.: Terrestrial ecosystem response to flash droughts over India, Journal of Hydrology, 605, 127 402, 2022.

Qing, Y., Wang, S., Ancell, B. C., and Yang, Z.-L.: Accelerating flash droughts induced by the joint influence of soil moisture depletion and atmospheric aridity, Nature communications, 13, 1–10, 2022.

Roman, D., Novick, K., Brzostek, E., Dragoni, D., Rahman, F., and Phillips, R.: The role of isohydric and anisohydric species in determining ecosystem-scale response to severe drought, Oecologia, 179, 641–654, 2015.

Running, S., Mu, Q., and Zhao, M.: MOD17A2H MODIS/terra gross primary productivity 8-day L4 global 500m SIN grid V006, NASA EOSDIS Land Processes DAAC, 2015.

Running, S. W., Nemani, R. R., Heinsch, F. A., Zhao, M., Reeves, M., and Hashimoto, H.: A continuous satellite-derived measure of global terrestrial primary production, Bioscience, 54, 547–560, 2004.

Sade, N., Gebremedhin, A., and Moshelion, M.: Risk-taking plants: anisohydric behavior as a stress-resistance trait, Plant signaling & behavior, 7, 767–770, 2012.

Sanaullah, M., Chabbi, A., Rumpel, C., and Kuzyakov, Y.: Carbon allocation in grassland communities under drought stress followed by 14C pulse labeling, Soil Biology and Biochemistry, 55, 132–139, 2012.

Savitzky, A. and Golay, M. J.: Smoothing and differentiation of data by simplified least squares procedures., Analytical chemistry, 36, 1627–1639, 1964.

Schmid, H.: Source areas for scalars and scalar fluxes, Boundary-Layer Meteorology, 67, 293–318, 1994.

Sellers, P. J., Dickinson, R., Randall, D., Betts, A. K., Hall, F. G., Berry, J. A., Collatz, G., Denning, A., Mooney, H. A., Nobre, C. A., et al.: Modeling the exchanges of energy, water, and carbon between continents and the atmosphere, Science, 275, 502–509, 1997.

Soil Survey Staff, Natural Resources Conservation Service, U. S. D. o. A.: Web Soil Survey. Available online. Accessed 07 December 2022, https://www.nrcs.usda.gov/resources/data-and-reports/web-soil-survey.

Stöckli, R., Rutishauser, T., Dragoni, D., O'keefe, J., Thornton, P., Jolly, M., Lu, L., and Denning, A.: Remote sensing data assimilation for a prognostic phenology model, Journal of Geophysical Research: Biogeosciences, 113, https://doi.org/10.1029/2008JG000781, 2008.

Sulla-Menashe, D. and Friedl, M. A.: User guide to collection 6 MODIS land cover (MCD12Q1 and MCD12C1) product, USGS: Reston, VA, USA, 1, 18, 2018.

Svoboda, M., LeComte, D., Hayes, M., Heim, R., Gleason, K., Angel, J., Rippey, B., Tinker, R., Palecki, M., Stooksbury, D., et al.: The drought monitor, Bulletin of the American Meteorological Society, 83, 1181–1190, 2002.

Tanré, D., Kaufman, Y., Herman, M., and Mattoo, S.: Remote sensing of aerosol properties over oceans using the MODIS/EOS spectral radiances, Journal of Geophysical Research: Atmospheres, 102, 16 971–16 988, https://doi.org/10.1029/96JD03437, 1997.

Tao, J. and Barros, A.: Coupled prediction of flood response and debris flow initiation during warm-and cold-season events in the Southern Appalachians, USA, Hydrology and Earth System Sciences, 18, 367–388, 2014.

Tao, J. and Barros, A. P.: Prospects for flash flood forecasting in mountainous regions–An investigation of Tropical Storm Fay in the Southern Appalachians, Journal of Hydrology, 506, 69–89, 2013.

Thornthwaite, C. W. and Mather, J. R.: Instructions and tables for computing potential evapotranspiration and the water balance., Publications on Climatology, 10, 185–310, 1957.

Tobin, K. J., Bennett, M. E., and Torres, R.: Long-term root zone moisture trends across CONUS from a new root-zone soil moisture product called SMERGE, in: AGU Fall Meeting Abstracts, vol. 2019, pp. H51S–1750, 2019.

Towne, G. and Owensby, C.: Long-term effects of annual burning at different dates in ungrazed Kansas tallgrass prairie., Rangeland Ecology & Management/Journal of Range Management Archives, 37, 392–397, 1984.

Trenberth, K. E., Dai, A., Van Der Schrier, G., Jones, P. D., Barichivich, J., Briffa, K. R., and Sheffield, J.: Global warming and changes in drought, Nature Climate Change, 4, 17–22, 2014.

Urban, J., Ingwers, M., McGuire, M. A., and Teskey, R. O.: Stomatal conductance increases with rising temperature, Plant signaling & behavior, 12, e1356 534, 2017.

Vargas Zeppetello, L. R., McColl, K. A., Bernau, J. A., Bowen, B. B., Tang, L. I., Holbrook, N. M., Gentine, P., and Huybers, P.: Apparent surface conductance sensitivity to vapour pressure deficit in the absence of plants, Nature Water, pp. 1–11, 2023.

Wang, J., Rich, P. M., and Price, K. P.: Temporal responses of NDVI to precipitation and temperature in the central Great Plains, USA, International journal of remote sensing, 24, 2345–2364, 2003.

Wilson, K., Goldstein, A., Falge, E., Aubinet, M., Baldocchi, D., Berbigier, P., Bernhofer, C., Ceulemans, R., Dolman, H., Field, C., et al.: Energy balance closure at FLUXNET sites, Agricultural and Forest Meteorology, 113, 223–243, 2002.

Wolf, S., Keenan, T. F., Fisher, J. B., Baldocchi, D. D., Desai, A. R., Richardson, A. D., Scott, R. L., Law, B. E., Litvak, M. E., Brunsell, N. A., et al.: Warm spring reduced carbon cycle impact of the 2012 US summer drought, Proceedings of the National Academy of Sciences, 113, 5880–5885, 2016.

Wu, G., Guan, K., Li, Y., Novick, K. A., Feng, X., McDowell, N. G., Konings, A. G., Thompson, S. E., Kimball, J. S., De Kauwe, M. G., et al.: Interannual variability of ecosystem iso/anisohydry is regulated by environmental dryness, New Phytologist, 229, 2562–2575, 2021.

Xia, Y., Mitchell, K., Ek, M., Sheffield, J., Cosgrove, B., Wood, E., Luo, L., Alonge, C., Wei, H., Meng, J., et al.: Continental-scale water and energy flux analysis and validation for the North American Land Data Assimilation System project phase 2 (NLDAS-2): 1. Intercomparison and application of model products, Journal of Geophysical Research: Atmospheres, 117, 2012.

Xu, T., Chen, F., He, X., Barlage, M., Zhang, Z., Liu, S., and He, X.: Improve the performance of the noah-MP-crop model by jointly assimilating soil moisture and vegetation phenology data, Journal of Advances in Modeling Earth Systems, 13, e2020MS002 394, 2021.

Yan, K., Park, T., Yan, G., Chen, C., Yang, B., Liu, Z., Nemani, R. R., Knyazikhin, Y., and Myneni, R. B.: Evaluation of MODIS LAI/FPAR product collection 6. Part 1: Consistency and improvements, Remote Sensing, 8, 359, 2016.

Yao, T., Liu, S., Hu, S., and Mo, X.: Response of vegetation ecosystems to flash drought with solar-induced chlorophyll fluorescence over the Hai River Basin, China during 2001–2019, Journal of Environmental Management, 313, 114 947, 2022.

Yildiz, O. and Barros, A. P.: Climate variability, water resources, and hydrologic extremes—Modeling the water and energy budgets, Climate and Hydrology, in Mountain Areas, pp. 291–306, 2005.

Yildiz, O. and Barros, A. P.: Elucidating vegetation controls on the hydroclimatology of a mid-latitude basin, Journal of Hydrology, 333, 431–448, 2007.

Yildiz, O., Barros, A. P., et al.: Evaluating spatial variability and scale effects on hydrologic processes in a midsize river basin, Sci. Res. Essays, 4, 217–225, 2009.

Yuan, X., Wang, L., Wu, P., Ji, P., Sheffield, J., and Zhang, M.: Anthropogenic shift towards higher risk of flash drought over China, Nature communications, 10, 1–8, 2019.

Zeng, X.: Global vegetation root distribution for land modeling, Journal of Hydrometeorology, 2, 525–530, 2001.

Zeng, Z., Wu, W., Li, Y., Huang, C., Zhang, X., Peñuelas, J., Zhang, Y., Gentine, P., Li, Z., Wang, X., et al.: Increasing meteorological drought under climate change reduces terrestrial ecosystem productivity and carbon storage, One Earth, 6, 1326–1339, 2023.

Zhang, M. and Yuan, X.: Rapid reduction in ecosystem productivity caused by flash droughts based on decade-long FLUXNET observations, Hydrology and Earth System Sciences, 24, 5579–5593, 2020.

Zhang, M., Yuan, X., and Otkin, J. A.: Remote sensing of the impact of flash drought events on terrestrial carbon dynamics over China, Carbon Balance and Management, 15, 1–11, https://doi.org/10.1186/s13021-020-00156-1, 2020.

Zhou, S., Duursma, R. A., Medlyn, B. E., Kelly, J. W., and Prentice, I. C.: How should we model plant responses to drought? An analysis of stomatal and non-stomatal responses to water stress, Agricultural and Forest Meteorology, 182, 204–214, 2013.